Department of Chemical and Metallurgical Engineering

Tar reforming in biomass gasification gas cleaning

Noora Kaisalo

Aalto University

DOCTORAL DISSERTATIONS

Aalto University publication series
DOCTORAL DISSERTATIONS 132/2017
VTT SCIENCE 160

Tar reforming in biomass gasification gas cleaning

Noora Kaisalo

A doctoral dissertation completed for the degree of Doctor of Science (Technology) to be defended, with the permission of the Aalto University School of Chemical engineering, at a public examination held at the lecture hall Ke2 of the school on 18th August 2017 at 12:00.

Aalto University
School of Chemical Engineering
Department of Chemical and Metallurgical Engineering
Industrial Chemistry

Supervising professor
Professor Riikka Puurunen, Aalto University, Finland

Thesis advisors
Dr. Pekka Simell, VTT Technical Research Centre of Finland Ltd, Finland
Research Professor Juha Lehtonen, VTT Technical Research Centre of Finland Ltd, Finland

Preliminary examiners
Professor Lars J. Pettersson, KTH Royal Institute of Technology, Sweden
Professor Hermann Hofbauer, TU Wien, Austria

Opponent
Dr. Tilman J. Schildhauer, Paul Scherrer Institute, Switzerland

Aalto University publication series
DOCTORAL DISSERTATIONS 132/2017

VTT SCIENCE 160

ISBN 978-952-60-7525-9 (printed)
ISBN 978-952-60-7524-2 (pdf)
ISSN-L 1799-4934
ISSN 1799-4934 (printed)
ISSN 1799-4942 (pdf)
http://urn.fi/URN:ISBN:978-952-60-7524-2

ISBN 978-951-38-8561-8 (printed)
ISBN 978-951-38-8560-1 (pdf)
ISSN-L 2242-119X
ISSN 2242-119X (printed)
ISSN 2242-1203 (pdf)
http://urn.fi/URN:ISBN:978-951-38-8560-1

Unigrafia Oy
Helsinki 2017

Finland

NORDIC ECOLABEL
441 697
Printed matter

Aalto University

Abstract

Aalto University, P.O. Box 11000, FI-00076 Aalto www.aalto.fi

Author
Noora Kaisalo

Name of the doctoral dissertation
Tar reforming in biomass gasification gas cleaning

Publisher School of Chemical Engineering

Unit Department of Chemical and Metallurgical Engineering

Series Aalto University publication series DOCTORAL DISSERTATIONS 132/2017

Field of research Industrial Chemistry

Manuscript submitted 1 February 2017 **Date of the defence** 18 August 2017

Permission to publish granted (date) 26 April 2017 **Language** English

☐ **Monograph** ☒ **Article dissertation** ☐ **Essay dissertation**

Abstract

Thermochemical conversion of biomass can be used to produce synthesis gas via gasification. This synthesis gas can be further upgraded to renewable fuels and chemicals provided that the gas is ultra clean. To achieve this, impurities, such as light hydrocarbons and tar compounds present in the gasification gas can be converted to syngas by reforming.

The amount of tar in gasification gas can be reduced already in the gasifier by using catalytically active bed materials. Typical bed materials in fluidized bed gasification are sand, olivine, dolomite and MgO. The tar conversion activity of dolomite and MgO were found to be high at atmospheric pressure. However, the activity was lost when the pressure was increased to 10 bar.

Gasification gas contains, in addition to tar, ethene, which may contribute to further tar formation in high temperature zones of the process, especially at elevated pressures. Ethene forms tar compounds by radical chain reactions. The tar formed by thermal reactions of ethene resembles the tar from high temperature fluidized bed gasification, which contains mainly secondary and tertiary tar compounds.

Carbon formation on the reformer catalysts presents a challenge in biomass gasification gas cleaning. The presence of sulfur in the gas, mainly in the form of H2S, also complicates reforming. Typical catalysts used in the reformer after the gasifier are precious metal and nickel catalysts. The heat for reforming can be brought either indirectly in the case of steam reforming or by adding oxygen to the feed for autothermal reforming. Nickel and precious metal catalyst activities were analysed in experiments of around 500 hours with several different gas compositions. Catalyst deactivation was higher with steam than autothermal reforming. The use of catalytically active bed materials to reduce tar concentration already in the gasifier is especially favourable for steam reforming as the catalyst deactivation rate was decreased by the lower hydrocarbon content of the gas.

Benzene, a highly stable compound, is a typical residual compound in the gas after the reformer. Thus, the reformer could be designed based on the reforming kinetics of benzene, for example in the production of synthetic natural gas. For this purpose, qualitative analysis of the effect of the main gasification gas compounds (H2, CO, CO2, H2O) on reforming kinetics were studied with a nickel catalyst. Benzene reforming can be described by first order kinetics if the parameters are estimated for the specific gas composition.

Keywords biomass, gasification, reforming, tar, synthesis gas, nickel catalyst, precious metal catalyst

ISBN (printed) 978-952-60-7525-9 **ISBN (pdf)** 978-952-60-7524-2

ISSN-L 1799-4934 **ISSN (printed)** 1799-4934 **ISSN (pdf)** 1799-4942

Location of publisher Helsinki **Location of printing** Helsinki **Year** 2017

Pages 132 **urn** http://urn.fi/URN:ISBN:978-952-60-7524-2

Aalto-yliopisto

Tiivistelmä

Aalto-yliopisto, PL 11000, 00076 Aalto www.aalto.fi

Tekijä
Noora Kaisalo

Väitöskirjan nimi
Tervan reformointi biomassan kaasutuskaasun puhdistuksessa

Julkaisija Kemian tekniikan korkeakoulu

Yksikkö Kemian tekniikan ja metallurgian laitos

Sarja Aalto University publication series DOCTORAL DISSERTATIONS 132/2017

Tutkimusala Teknillinen kemia

Käsikirjoituksen pvm 1.2.2017 **Väitöspäivä** 18.08.2017

Julkaisuluvan myöntämispäivä 26.4.2017 **Kieli** Englanti

☐ **Monografia** ☒ **Artikkeliväitöskirja** ☐ **Esseeväitöskirja**

Tiivistelmä

Biomassan termokemiallisella konversiolla voidaan tuottaa synteesikaasua kaasutusreitin kautta. Synteesikaasu voidaan jatkojalostaa uusiutuviksi polttoaineiksi sekä kemikaaleiksi. Synteesisovelluksia varten kaasun tulee olla ultrapuhdasta. Tämän saavuttamiseksi epäpuhtaudet, kuten keveät hiilivedyt ja tervayhdisteet voidaan konvertoida synteesikaasuksi reformoimalla. Tervan määrää kaasutuskaasussa voidaan vähentää jo kaasuttimessa käyttämällä katalyyttisesti aktiivisia petimateriaaleja. Leijukerroskaasutuksessa tyypillisesti käytettyjä petimateriaaleja ovat hiekka, oliviini, dolomiitti ja MgO. Dolomiitin ja MgO:n aktiivisuus tervakonversion suhteen oli korkea ilmanpaineessa. Jos painetta nostettiin 10 bar:iin, katalyyttinen aktiivisuus käytännössä katosi.

Kaasutuskaasu sisältää tervan lisäksi eteeniä, joka voi lisätä tervan muodostusta erityisesti paineistetuissa olosuhteissa prosessin kohdissa, joissa on korkea lämpötila. Eteeni muodostaa tervayhdisteitä radikaaliketjureaktioilla. Terva, joka muodostuu eteenin termisistä reaktioista, muistuttaa korkean lämpötilan leijukerroskaasuttimen tervaa, joka koostuu pääasiassa sekundäärisistä ja tertiäärisistä tervayhdisteistä.

Hiilen muodostus reformointikatalyyteille on haaste biomassan kaasutuskaasun puhdistuksessa. Lisäksi kaasun sisältämä rikki, joka on pääasiassa rikkivedyn muodossa, vaikeuttaa reformointia. Tyypillisesti kaasuttimen jälkeisessä reformerissa käytettyjä katalyyttejä ovat jalometalli- ja nikkelikatalyytit. Reformoinnin vaatima lämpö voidaan tuoda reaktoriin, joko epäsuorasti höyryreformoinnin tapauksessa tai lisäämällä happea kaasuun autotermisessä reformoinnissa. Nikkeli- ja jalometallikatalyyttien aktiivisuutta seurattiin noin 500 tunnin kokeissa useilla eri kaasukoostumuksilla. Katalyyttien deaktivoituminen oli nopeampaa höyryreformoinnissa kuin autotermisessä reformoinnissa. Katalyyttisesti aktiivisten petimateriaalien käyttö alentamaan tervan määrää jo kaasuttimessa on erityisen suositeltavaa höyryreformoinnin kannalta, sillä höyryreformoinnissa katalyyttien deaktivoitumisnopeus aleni, kun hiilivetyjen määrää kaasussa vähennettiin.

Bentseeni hyvin stabiilina yhdisteenä on tyypillinen jäännöskomponentti kaasussa reformoinnin jälkeen. Tästä johtuen reformeri voidaan suunnitella bentseenin reformointikinetiikkaan perustuen esimerkiksi synteettisen maakaasun valmistuksessa. Tätä varten tutkittiin kaasutuskaasun pääkomponenttien (H_2, CO, CO_2, H_2O) kvalitatiivista vaikutusta reformointi kinetiikkaan nikkelikatalyytillä. Bentseenin reformointireaktiota voidaan kuvata ensimmäisen kertaluvun kinetiikalla, mikäli parametrit estimoidaan kyseessä olevalle kaasukoostumukselle.

Avainsanat biomassa, kaasutus, reformointi, terva, synteesikaasu, nikkelikatalyytti, jalometallikatalyytti

ISBN (painettu) 978-952-60-7525-9 **ISBN (pdf)** 978-952-60-7524-2

ISSN-L 1799-4934 **ISSN (painettu)** 1799-4934 **ISSN (pdf)** 1799-4942

Julkaisupaikka Helsinki **Painopaikka** Helsinki **Vuosi** 2017

Sivumäärä 132 **urn** http://urn.fi/URN:ISBN:978-952-60-7524-2

Preface

The work presented in this thesis has been carried out at VTT Technical Research Centre of Finland Ltd during years 2012-2017. I would like to acknowledge financial support from VTT Technical Research Centre of Finland Ltd and Tekes -- the Finnish Funding Agency for Innovation through Vetaani and 2G2020 projects.

I would like to express my gratitude to my instructor Dr. Sc. Pekka Simell for sustained support and advice. I thank my original thesis supervisor Professor Juha Lehtonen for his interest and guidance in my work, and Professor Riikka Puurunen who agreed to be the official supervisor in 2017.

My sincere thanks to my co-authors Johanna Kihlman and Sanna Tuomi for fruitful and inspiring discussions. I am indebted to Mari-Leena Koskinen-Soivi, Katja Heiskanen and Päivi Jokimies for the experimental work and expertise in laboratory. Warm thanks to my co-authors Ilkka Hannula, Esa Kurkela, Ilkka Hiltunen and Matti Nieminen. I thank my colleagues at Biologinkuja 5 for providing a pleasant working atmosphere.

For my parents, Leena and Yki: thank you for your encouragement during my studies. My friends, I appreciate your support and taking my mind of work. Aapo, thank you for support to make this thesis ready.

Espoo, April 2017
Noora Kaisalo

List of publications

This thesis is based on the following original publications which are referred to in the text as I–V. The publications are reproduced with kind permission from the publishers.

I Noora Kaisalo, Mari-Leena Koskinen-Soivi, Pekka Simell, Juha Lehtonen. Effect of process conditions on tar formation from thermal reactions of ethylene. *Fuel*, 2015, Volume 153, pages 118-127. DOI: 10.1016/j.fuel.2015.02.085

II Sanna Tuomi, Noora Kaisalo, Pekka Simell, Esa Kurkela. Effect of pressure on tar decomposition activity of different bed materials in biomass gasification conditions. *Fuel*, 2015, Volume 158, pages 293-305. DOI: 10.1016/j.fuel.2015.05.051.

III Noora Kaisalo, Johanna Kihlman, Ilkka Hannula, Pekka Simell. Reforming solutions for biomass-derived gasification gas – Experimental results and concept assessment. *Fuel*, 2015, Volume 147, pages 208-220. DOI: 10.1016/j.fuel.2015.01.056.

IV Noora Kaisalo, Pekka Simell, Juha Lehtonen. Benzene steam reforming kinetics in biomass gasification gas cleaning. *Fuel*, 2016, Volume 182, pages 696-703. DOI: 10.1016/j.fuel.2016.06.042.

V Pekka Simell, Ilkka Hannula, Sanna Tuomi, Matti Nieminen, Esa Kurkela, Ilkka Hiltunen, Noora Kaisalo, Johanna Kihlman. Clean syngas from biomass—process development and concept assessment. *Biomass Conversion and Biorefinery*, 2014, Volume 4, pages 357-370. DOI10.1007/s13399-014-0121-y.

Author's contributions

Publication I: "Effect of process conditions on tar formation from thermal reactions of ethylene"

Author contributions: N. Kaisalo designed the experiments and calculated the results and was the main contributor in interpreting the results and writing of the manuscript. M-L Koskinen-Soivi carried out the experiments and gas chromatography analysis. P. Simell instructed the work, took part in planning of the experiments and commented the manuscript. J. Lehtonen reviewed and commented the manuscript.

Publication II: Effect of pressure on tar decomposition activity of different bed materials in biomass gasification conditions

Author contributions: S. Tuomi designed the biomass gasification experiments and calculated and analysed the results. N. Kaisalo designed the laboratory experiments and calculated and analysed the results of those. S. Tuomi and N. Kaisalo co-authored the article. P. Simell and E. Kurkela took part in the experimental design and commented on the manuscript.

Publication III: Reforming solutions for biomass-derived gasification gas – Experimental results and concept assessment

N. Kaisalo and J. Kihlman planned the experiments, calculated and analysed the results and wrote the experimental part of the article. N. Kaisalo carried out two of the experiments. I. Hannula carried out and wrote the concept assessment section of the article. P. Simell commented on the experimental design and the manuscript.

Publication IV: Benzene steam reforming kinetics in biomass gasification gas cleaning

N. Kaisalo designed the experiments, analysed the results, carried out the modelling work and wrote the manuscript. P. Simell participated in experimental design and result analysis. J. Lehtonen guided and assisted in the modelling work and commented on the manuscript.

Publication V: Clean syngas from biomass—process development and concept assessment

Author contributions: P. Simell was the main writer of the manuscript and the main developer of the catalytic reforming work reported in article. I. Hannula carried out and wrote the techno-economical assessment. S. Tuomi and M. Nieminen were responsible for the filtration part of the article. E. Kurkela and I. Hiltunen were responsible for the pilot-scale experimental planning and results. N. Kaisalo planned the laboratory catalyst testing experiments and calculated and wrote the results. J. Kihlman took part in experimental planning of reforming experiments and commented on the article.

Contents

List of abbreviations and symbols

Abbreviations

Air gaga	air gasification gas
BFB	bubbling fluidized bed
Bz	benzene
CFB	circulating fluidized bed
CHP	combined heat and power
DFB	dual fluidized bed
FID	flame ionization detector
FT	Fischer-Tropsch
FTIR	Fourier transformation infrared spectroscopy
GC	gas chromatograph
HACA	hydrogen abstraction and acetylene addition
HAVA	hydrogen abstraction and vinyl radical addition
HC	hydrocarbon
LH	low hydrocarbon content gas
MAC	methyl addition and cyclization
MH	medium hydrocarbon content gas
PAC	phenyl addition and cyclization
PDU	process development unit
SNG	synthetic natural gas
TCD	thermal conductivity detector
WGS	water gas shift

Symbols

c_i	concentration of a compound i (mol/m^3)
E_a	activation energy (kJ/mol)
ΔH_i	adsorption enthalpy of a compound i (kJ/mol)
K_i	equilibrium constant for adsorption of a compound i
K_{ref}	equilibrium constant at reference temperature, 850 °C
k’	apparent reaction rate constant (m^3/(s*kg_{cat}))
k_{ref}	apparent reaction rate constant at reference temperature, 850 °C (m^3/(s*kg_{cat}))
m_{cat}	mass of the catalyst (kg)
n_i	molar flow of a compound i (mol/h)
p_i	partial pressure of a compound i (Pa)
R	gas constant (kJ/(K*mol))
r_i	rate of reaction of a compound i (mol/kg_{cat}*h)
T	temperature, K
z	dimensionless weight of the catalyst bed
α, β	reaction orders
Θ_s	surface coverage by sulfur

1. Introduction

1.1 Background and motivation

Levels of anthropogenic greenhouse gas emissions in the atmosphere have been rising since the beginning of the industrial era (1750), yet around half of all emissions occurred since 1970 [1]. Increasing carbon dioxide emissions have been identified as a primary cause of global warming [1]. The Paris Agreement on climate change, which entered into force in 2016, sets goals for greenhouse gas emission reductions [2]. For example, the EU has committed under the Paris Agreement to reducing greenhouse gas emissions by at least 40% by 2030 compared to 1990 levels [3]. To mitigate CO_2 emissions and achieve climate objectives, the use of renewable energy sources is essential. In addition to environmental drivers, also political drivers exist for the exploitation of locally produced energy sources instead of dependency on geographically limited oil reserves.

Biomass is an important part of the renewable energy mix alongside with solar, wind and hydropower. Use of cellulosic biomass, especially wastes and residues, avoids competition with the food chain. Searle and Malins [4] have evaluated the total amount of sustainably available cellulosic waste and residue to be around 220 million tonnes per year in the EU. The amount of forest residue was evaluated at 40 million tonnes per year. The amount of all sustainably available cellulosic waste and residue corresponds to 1 million barrels of oil equivalent per day, which would mean 13% of road fuel consumption in the EU in 2020. However, they evaluated that only 8% of forest residue in the EU was used in 2013. In Finland, forest industry residues are a major potential biomass feedstock. By using biomass for fuel or chemical production, dependency on imported oil can be reduced.

Thermochemical conversion of biomass is an option for the production of renewable fuels or chemicals. By gasification, solid biomass can be converted to synthesis gas (syngas), which is a platform for various end products from combined heat and power (CHP) production to fuels and chemicals. An essential aspect of biomass conversion to syngas is the cleaning of the gas from various impurities. A typical feature of biomass gasification is tar formation. Tar consists of a range of aromatic hydrocarbons; by converting them by reforming to H_2 and CO, the syngas yield increases. However, the reforming conditions are challenging and require understanding of how the process conditions affect the operation of the reformer.

1.2 Scope of the thesis

The thesis comprises five publications related to catalytic gas cleaning of hydrocarbons either in a gasifier or in a reformer after the gasifier. The relations of the publications to each other and to the gasification process are presented in Figure 1. The scope of the thesis was mainly to investigate the reformer. The hydrocarbon

load and gas composition from the gasifier affect the reformer operation, for example, by affecting the carbon formation. Thus, the reformer studies were supported by studies of thermal reactions of ethene and the catalytic activity of the bed materials of the fluidized bed gasifier.

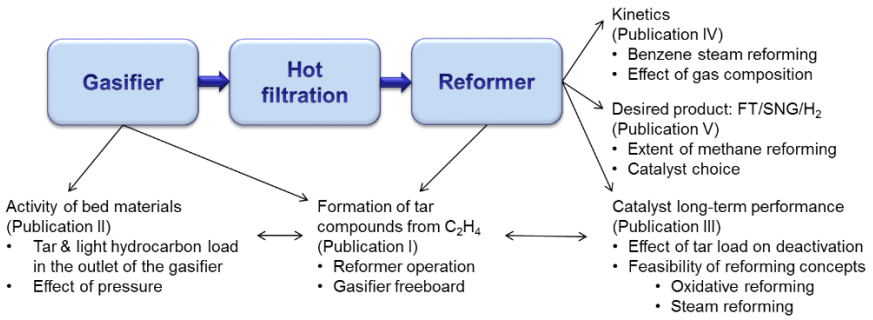

Figure 1. Relation of thesis publications to each other and to the gasification process.

The formation of tar compounds from ethene was studied in Publication I. Light hydrocarbons in the biomass gasification gas may form tar compounds in high temperatures and thus affect the operation of the reformer by adding the hydrocarbon load on the catalyst. Such high temperature zones may exist, for example, in the inlet area of the reformer or in the gasifier free board.

The hydrocarbon and tar content of biomass gasification gas can be reduced already in the gasifier by catalytically active bed materials. Publication II addresses the questions: Can catalytically active bed materials help to achieve conditions where reforming can be done easily and how does pressure affect their efficiency in reducing tar levels?

Pressurizing the gasification and gas cleaning processes is beneficial for process economics and efficiency, but it may present operational challenges for reforming. Thus, the thermal reactions of ethene (Publication I) and the activity of the bed materials (Publication II) were studied under pressurized conditions.

Steam and autothermal reforming of tar and light hydrocarbons with nickel and precious metal catalysts were studied in Publications III and V. The catalyst lifetime in both reforming modes and the effect of hydrocarbon load in the gas was investigated in Publication III by long-term catalyst testing. Publication V focused on the effect of the catalyst choice on methane conversion. The desired level of methane conversion in reforming depends on the process concept.

Benzene steam reforming kinetics was studied in Publication IV. The study addresses the effect of gas composition on the kinetics of benzene steam reforming.

2. Biomass gasification gas cleaning from tar and light hydrocarbons

2.1 Process description

Gasification of biomass in fluidized bed gasifiers has been identified to be feasible for forest residue gasification at scale of around 100-300 MW fuel input [5]. The gasification reactions are endothermic and thus require heat. The heat for the reactions can be brought directly by partly oxidizing the feedstock with air or oxygen. Alternatively, steam can be used as a gasification medium, in which case the heat for the reactions needs to be brought indirectly by circulating the hot bed material. The fluidized bed gasifiers can be operated as circulating or bubbling fluidized beds. In dual fluidized bed gasifiers, the gasification of biomass takes place in one fluidized bed and the combustion of residual char in the other. The heat is transferred between the fluidized beds by the bed material. The circulating fluidized bed (CFB) and dual fluidized bed (DFB) gasifiers at VTT are presented in Figure 2 and Figure 3, respectively.

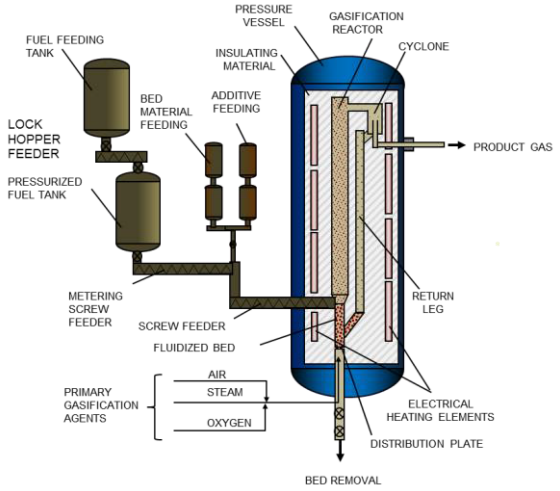

Figure 2. CFB gasifier at VTT

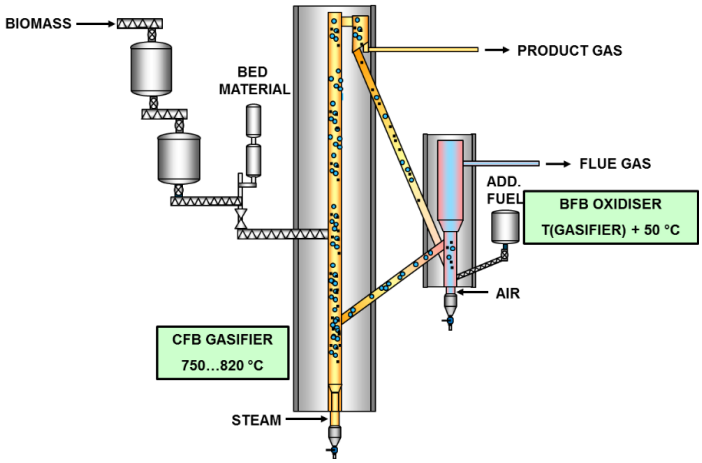

Figure 3. DFB gasifier at VTT

The gas composition obtained by gasification depends on the gasifying agent, process conditions and feedstock. Typical gasification temperatures in fluidized bed gasifiers are 750 – 950 °C. With air gasification, a downside is that the product gas is diluted by N_2. For synthesis purposes, the nitrogen is an inert gas and dilution by it would lead to high costs of gas compression [6]. The air gasification gas also has low energy contents: 3-7 MJ/Nm^3 compared to 7-15 MJ/Nm^3 for oxygen gasification gas [7].

The gas exiting the gasifier contains impurities that need to be removed for the advanced use of biomass gasification gas. For example, the synthesis processes require ultra clean syngas. An example process concept for the production of synthetic fuels by Fischer-Tropsch (FT) synthesis is presented in Figure 4 (Publication V). The particulates in the gas exiting the gasifier can be removed by a hot gas filter, whereas the tar compounds and light hydrocarbons can be converted by reforming to syngas. For tar removal, another possibility is scrubbing by an organic solvent [8,9]. However, the gasification gas also contains minor impurities, such as H_2S, COS, NH_3 and alkali metals. Especially sulfur compounds further complicate the reforming of hydrocarbons by poisoning the catalyst. In addition to hydrocarbons, ammonia is partly converted to N_2 in the reformer [10]. The alkali metals, in turn, will condense in hot gas filtration taking place at around 500 °C [11]. The final conditioning of gas for synthesis purposes can be realized by conventional commercial technologies for acid gas removal, such as the Rectisol process, and the H_2/CO ratio can be adjusted by a water gas shift reactor [12].

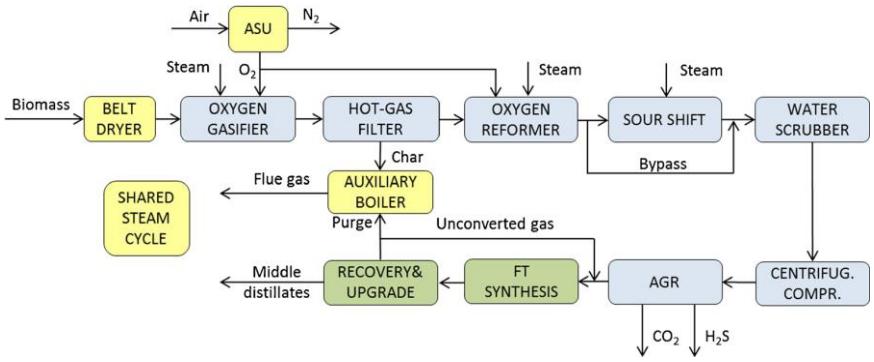

Figure 4. Stand-alone biomass gasification concept producing FT liquids.

Figure 5 presents the concepts for FT, synthetic natural gas (SNG) or H_2 production by gasification developed at VTT. The O_2-steam blown gasification concept with FT synthesis has been demonstrated in Varkaus [13] and the gasification and gas cleaning has been tested extensively at VTT's process development unit (PDU) [14,15]. Prior to the demonstration, the gasification and gas cleaning by filtration and reforming were developed at VTT and tested on VTT's 0.5 MW fuel input PDU test rig. The gas cleaning was realized by hot gas filtration and reforming of hydrocarbons followed by final gas ultra-cleaning and conditioning at Varkaus. Kurkela et al. [14] have reported the results of a 215 h-run of gasification and gas cleaning on the PDU. The concepts based on steam gasification in DFB combined with filtration at the gasifier outlet temperature followed by steam or oxidative reforming are under development.

For the pressurized oxygen blown gasification concept, Hannula and Kurkela [12] have calculated the cost estimates for the production of FT liquids in a stand-alone plant. Forest residues were used as feedstock for plants with 300 MW biomass input. The cost estimates were developed for a so-called N^{th} plant, i.e. after the technology has been commercialized. The thermal efficiency of producing FT liquids was calculated to be 52% (LHV). The levelized production cost was estimated at 75 €/MWh. The total capital investment cost for the plant was estimated at 370 M€. The gasifier accounted for 51 M€ and hot gas cleaning including the filtration and reformer for 38 M€. The share of the reformer in the cost of the hot gas cleaning train was about 75%.

Pressurised oxygen blown gasification is targeted at a relatively large scale, around 300 MW fuel input, to be economic, whereas steam gasification would be suitable for 100-200 MW scales where the production of oxygen would render the process uneconomic [16]. For example, in the oxygen blown gasification concept, the investment cost of the air separation unit was evaluated at 47 M€ [12]. In addition, steam gasification is suitable for uses where high H_2/CO ratios are desirable, such as SNG production, since the large steam input drives the water-gas shift reaction on the side of H_2 (Publication III).

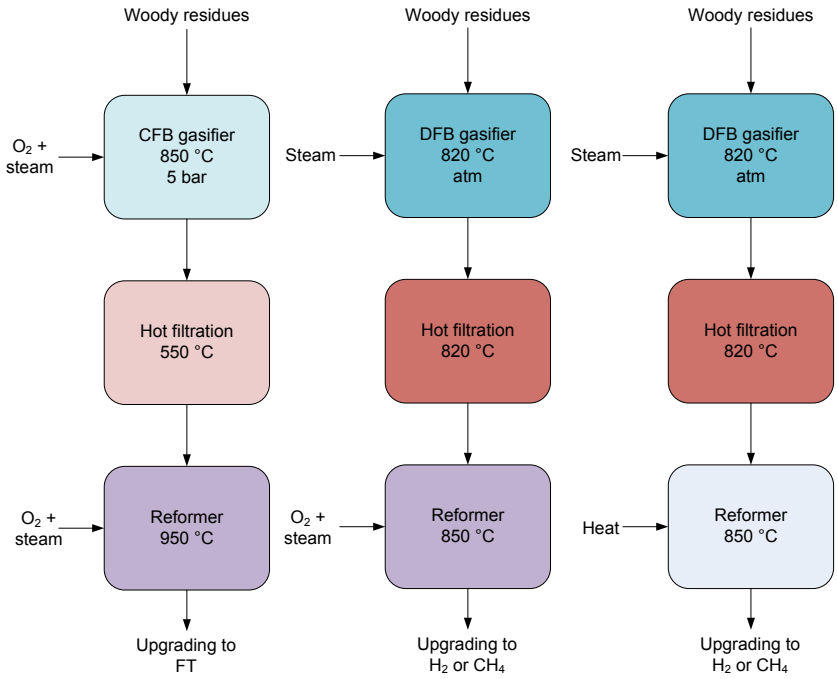

Figure 5. Gasification and gas cleaning concepts for FT production by steam-oxygen blown gasification, and steam gasification concepts for SNG and H_2 production with autothermal or steam reforming.

Pressurizing the process is of interest for concepts where the final steps are at high pressure, such as FT or methanol synthesis. Pressurization reduces the production cost by reducing the compression costs [17]. For example, in methanol production by oxygen-blown gasification of biomass, the production costs decrease around 3-4% by increasing the gasification pressure from 1 to 5 bar [6]. However, high pressure may lead to operational problems, such as ash sintering and melting [15].

Steam-blown DFB gasifiers are more suitable for relatively low pressure due to more difficult operation of the dual fluidized bed, whereas oxygen blown gasifiers could be pressurized to higher pressures close to synthesis pressures [17]. The low operation pressure makes the DFB gasifier suitable for relatively low pressure synthesis, such as methanation, or for H_2 production. The economic feasibility of both gasification concepts is strongly dependent on the integration of the process with forest industry or other heat-consuming industry [6], Publication III.

Biomass gasifiers are industrially used for CHP production, for example, air-blown CFB gasifiers in Finland and indirectly heated DFB steam gasifiers in Austria and Germany [14]. The Güssing gasifier in Austria is a steam-blown DFB reactor operating at 8 MW of fuel [18]. There are several other gasifiers based on the same technology in Senden 15 MW_{th}, Villach 15 MW_{th}, Oberwart 8.5 MW_{th} [19]. These

DFB gasifiers have been equipped with gas cleaning by scrubbing with organic solvent [19]. In addition to CHP production, a biomass gasification plant in Gothenburg produces 20 MW of SNG [20]. There the gasification process is based on a similar steam-blown DFB concept as the Güssing plant. Gas cleaning for the synthesis is carried out by scrubbing the tars and converting the remaining light hydrocarbons in a reformer before the synthesis.

2.2 Tar compounds and light hydrocarbons in the gasification gas

Tar compounds are formed during gasification when biomass decomposes in pyrolysis and gasification reactions. Primary tar compounds are mostly oxygenated compounds that are decomposition products of biomass [8,21]. These compounds react further and form secondary and tertiary tar compounds [8], which consists of compounds that do not exist in the source biomass [22]. The secondary tar is described as alkylated one- and two-ring aromatic compounds including heterocyclic compounds [21], whereas tertiary tar consists of aromatic hydrocarbons such as benzene, naphthalene and various polycyclic aromatic hydrocarbons (PAH) [22]. In addition to describing tar compounds by their formation process [23], tar is typically classified based on the number of rings in the tar compound [8,24] or by boiling point distribution or physical properties [25]. In tar protocol [26], tar is defined as aromatic compounds that are heavier than benzene. Furthermore, an operational definition for tar depending on the end-use application has been used [22].

During the gasification process, radicals and small hydrocarbon molecules are formed from biomass pyrolysis vapours [27]. At high temperatures these light compounds react to form tar compounds in pyrolysis reactions, the majority of which takes place in the gas phase by free radical mechanisms [28]. A schematic figure of tar formation is presented in Figure 6. Shukla and Koshi [29,30] have explained aromatic growth by various radical reaction mechanisms such as hydrogen abstraction and acetylene addition (HACA), hydrogen abstraction and vinyl radical addition (HAVA), phenyl addition and cyclization (PAC) and methyl addition and cyclization (MAC). Via the radical chain reactions, the tertiary and secondary tar compounds can be formed at high temperature from light hydrocarbons, such as ethene, in the gasification gas.

The composition and amount of tar depends on the gasifier type and gasification temperature. Tar from the fluidized bed gasifier can be characterized as secondary and tertiary tar [8]. Increasing gasification temperature typically reduces the amount of tar but increases the share of heavier compounds. The effect of pressure on tar composition has been less studied and not in a systematic manner [21,31–34]. Based on these studies, no general trend of tar amount evolution with pressure increase can be deduced. However, it can be seen that with pressure increase the composition of tar shifts more towards heavier compounds.

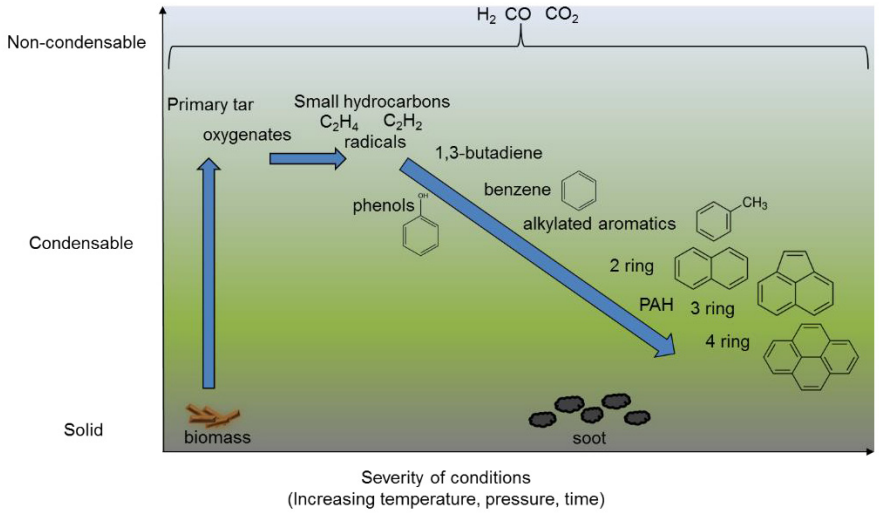

Figure 6. Scheme of tar formation and maturation during gasification process with exemplar compounds

In addition to tar and main gasification product gases (CO, CO_2, H_2), the main light hydrocarbon compounds are typically methane and ethene [15,35]. In steam gasification, the ethene content is typically higher, up to 4 vol-% in dry gas [35], than in air or steam-oxygen blown gasification, where it reaches 0.2-1.2 vol-% in dry gas [11,15]. Often the light hydrocarbons are not reported in detail in biomass gasification studies since they are not considered as problematic as tar compounds. However, they may contribute to further tar formation in the process.

2.3 Catalytically active gasifier bed materials

In fluidized bed gasifiers, catalytically active bed materials can be used to ease the cleaning of biomass gasification gas by reducing tar load. In addition to their catalytic tar decomposing effect, the bed materials affect the sintering properties of the bed. By selecting a proper bed material, higher temperatures or pressures may be used in the gasifier without problems.

The typical bed materials used in biomass gasification are low-cost natural minerals. Catalytically active materials, such as dolomite, olivine, magnesite and limestone, may be used alone or mixed with sand. Catalytically active bed materials are reviewed by, e.g., Abu El-Rub et al. [36], Sutton et al. [37], Dayton [38] and Shen & Yoshikawa [39].

Dolomites are the most widely studied non-metallic catalyst for biomass gasification gas cleaning [38]. The use of dolomites has been studied as bed materials as well as catalysts for a separate reformer after the gasifier. Dolomite is used at the

commercial scale in the Skive plant in Denmark, for example [40]. Dolomites are calcium magnesium ores ($CaCO_3 \cdot MgCO_3$), the exact composition of which depends on their geological origin [41,42]. Dolomites are effective in reducing heavier tar compounds, but less effective for benzene, naphthalene and methane decomposition [38]. Tuomi et al. [43] report the activity of dolomite compared to sand: with dolomite as a bed material the tar level was 5.7 g/Nm^3, whereas sand as a bed material lead to a tar concentration of 20 g/Nm^3 in steam gasification of wood at 800 °C. Dolomite has been reported to be especially effective for tar compounds formed in steam gasification compared to more refractory tar of air gasification gas [42].

For dolomite to be active it has to be calcined, as the carbonate form is not nearly as active as the oxide form [41]. The calcination temperature depends on the partial pressure of CO_2. If the partial pressure of CO_2 increases over the calcination/carbonation limit of dolomite, the calcium in dolomite forms carbonate. This limits the usage of dolomites to low pressures. A downside of dolomite is that in calcined form it is brittle and suffers from attrition in the fluidized bed [38]. In addition, at pressures higher than 4 bar, bed sintering and formation of agglomerates has been observed with dolomite[15].

Olivine has been studied as an alternative to dolomite. The key advantage of olivine over dolomite is its attrition resistance comparable to sand [44]. However, its activity is generally somewhat lower than that of dolomite [25,44–48]. Olivine is a silicate mineral that contains magnesium and iron $(Mg,Fe)_2SiO_4$. Olivine is used, for example, in steam gasification plants using woody biomass as feedstock at Güssing [49] and at Gothenburg [20].

Olivine is activated during the gasification of biomass by formation of a calcium-rich layer on top of the particles from biomass ash and possible bed additives, such as dolomite [50,51]. At the Gothenburg biomass gasification plant, olivine is activated by addition of K_2CO_3 to the gasifier [20]. The addition of K_2CO_3 reduced tar amounts from 43.1 g/Nm^3 to 13.1 g/Nm^3. Marinkovic et al. [52] have investigated how olivine activates during gasification. They followed tar concentrations over three days without replacing the bed material and tar levels were reduced 30% from the levels of the first day. They did not observe migration of iron to the surface of the particles. They explained the activity of olivine as being due to the potassium in the biomass remaining in its active form and catalysing the gasification reactions, whereas sand binds potassium leading to low tar decomposition activity. In addition, Devi et al. [53,54] have reported that calcination may improve the catalytic activity of olivine.

Magnesium oxide has also been tested as a bed material. Kurkela et al. [15] reported in pressurized steam-oxygen gasification of woody biomass that tar levels were almost similar with magnesium oxide as with dolomite. They also observed that magnesium oxide could be used as bed material even at 6 bar pressure without the bed sintering problems encountered with dolomite.

2.4 Tar reformer

2.4.1 Catalysts and reactions

For synthesis purposes, secondary cleaning measures are required to convert tar compounds and light hydrocarbons to synthesis gas. In the gasifier itself, tar levels lower than 2-4 g/Nm^3 are difficult to achieve due to insufficient contact between the gas and bed material [55]. Reforming is widely studied and shown to be an efficient technology for gas cleaning. In addition to reforming, tar compounds can be decomposed to syngas by thermal cracking. However, thermal cracking suffers from soot formation and efficiency penalty since the temperature needs to be >1100 °C [39, 58], which is higher than typical gasifier outlet temperatures. This high temperature can be achieved by partial oxidation of the gas. Reforming of tar, instead, takes place approximately at the gasifier outlet temperatures.

Steam reforming of hydrocarbons is a well-established industrial process for natural gas and naphtha feeds. Reforming of biomass gasification gas, however, has some special features compared to natural gas or naphtha reforming. The hydrocarbons that need to be reformed from biomass gasification gas are aromatic tar compounds and light olefins, such as ethene, which are more prone to carbon formation than typical steam reformer feedstocks. Another special feature is that the gas contains sulfur compounds. Sulfur is mostly in the form of H_2S (around 100 ppm) and a few ppm of COS. Kaufman-Rechulski et al. [57] have reported small amounts of organic sulfur compounds, such as thiophene, methyl-thiophenes and benzo[b]thiophene, in air gasification of wood at 730-740 °C with a total concentration of organic sulfur compounds of 3.2-8.5 mg S/Nm^3. Sulfur compounds complicate reforming by poisoning the catalyst. However, study by Hepola [58] shows that catalyst activity can be retained by using reforming temperatures above 900 °C.

Steam reforming reactions for benzene are presented in reactions (1) and (2). Since the gasification gas contains CO_2, the dry reforming reaction (3) may take place as well. In addition to reforming reactions, the water-gas shift (WGS) reaction (4) takes place simultaneously with reforming reactions, affecting the product distribution [59]. Also, due to high temperatures, hydrocarbons may crack thermally (5). Since steam reforming reactions are strongly endothermic, heat is required to process the gas. The reformer may be an indirectly heated steam reformer or an autothermal reformer where the heat for reforming is obtained by partial oxidation (6) by adding air or oxygen to the gasification gas.

$$C_6H_6 + 6H_2O \rightarrow 6CO + 9H_2 \quad (1)$$

$$C_6H_6 + 12H_2O \rightarrow 6CO_2 + 15H_2 \quad (2)$$

$$C_6H_6 + 6CO_2 \rightarrow 12CO + 3H_2 \quad (3)$$

$$CO + H_2O \leftrightarrow CO_2 + H_2 \quad (4)$$

$$C_6H_6 \rightarrow wC_xH_y + (3 - wy/2)H_2 \quad (5)$$

$$C_6H_6 + 3O_2 \rightarrow 6CO + 3H_2 \quad (6)$$

Several types of catalysts have been studied for reforming hydrocarbons in biomass gasification gas and these are reviewed in [38,39,56,60,61]. Typical catalysts are nickel and precious metal catalysts. Nickel catalysts have been traditionally used in industrial steam reforming of natural gas. Steam reforming nickel catalysts are active in tar and methane conversion and, in addition, have WGS activity and are effective in ammonia conversion [38]. Their disadvantage is that they are prone to coke formation. Precious metals are less prone to this, but their price is high. Kurkela et al. [17] reported in biomass gasification gas reforming that at pressurized conditions carbon formation was more of a problem with a nickel catalyst than with precious metals. In addition to better carbon gasification with precious metals compared to nickel, they are reported to be more resistant to sulfur poisoning. Rönkönen et al. [62] reported that the Rh/ZrO_2 catalyst was more resistant to sulfur poisoning than the Ni/ZrO_2 catalyst in tar reforming. In addition, Rhyner et al. [63] observed that precious metal catalysts are highly active in converting organic sulfur compounds.

2.4.2 Demonstration plants with a reformer

Catalytic gas cleaning developed by VTT has been demonstrated at the Skive, Kokemäki and Varkaus plants. In Skive and Kokemäki, the gas was unfiltered and monoliths were used, whereas in Varkaus the gas was filtered before reforming. Filtering the gas before reforming allows the use of fixed bed of catalyst particles instead of monoliths, which makes the catalyst packing more simple [14]. Most of the demonstration results and details of reformers are confidential information and are not published.

At Kokemäki, a tar reformer was connected to a fixed bed updraft type Novel gasifier with a plant capacity range of 1-4 MW [64]. The reformer at Kokemäki was operated in catalytic partial oxidation mode, whereas the reformer at Skive operates in steam reforming mode [65]. Kurkela et al. [64] reported that the reformer of Kokemäki gasifier consisted of zirconia and nickel monoliths operated at a temperature range of 700-900 °C. Several catalysts were tested in slip stream and the optimized version was tested for 750 h showing stable activity. Heavy tar conversion of 75% and naphthalene conversion of 50% were achieved allowing use of the gas in a gas engine.

VTT has patented [55,66–68] a staged reformer which consists of three stages. The reactor concept is presented in Figure 7. In the first stage, heavy tar compounds are partially oxidized by a zirconia catalyst. The zirconia pre-reformer part is followed by a precious metal catalyst, which is used to further reduce the amount of tar and light intermediates, such as ethene and butadiene, in the gas. The last nickel stage is for final conversion of tar and methane. Zirconia and precious metal catalysts are needed to protect the nickel catalyst from carbon formation. The reformer is operated autothermally by feeding O_2 to different stages. The use of ZrO_2 catalyst allows lower operational temperatures, and the temperature of the reformer is gradually increased from around 600 °C in the ZrO_2 stage to 950 °C at the outlet.

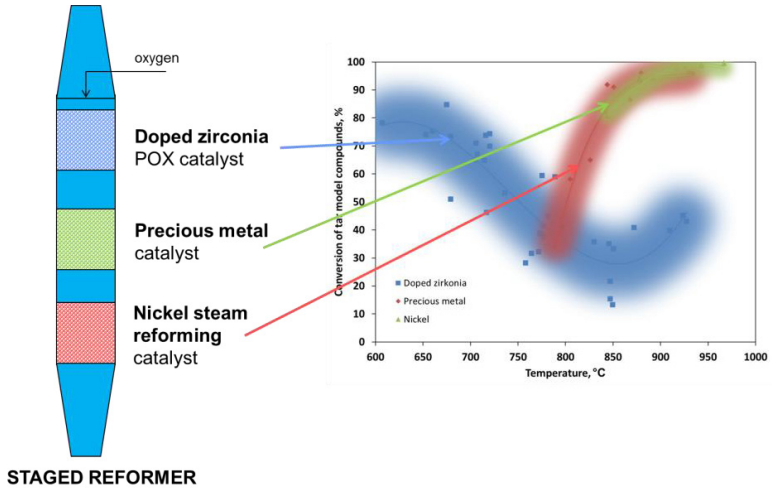

Figure 7. Staged reformer concept developed by VTT.

The staged reformer concept with zirconia catalyst as a pre-reformer stage has been demonstrated to be technically feasible in connection with oxygen blown gasifier. Kurkela et al. [14] reported a 215 h gasification experiment at 2 bar pressure where the staged reformer was used connected to an oxygen blown gasifier and a hot gas filter. In the experiment, the pre-reformer consisted of a ZrO_2 and a precious metal catalyst in monolith form, whereas the nickel catalyst in the final stage of the reformer was in particulate form. The oxygen was fed in the pre-reformer and O_2/steam mixture to the nickel bed to achieve the target operation temperatures. In the pre-reformer, the temperature was increased from the filtration temperature of 550 °C to 800-850 °C. No signs of coke formation during the experiment were observed. In the reformer, complete C_2 conversion was obtained. Tar conversion was 98-99% and benzene conversion 93-99%, whereas methane conversion was 55-80%. The highest conversions were obtained with crushed wood pellets due to lower sulfur content of the feedstock compared to bark or forest residues.

2.4.3 Carbon formation on the catalyst

Catalyst deactivation by carbon formation on the catalysts is one of the main problems in tar reforming. To be economically feasible, the catalyst lifetime in the reformer should be at least 1-2 years (Publication V), which means that coke formation should be completely avoided.

Carbon may form on the catalyst by many routes. Rostrup-Nielsen [69] has classified the formation of carbon on the catalyst based on operation conditions. At low

temperatures, encapsulating gum may be formed by polymerization reactions of adsorbed hydrocarbons. At intermediate temperatures on nickel catalysts, carbon may form whiskers which mechanically destroy the catalyst. With precious metals, whisker carbon formation is avoided since they do not dissolve carbon [70]. Pyrolytic carbon and soot are formed at high temperatures and are therefore the most relevant for biomass gasification gas cleaning conditions due to high temperatures in the reformer.

Pyrolytic carbon is formed from hydrocarbons by thermal cracking reactions [71]. Firstly, the unsaturated molecules and hydrocarbon radicals are formed at high temperature. Secondly, they polymerize and dehydrogenate forming larger, tar-like compounds that deposit on the reactor walls and catalyst surfaces covering and encapsulating the particles and filling the voids. Thirdly, the deposited compounds dehydrogenate further to form solid coke leading to blockage of the reactor. The low activity of the catalyst may lead to takeover of thermal cracking reactions leading to soot formation [70].

Process parameters, such as temperature, pressure, steam-to-carbon or oxygen-to-carbon ratio and the nature of hydrocarbons affect the carbon formation on the catalyst. The O/C and H_2O/C ratios of the inlet gas are typically used to describe the conditions in which the steam reformer can be operated in coke-free conditions. The minimum H_2O/C ratio is based on experimental knowledge, not on any fundamental or theoretical calculations although a principle of equilibrated gas can be applied for methane steam reforming [69]. A safe H_2O/C ratio depends on the catalyst type: nickel or precious metal, as well as on the nature of the hydrocarbons in the feed. Unsaturated hydrocarbons form carbon more easily than saturated ones [72]. For example, compared to n-paraffins, benzene and ethene showed much higher coking rates [73]. Consequently, the hydrocarbons in biomass gasification gas form carbon more easily than natural gas.

2.4.4 Kinetics of tar reforming

Kinetic studies of steam reforming of biomass gasification gas are carried out either by using a side-stream of real gasifiers or with model gas mixtures in the laboratory. In studies using real biomass gasification gas, the tar compounds have been typically combined in one or several lumps. The data obtainable for modelling from side stream studies with real gasifiers is more limited in the sense that the gas composition cannot be varied as freely as with model gases. On the other hand, many studies conducted with model gases and tar model compounds do not include, for example, H_2S in the gas feed, even though it is present in biomass gasification gas at levels of 40-120 ppm (Publication V) and is a known catalyst poison. The models used in kinetic studies of tar reforming are often first order kinetic models towards tar or tar model compounds. The kinetics of steam reforming of tar compounds has been reviewed by Font Palma [74].

Steam reforming is a fast, strongly endothermic surface reaction, which is easily limited by mass and heat transfer. Thus, for kinetic studies, the conditions have to

be chosen carefully. In typical industrial natural gas (or naphtha) steam reformers, the effectiveness factor for the catalyst particles is very low [71]. Gas film diffusion limits the reaction rate severely with industrial-scale catalyst particles [75].

Jess [76] has studied benzene and naphthalene steam reforming with a nickel catalyst in gas atmospheres consisting of H_2, H_2O and N_2. For benzene, the first-order kinetics was assumed, but with naphthalene the reaction order was modelled to be 0.2 and for H_2 and H_2O the orders were 0.3 and 0, respectively. The activation energy for naphthalene reforming was 332 kJ/mol, whereas for benzene it was 196 kJ/mol. Swierczynski et al. [77] studied toluene reforming on a Ni/olivine catalyst in H_2O and argon atmosphere. They used first-order kinetics for modelling. Corella et al. [78] used a lump model for the kinetics of tar reforming for tar from the air gasifier. Their model consists of six tar compound lumps for which they have established a reaction network in which each of the reactions is represented by the first-order kinetics.

A power law model for naphthalene reforming without H_2S in the feed was used by Devi et al. [79]. The reaction order for naphthalene in their study was 2.04, which is quite far from the reaction order obtained by Jess [76], which was 0.2. The gas composition used by Devi et al. included H_2, H_2O, CO and CO_2, whereas the gas composition used by Jess consisted only of H_2 and H_2O.

Simell et al.[80,81] have used a Langmuir-Hinshelwood type model for steam and dry reforming of benzene on a dolomite catalyst. They found that hydrogen inhibits the reforming reaction rate. In contrast, Depner and Jess [75] studied kinetics of methane, benzene and naphthalene reforming on Ni/MgO catalyst and, in their model, steam or hydrogen had no influence on the reforming rate. Their gas contained H_2, H_2O and H_2S but no CO or CO_2 in the feed.

Rhyner et al. [82] have studied kinetics on precious metal catalyst in the presence of sulfur compounds. For methane steam reforming and for WGS reaction, they used a Langmuir-Hinshelwood type kinetic model with a sulfur adsorption term in denominator. For tar, ethene and sulfur containing hydrocarbons they used first-order power law kinetics.

3. Experimental

3.1 Test apparatus

The experimental work in this study was based on a laboratory-scale fixed bed reactor. The general layout of the system is presented in Figure 8. The gases were fed from the gas cylinders by mass flow controllers. The ion exchanged water and tar model compounds were fed by the HPLC pumps. Water was fed through a vaporizer to the heated line with the gases, whereas tar was fed straight to the heated gas line. The experiments were conducted in a quartz reactor placed in a three-zone furnace; in the pressurized experiments the quartz reactor was placed in a pressure vessel made of steel. The products were analysed by an online gas chromatograph (GC/FID and/or GC/TCD), FTIR and gas analyser.

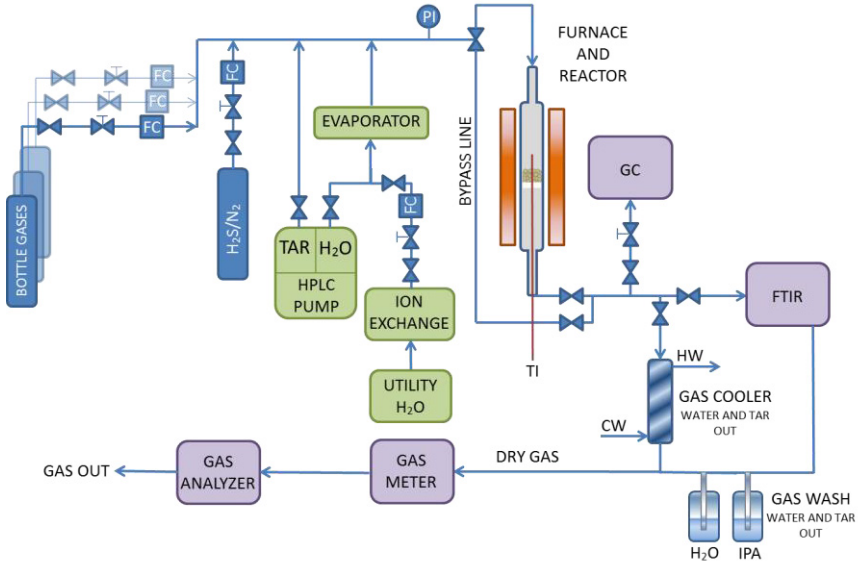

Figure 8. General layout of the experimental set-up

For studies of thermal reactions of ethene (Publication I), an empty quartz reactor tube was used with an inner diameter of 10 or 15 mm depending on the conditions. The reactor was equipped with a thermocouple pocket of 4 mm. The temperature profile of the reactor was measured under N_2 flow. During the experiments, the thermocouple was placed at the maximum point of this profile. The measured temperature was used in the calculation of the residence time. The flow was adjusted to maintain a constant residence time when changing the temperatures and pressures. Typically, each experimental condition was kept for 2-3 h. For the analysis of H_2 a gas analyser was used, whereas hydrocarbons were analysed by online GC/FID. In

addition to the online analysis, gas bags and liquid tar samples were taken at certain experimental conditions.

In the bed material tests (Publication II), the gas flow was adjusted to keep the residence time at 0.1 s when the pressure was varied. To keep the residence time constant, two different quartz reactors were used with inner diameters of 16 mm and 27 mm. The temperature was measured from the centre of the catalyst bed. Each experimental condition was maintained for around 2 h. The dolomite was calcined at 900 °C in experiments where conditions were such that the dolomite was in oxide form. The experiments with dolomite in carbonate form were done separately from the experiments in which dolomite was in oxide form.

In catalyst testing experiments (Publication V) and in long-term experiments (Publication III), a gas flow of 2 dm^3/min was used. The quartz reactor had an inner diameter of 27 mm and was equipped with a 4 mm thermocouple pocket. Temperature was measured below the catalyst bed. The catalyst was reduced in-situ by exposure to model gasification gas. In the catalyst testing experiments (Publication V), the duration of each experimental condition was around 1.5-2 h.

In the steam reforming kinetics study (Publication IV), a reactor with an inner diameter of 10 mm with a 4 mm thermocouple pocket was used. The gas flow used in the experiments was 1 dm^3/min. The catalyst was reduced in-situ with a H_2:N_2 1:1 mixture for 1 h. The first experimental condition was run for at least 4 h to stabilize the catalyst activity. Further conditions were run for 1-2 h. Every fifth experimental condition was a reference condition where the catalyst activity was checked.

3.2 Composition of the feed gases

In the studies of thermal reactions of ethene (Publication I), the gas consisted of 5 vol-% of ethene in nitrogen. The gas compositions used in the catalyst activity testing (Publication V) and in long-term experiments (Publication III) are presented in Table 1. The gas compositions corresponded to different kinds of biomass gasification gases. The low hydrocarbon content gas (LH) corresponded to steam gasification gas with dolomite as the bed material. The medium hydrocarbon content gas represented steam gasification gas with sand as the bed material, which was also close to the composition of steam-oxygen blown gasification gas. The tar model compound mixture contained 10 wt-% benzene, 80 wt-% toluene and 10 wt-% naphthalene. The gas composition (Air gaga, Table 1) used for testing the activity of the bed materials was based on the atmospheric air gasification of crushed bark pellets in BFB with sand as bed material.

The gas mixtures used for benzene steam reforming kinetic studies contained, depending on the conditions, CO, CO_2, H_2, N_2, H_2S and H_2O in addition to benzene. In the kinetic experiments, pure benzene was used instead of a tar model compound mixture. An H_2S level of 100 ppm was chosen based on the typical concentration of H_2S in biomass gasification gas.

Table 1. Dry gas compositions used in long-term reforming experiments (LH is low hydrocarbon content gas and MH is medium hydrocarbon content gas) (Publication III), the composition of air gasification gas (Air gaga) used in activity testing of bed materials (Publication II), and the gasification gases (Gasification gas 1 and 2) used in kinetic experiments (Publication IV).

	LH	MH	MH+O_2	Air gaga	Gasification gas 1	Gasification gas 2
CO, vol-%	19.2	25.0	25.0	15.0	12.5	25.0
CO_2, vol-%	22.7	20.0	20.0	15.0	15.0	20.0
H_2, vol-%	50.6	35.0	35.0	20.0	11.0	35.0
CH_4, vol-%	6.3	10.0	10.0	3.4	0.0	0.0
O_2, vol-%	0.0	0.0	3.4	0.0	0.0	0.0
N_2, vol-%	0.0	7.8	4.4	45.4	61.5	20.0
C_2H_4, vol-%	1.0	2.0	2.0	1.0	0.0	0.0
NH_3, vol-%	0.2	0.2	0.2	0.2	0.0	0.0
H_2S, ppm	100	100	100	100	100	100
Tar, g/Nm^3	10	20	20	10	14	14
H_2O, vol-%	30.0	40.0	40.0	12.0	10	10

3.3 Catalyst materials

The catalytic activity of gasification bed materials (Publication II) was investigated with dolomite (Myanit D, Sweden), MgO (M85, Slovakia), olivine and silica sand (Maxit hiekkatuote). The silica sand was considered an inert reference material. The properties of the bed materials are shown in Table 2. The particle size of the bed materials was 0.25-0.56 mm in the laboratory experiments, whereas a smaller fraction of 0.10-0.25 mm was used in the gasification experiments.

Table 2. Properties of the tested bed materials.

Bed material	Sand	Dolomite (Myanit D)	MgO (M85)	Olivine A	Olivine B/kaolin mixture
BET surface area[a], m^2/g	3.1	5.2[b]	16.2	3.5	4.9
Element, wt-% (XRF)					
Na	2.1	-	-	-	0.02
Mg	0.56	12	50	29	24
Al	6.7	0.44	0.14	0.52	2
Si	35	2.3	0.42	19	18
P	0.07	-	0.02	-	-
S	-	-	0.05		0.01
Cl	0.01	-	0.06		0.01
K	2.8	0.08	0.02	0.04	0.06
Ca	2.2	21	4.1	0.08	2.1
Ti	0.14	0.01	0.01	-	0.08
V	-	-	-	-	-
Cr	-	-	-	0.19	0.3
Mn	0.03	0.07	0.40	0.09	0.11
Fe	1.8	0.4	6.0	6.4	7.2
Co	-	-	-	0.02	0.02
Ni	-	-	-	0.44	0.49
Cu	0.01	-	-		-
Zn	-	-	-		-
Rb	0.01	-	-	-	-
Sr	0.04	-	-	-	-
Zr	0.01	-	-	-	-
Ba	0.09	-	-	-	-

[a] Determined from unused bed material samples

[b] Determined from the carbonate form ($CaCO_3 \cdot MgCO_3$)

"-" = below detection limit (< 0.01 wt-%)

The precious metal and nickel catalysts used for reforming in the catalyst activity testing (Publication V) and in long-term experiments (Publication III) were commercial catalysts. The catalysts used in the experiments are listed in Table 3. Catalyst particles of around 2-3 mm were applied in the long-term experiments and catalyst

activity testing. In the kinetic experiments (Publication IV), nickel catalyst powder of 0.2-0.3 mm particle size was used to avoid mass transfer limitations. The nickel catalyst in the kinetic studies contained 14.7 wt-% of NiO on α-Al_2O_3 support. In the kinetic experiments, the nickel catalyst was diluted with SiC to 1:1 volume ratio to obtain more isothermal behaviour in the catalyst bed.

Table 3. Catalysts used in experiments

Catalyst	Shape	Particle size, mm
Nickel	cylinder	3x3
Nickel in kinetic studies	irregular particles	0.20-0.30
PM1	sphere	2.5
PM2	cylinder	3x3
PM3	cylinder	3x3
PM5	sphere	2.6
PM6	sphere	1.9

4. Results and discussion

4.1 Tar formation from ethene

High temperatures in the gasification process may induce thermal reactions of hydrocarbons leading to heavier tar compounds and pyrolytic carbon formation. Biomass gasification gas typically contains C_2 hydrocarbons especially ethene and acetylene, which can react at high temperatures to form tar and soot. Typical ethene concentration at the gasifier outlet is 0.2-4% depending on the gasification conditions [15,35,43]. The tar compounds formed from ethene may cause problems in reforming of gasification gas. High temperature spots causing tar formation may form in autothermal reforming near to where oxygen is fed. Thus, ethene may form tar and soot and plug the front face of the catalyst or cause coke formation in the catalyst bed. Operation pressure has a strong effect on tar formation from light hydrocarbons, which is an essential question when considering pressurizing the gasification and gas cleaning process.

The effect of process conditions on tar formation from ethene was studied with an empty quartz reactor (Publication I). In the experiments, 5 vol-% of ethene was used in nitrogen atmosphere. First, the temperature region of 787-978 °C was screened at atmospheric pressure with a 0.3 s residence time. As can be seen from Figure 9, the formation of tar and benzene increased steeply with temperature, likewise the ethene conversion. A reaction temperature of around 950 °C was chosen for further experiments in which pressure and residence time effects were investigated.

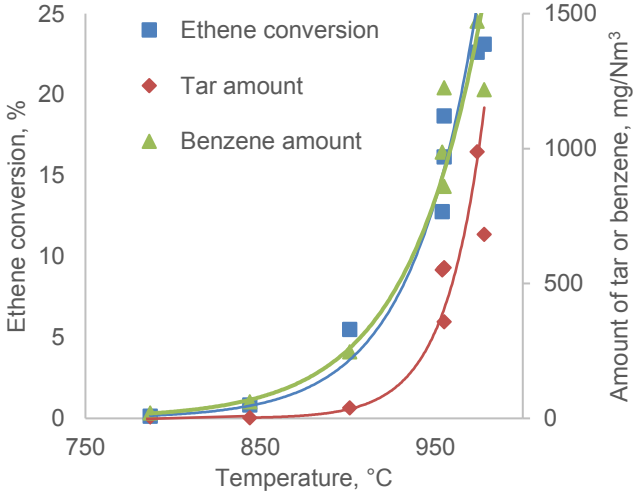

Figure 9. Conversion of ethene and amount of tar formed from ethene as a function of temperature.

The main compounds formed in thermal reactions of ethene were hydrogen, methane, acetylene and 1,3-butadiene. The most abundant aromatic compound formed was benzene. The pressure increase from 1 to 3.5 bar increased the ethene conversion and the selectivity to tar, Figure 10. With increasing pressure, the composition of products shifted more towards heavier compounds. The same change in composition with increasing pressure has been observed in biomass gasification [21,31,32]. When the pressure was further increased to 6 bar with a longer residence time of 2 s, the amount of tar was not increased considerably, likely due to soot formation. Although the amount of soot was not measured, the large error in the carbon balance indicates that soot formation was likely.

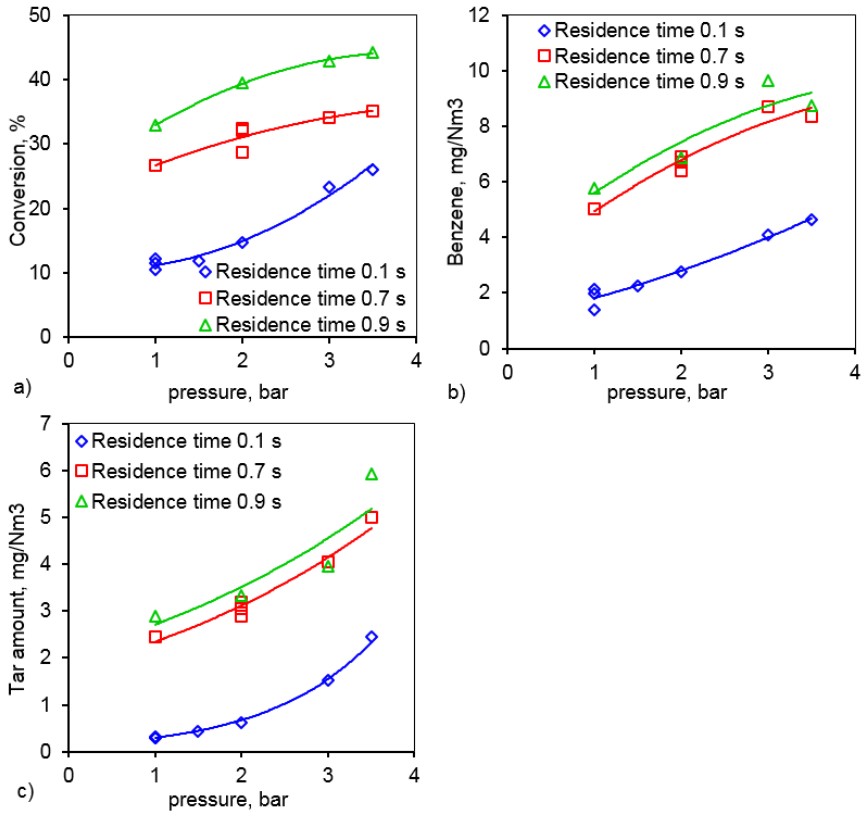

Figure 10. a) Conversion of ethene, b) amount of benzene formed and c) tar amount at 954 °C.

The observed effect of pressure on tar formation and the change in composition towards heavy tar compounds with increasing pressure indicates that when designing pressurized gasification gas cleaning, the thermal reactions of light hydrocarbons should be taken into account. However, their effect in biomass gasification

gas, which contains hydrogen and steam, is not likely to be as pronounced as they affect the radical chain reactions by terminating them.

Since the thermal reactions of ethene produce similar compounds to those formed during biomass gasification, ethene could be used to produce a mixture of tar for gas cleaning studies at the laboratory or bench scale. In Table 4, typical tar compositions of fluidized bed gasification processes are compared with the tar composition from thermal reactions of ethene. The tar composition from the thermal reactions of ethene resembles the tar formed in high temperature gasification, which mainly contains more stable aromatic compounds instead of oxygenated compounds. Tuomi et al. [83] have used ethene pyrolysis combined with natural gas partial oxidation to produce model tar and biomass gasification gas for bench-scale filtration studies.

Table 4. Tar product distribution in different types of gasification experiments and selected results of thermal reaction of ethene for comparison.

	CFB air	CFB O_2/H_2O	BFB H_2O	BFB H_2O	BFB air	BFB air	C_2H_4	C_2H_4	C_2H_4
Ref	[84]	[14]	[43]	[43]	Publication II	Publication II	Publication I	Publication I	Publication I
Raw material	sawdust	forest wood residue	wood	wood	bark	bark	C_2H_4	C_2H_4	C_2H_4
Bed material	sand	sand/ dolomite	sand	dolomite	sand	dolomite	-	-	-
P, bar	5	2	1	1	1	1	1	3	6
T, °C	940	930	800	800	850	850	954	956	954
residence time, s	4	3	6	6	7	7	0.9	0.9	2
benzene, g/Nm^3	7.1	13.6	11.8	7.4	7.1	3.4	2.8	6.2	8.9
Total tar, g/Nm^3	4.3	5.7	20.5[b]	4.7[b]	3.7	0.5	2.1	3.9	6.9
1-ring[a], %	6	6	20	32	20	34	42	39	19
2-ring, %	49	64	29	38	57	61	45	47	54
3-ring, %	29	22	14	14	14	0	8	8	12
4-ring, %	14	6	2	2	2	0	5	6	15
Heterocyclic, %	2	2	11	7	4	2	0	0	0
Tot, %	100	100	76	91	100	100	100	100	100

[a] Benzene is not included in 1-ring compounds

[b] Unidentified tar compounds included in total amount of tar

4.2 Catalytic activity of gasification bed materials in tar reduction

Tar concentration can be reduced already in the gasifier by catalytically active bed materials, which makes the operation of the reformer easier. The catalytic activity of the different bed materials was studied in Publication II. The activity of the bed materials was first compared in atmospheric air gasification of bark in a BFB gasifier. Figure 11 shows the amount and composition of tar from biomass gasification experiments. Dolomite and MgO were clearly the most active, with olivine/kaolin mixture being less active but still giving tar amounts of around half of that produced with silica sand as the bed material. In addition to reducing the amount of tar, the catalytically active bed materials changed the tar composition to lighter compounds compared to silica sand. With dolomite as the bed material, the tar contained no three- or four-ring compounds and with MgO three-ring compounds were present only in trace amounts.

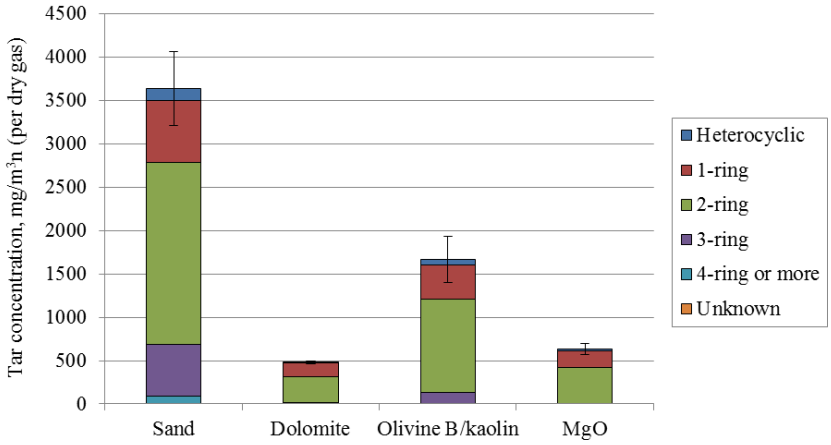

Figure 11. Tar concentration (in dry gas) in fluidized-bed experiments. Error bars represent the standard deviations of total tar concentrations.

The catalytic activity of the bed materials in pressurized conditions was tested in a fixed bed reactor with a model gasification gas composition (air gaga, Table 1). The aim in the laboratory experiments was to compare the tar reforming activity of the bed materials. The easily controllable laboratory conditions were more suitable for this purpose than experiments in a fluidized-bed gasifier. The model gas composition resembled the gas composition in the air gasification of bark pellets with silica sand as the bed material. The dolomite, MgO and silica sand were the same materials as used in the biomass gasification experiments, whereas pure olivine A instead of olivine B/kaolin mixture was used in the laboratory experiments.

The total hydrocarbon conversion was calculated to clarify the effect of the bed material. As can be seen from Figure 12, MgO was the most active of the tested bed materials, followed closely by dolomite. Conversely, olivine A behaved almost like inert silica sand. However, when the pressure was increased from atmospheric to 10 bar, all bed materials were equally inactive and the total hydrocarbon conversion was only around 5% at 850 °C as well as at 900 °C.

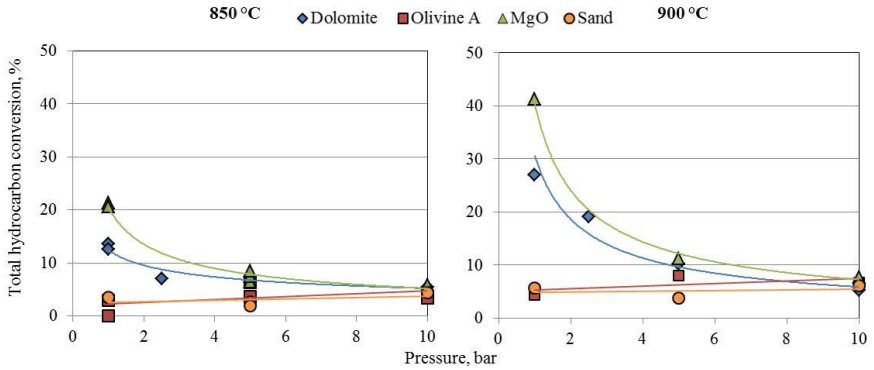

Figure 12. Total conversion of hydrocarbon based on carbon moles at 850 °C (left) and 900 °C (right).

According to the literature [50,51], olivine is activated by formation of a calcium-rich layer during biomass gasification due to contact with ash. In our experiments, fresh olivine was used, which might explain the observed low activity of the olivine. Our atmospheric gasification experiments were only 6-7 hours long, whereas, Marinkovic et al. [52] have observed the activation of olivine during gasifier operation to take place over three days. By conducting longer experiments or by using already activated olivine, the catalytic activity, at least in atmospheric pressure, might be higher than observed in these experiments. Other parameters possibly affecting the inactivity of olivine may be the origin of the olivine, possible thermal treatment, and also the lack of kaolin in the laboratory experiments.

When the pressure was increased, calcium in the dolomite changed from oxide to carbonate form. Figure 13 presents the oxidation/carbonation curve for $CaO/CaCO_3$. Magnesium in the dolomite was present as MgO [41] in all experimental conditions. In the laboratory studies, however, the decrease in catalytic activity in tar decomposition with increasing pressure was not only due to carbonation of dolomite. At 900 °C, the dolomite was in carbonate form only at 10 bar pressure; however, the conversion of hydrocarbons dropped most when the pressure was increased from 1 to 5 bar, as can be seen from Figure 12. The same behaviour was observed with MgO.

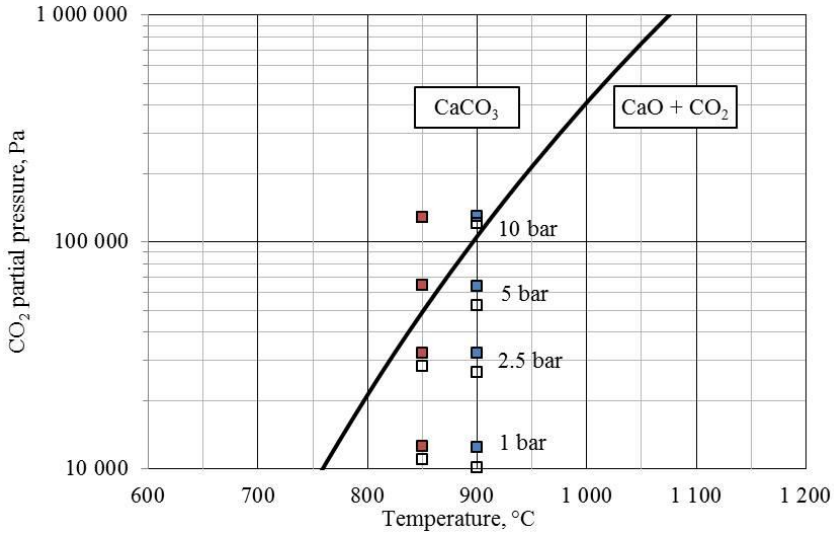

Figure 13. Equilibrium decomposition curve of $CaCO_3$ in relation to the partial pressures of CO_2 in dolomite test conditions. Filled symbols represent CO_2 partial pressures measured at the catalyst bed inlet and open symbols those measured at the catalyst bed outlet.

The effect of the calcination state of dolomite was also studied at 5 bar pressure at 850 °C by changing the CO_2 partial pressure so that calcium was at oxide form at 5 bar pressure (Table 5). Interestingly, the tar conversion was similar for both cases. Thus, in the conditions of the study, the decrease in the catalytic activity of dolomite with pressure was not due to the change of oxide to carbonate, which is in contrast with earlier results by Simell et al. [41]. A possible explanation for the contradicting results is a more realistic gas composition in this study, including ethene, which may contribute to tar formation. It should also be noted that the pressure level of this study was 1-10 bar, whereas Simell et al. studied tar conversion at a constant pressure of 20 bar by varying the CO_2 partial pressure.

Table 5. Benzene and tar conversions in tests with dolomite (5 bar and 850 °C) where the CO_2 content in the feed gas was varied.

Form of calcium	**oxide**	**carbonate**
CO_2 partial pressure, kPa	25.7	75.0
Toluene, %	92	99
Naphthalene, %	13	13
Total tars (excl. benzene), %	81	88
Total C conversion, %	3	7

As in the study of thermal reactions of ethene (Publication I), the conversion of ethene increased with pressure in the bed material experiments with model gasification gas (Figure 14). Ethene might be converted by steam reforming reaction to syngas or it might have reacted to form tar compounds. The formation of tar compounds other than in the feed (benzene, toluene, naphthalene) increased with pressure. The formation of these compounds might be due to thermal reactions of ethene or polymerization of tar compounds.

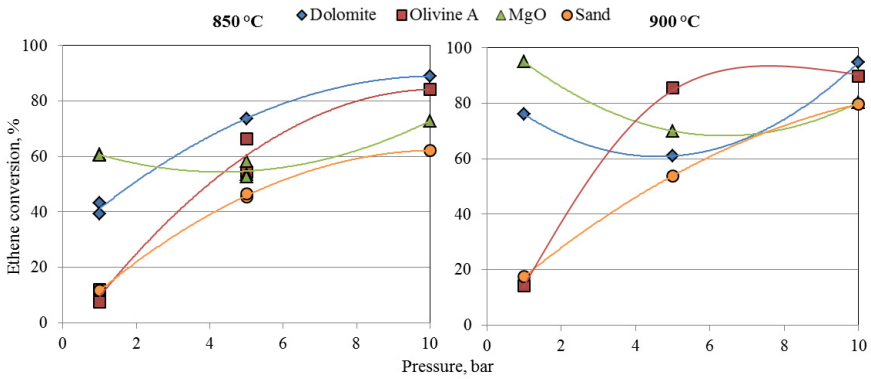

Figure 14. Conversion of ethene with different bed materials as a function of pressure.

4.3 Steam reforming versus autothermal reforming in biomass gasification gas cleaning

Steam and autothermal reforming can be applied in biomass gasification gas cleaning to convert tar and light hydrocarbons to syngas. In autothermal reforming, oxygen is used to partially oxidize the hydrocarbons and to produce heat for the reforming reactions. In contrast, the steam reformer needs to be heated indirectly, for example, by burning the flue gases of the process. Autothermal reforming also brings more oxygen to the gas, reducing the coke formation potential of the gas. On the other hand, if steam reforming of biomass gasification gas is technically feasible, the investment costs of the reformer could be reduced by omitting the air separation unit.

The activity of the nickel and three different precious metal catalysts was tested in steam and autothermal reforming modes (Publication V). Moreover, long-term stability was tested for both reforming modes (Publication III). The process concepts in which the reforming modes relate are presented in Figure 5. For steam-oxygen blown gasification, where the target product is FT-liquids, the high methane conversion is an asset. Based on techno-economical evaluation (Publication V), if methane

conversion is increased, for example, from 55% to 95%, the production costs of FT-liquids can be reduced by 5%. In the steam-blown gasification concept, the reforming mode was found to have only a limited impact on the amount of the main product, which was considered to be H_2 or SNG. However, because investment in the oxygen plant increases the production costs, the steam reforming concept could be an attractive choice for the steam gasification case. In the steam gasification concept, the reforming temperature can be lower than in the oxygen-blown gasifier case since low methane conversion is desired.

The activity comparison of the catalysts was based on the same geometrical catalyst surface area in the catalyst bed. For all the catalysts and for both steam and autothermal reforming experiments, the geometrical surface area was 125 cm^2. The gas compositions (MH and MH+O_2) used in the catalyst activity testing are presented in Table 1. Tar conversion was higher with the precious metal than the nickel catalyst, which is especially clear when comparing naphthalene conversions, Figure 15. Furthermore, ethene conversion was higher with the precious metal catalyst than with the nickel catalyst. The precious metal catalysts differed with regard to methane conversion; one of the precious metal catalysts (PM5) was clearly more active than the other precious metal catalysts, showing similar activity to a nickel catalyst. The precious metal catalyst that was highly active in methane conversion would be beneficial for the FT synthesis concept, whereas the other catalysts would be more suitable for SNG or H_2 production by steam gasification.

In addition to the catalyst choice, methane conversion can be affected by operating conditions; higher reforming temperatures favour higher methane conversion. High tar conversions, especially with precious metal catalysts, could be obtained already at around 850 °C, whereas for high methane conversions temperatures above 900 °C were required to achieve higher than 90% conversion. Lower methane conversion compared to tar or ethene conversion can be explained by the high stability of methane. It is also possible that the H_2S in the gasification gas deactivates the active sites for methane reforming more than the tar reforming site.

The addition of oxygen to the feed did not improve the methane reforming activity with the precious metal catalysts. However, tar conversion was slightly higher with oxygen addition, which could be seen especially in naphthalene conversion (Figure 15d). These activity experiments were only 1-3 h long per experimental condition, which was too short to observe possible deactivation of the catalyst. However, in an actual gasification process oxygen can be used to increase the reforming temperature and in that way increase the methane conversion.

To discover the long-term stability of the catalyst in different reforming conditions (Publication III), several precious metal and nickel catalysts were tested in extended experiments reaching around 500 h time on-stream. Steam and autothermal reforming modes were tested with medium hydrocarbon content gas (Table 1, MH and MH+O_2) representing oxygen-blown gasification gas. In steam reforming conditions, lower hydrocarbon content gas was also tested (Table 1, LH).

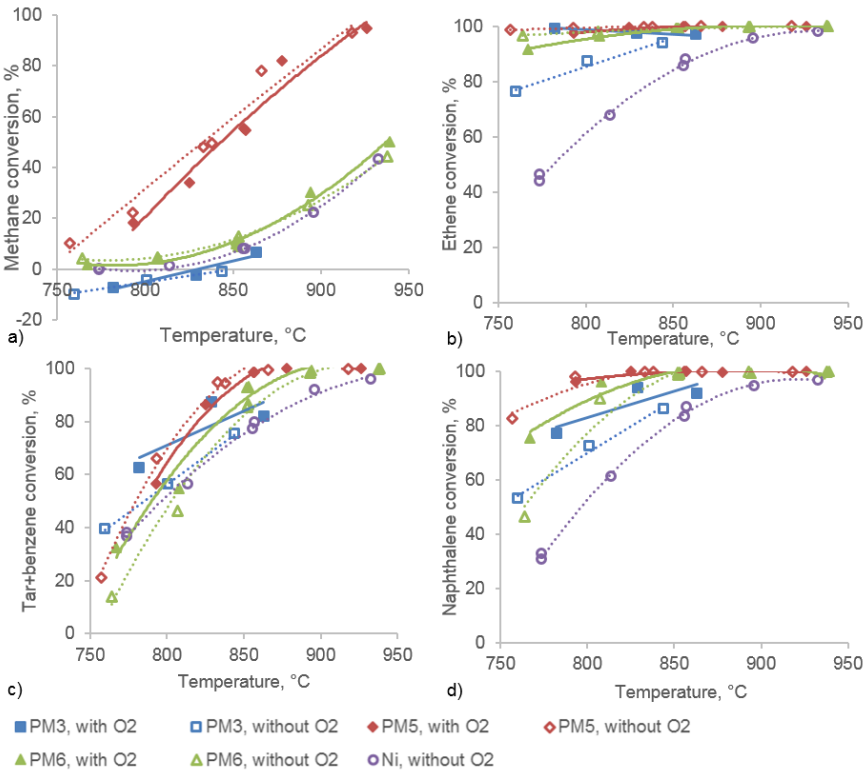

Figure 15. a) Methane, b) ethene, c) tar and benzene, and d) naphthalene conversion. Filled symbols with oxygen, empty symbols without oxygen.

The conversions of the hydrocarbons are presented in Figure 16. The levels of the conversions varied between the experiments, which was mostly due to different space velocities and geometrical surface areas. In addition, it should be noted that the oven temperature in the experiments with oxygen was 950 °C and without oxygen 900 °C. With the nickel catalyst, the initial tar conversion including benzene was high for all gas compositions. However, with precious metal catalysts the tar conversions were clearly higher for PM1 and PM2 catalysts with MH+O_2 gas than for PM3 catalyst with MH and LH gases. The higher activity of PM1 and PM2 is likely due to better catalyst formulation in addition to higher temperature. With oxygen addition, the temperature was higher and thus the conversions were also higher than with other gas compositions.

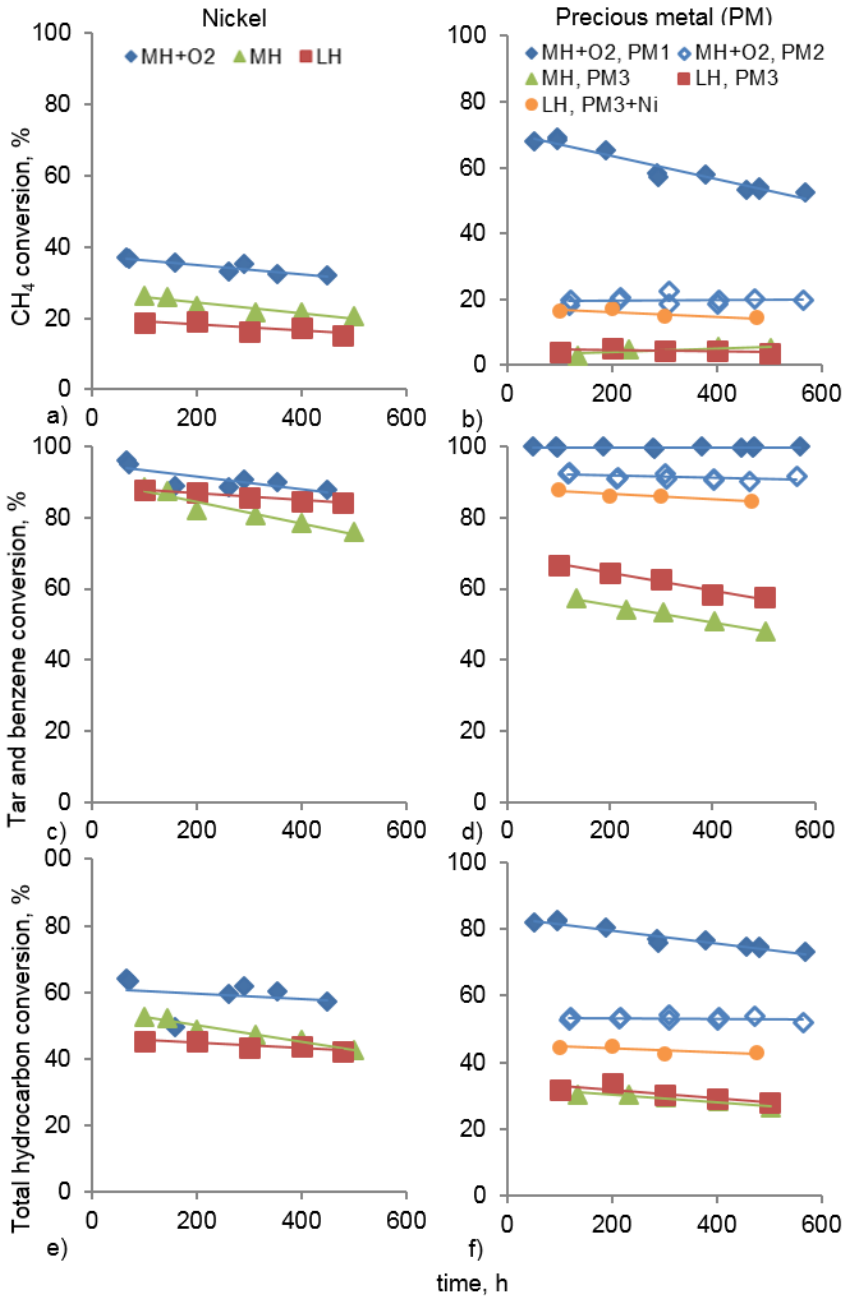

Figure 16. Methane conversion on a) nickel and b) precious metal catalyst, tar and benzene conversion on c) nickel and d) precious metal catalyst, and total carbon mol based hydrocarbon conversion on e) nickel and f) precious metal catalyst.

The rate of deactivation was calculated for total hydrocarbon conversion based on the number of carbon moles in hydrocarbons, Table 6. The deactivation rate was calculated after about 100 h onwards from start-up. As can be seen from Figure 16, the decrease in conversion was nearly constant over the time of the experiment. Figure 17 illustrates the starting phase of the experiment with the nickel catalyst. Deactivation was faster in the initial phase of the experiment, but then levelled-off to a nearly constant value, which is typical behaviour in catalyst deactivation [85]. Rostrup-Nielsen et al. [85] explain the exponential decrease in reaction rate at the beginning of the operation to be due to sintering. Sulfur poisoning of the catalyst reaches steady state in less than one hour [58].

Table 6. Activity decrease in total hydrocarbon conversion based on carbon moles in percentage units per 100 h after the initial activity decrease.

Catalyst	Gas	m_{cat} g	GHSV h^{-1}	Geometric surface area mm^2	Run time h	T at catalyst outlet °C	T oven °C	Decrease in total hydrocarbon conversion, %-units/100 h
Ni	MH+O_2	15.5	8800	11330	450	916	950	-0.8
Ni	MH	22.8	5400	16670	500	851	900	-2.5
Ni	LH	22.8	5400	16670	478	850	900	-0.8
PM1	MH+O_2	5.2	12000	12150	570	888	950	-2.0
PM2	MH+O_2	9.6	12000	8150	564	916	950	-0.1
PM3	MH	12.4	10200	15950	503	860	900	-1.0
PM3	LH	13.4	8600	11380	501	862	900	-1.2
PM3+Ni	LH	7.6+ 15.0	5400	6480+ 10940	477	868	900	-0.5

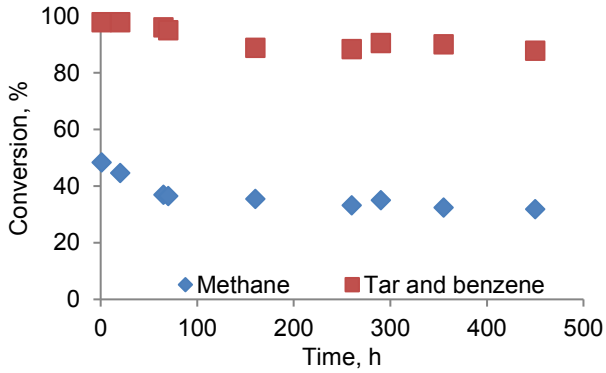

Figure 17. Methane and tar and benzene conversion with nickel catalyst with MH+O_2 gas.

With the nickel catalyst, the deactivation rate was highest for the MH gas without oxygen, whereas reducing the hydrocarbon content or adding oxygen to the feed resulted in the same deactivation rate in total hydrocarbon conversion (Table 6). With the PM1 catalyst, the percentage reduction in total hydrocarbon conversion with the MH+O_2 was high due to decrease in methane conversion, whereas tar conversion remained almost 100% throughout the experiment. The decrease in methane conversion was constant during the experiment without levelling off. Despite the relatively high deactivation rate, methane conversion was clearly higher than in other experiments. For the PM2 catalyst with MH+O_2 gas, conversion levels were lower but almost stable with only a 0.1 %-unit reduction per 100 h for total hydrocarbon conversion. With the PM3 catalyst, the total hydrocarbon conversion decrease was around the same for the MH and the LH, but slightly higher than for the nickel catalyst with LH gas. A combination of a precious metal and the nickel catalysts was also tested, and a low deactivation rate was obtained.

With the gasification gas experiments, the H_2O/C and O/C ratios were more descriptive and corresponded with the observed tendency to carbon formation if the carbon atoms only in the hydrocarbons were accounted for in the ratios. The MH gas contained two times the amount of ethene and tar model compound mixture compared to LH gas. The higher hydrocarbon content can be seen in the H_2O/C_{HC} and in O/C_{HC} ratios presented in Table 7. If CO and CO_2 were included, there was almost no difference at all in O/C ratio between the gas compositions, whereas a difference was observed in the experiments in carbon formation and catalyst deactivation.

With the MH+O_2 gas, the precious metal and nickel catalyst exhibited different carbon formation behaviour. After the experiment, the surface of the precious metal catalyst was clean of carbon (Figure 18a), which was not the case with the nickel catalyst (Figure 18b). The carbon formed on the nickel catalyst was characteristically pyrolytic carbon; the carbon had filled the voids of the top of the catalyst bed and encapsulated the catalyst particles. However, carbon did not form to an extent

that would have blocked the reactor or increased the pressure drop during the 450 h run time. Even though the precious metal catalyst seemed to be clean of carbon, the activity slightly decayed. To determine the cause of deactivation of the precious metal catalyst, detailed surface analysis of the catalyst would be needed to reveal possible sintering or other changes in catalyst structure.

Table 7. H_2O/C and O/C ratios for the tested gases, HC refers that only the hydrocarbons were calculated in the ratio.

Test gases	H_2O/C_{HC}	O/C_{HC}	H_2O/C	O/C
MH	3.8	7.6	1.07	2.1
MH+O_2	3.8	8.0	1.07	2.2
LH	4.3	10.7	0.83	2.1

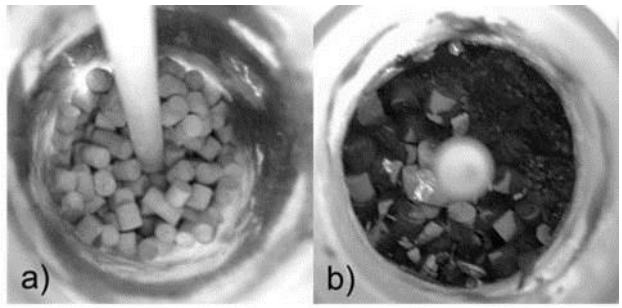

Figure 18. Top of the catalyst bed after experiment with MH+O_2 gas with a) PM2 catalyst, 564 h, and b) nickel catalyst, 450 h.

In industrial operation, the superficial gas velocities are typically higher than in the laboratory scale. In the industrial steam reformers the gas velocities in the tubes are in the range of 1.5 m/s [71], whereas in laboratory experiments the velocity was only 0.2 m/s. This might affect the radical formation in the reactor tube before the catalyst bed. The longer the residence time in the hot zone, the more time there is for radical formation [71], for example, from ethene, as was studied in Publication I. In addition, sulfur poisoning of the catalyst increases the risk of pyrolytic carbon formation from unconverted hydrocarbons [86].

4.4 Reactor modelling

The reactor model used for benzene steam reforming kinetics (Publication IV) was a pseudo-homogeneous plug flow model. Isothermal behaviour of the catalyst bed

was assumed based on the measured axial temperature gradient. The radial temperature gradient was assumed to be negligible due to the narrow reactor tube. Steam reforming is a fast surface reaction and the experiments easily suffer from mass transfer limitations. The mass transfer limitations were evaluated by calculating the criteria for inter- and intra-particle resistances. The Weisz-Prater criterion was used for intra-particle limitations and Mears' criterion for inter-particle limitations. Based on the calculated criteria, it was concluded that the mass transfer did not limit the reaction rate (Publication IV).

The parameter estimation was performed with MATLAB using the Nelder-Mead simplex and Levenberg-Marquardt algorithms to minimize the residual sum of squares of molar flow of benzene. The model equation (7) was an ordinary differential equation that was solved by the ODE15s.

$$\frac{dn_i}{dz} = -r_i * m_{cat} \tag{7}$$

Arrhenius (8) and Van't Hoff (9) equations were used in the temperature centralized forms to minimize the correlation between the parameters and to enhance the convergence of the model. The initial values for parameters for estimation routines were obtained by linearization of the Arrhenius equation.

$$k' = k_{ref} * \exp\left(-\frac{E_a}{R} * \left(\frac{1}{T} - \frac{1}{T_{ref}}\right)\right) \tag{8}$$

$$K_i = K_{ref} * \exp\left(-\frac{\Delta H_i}{R} * \left(\frac{1}{T} - \frac{1}{T_{ref}}\right)\right) \tag{9}$$

4.5 Kinetics of benzene reforming

The required degree of reforming varies depending on the end-use of the biomass gasification gas. For energy production, all condensable tar compounds should be removed. For synthesis purposes, however, the goal is to reform all hydrocarbons to syngas, except for methane synthesis where the conservation of methane in the gas is desirable. For cases where only tar compounds are to be reformed, benzene reforming kinetics could be used as the design basis. When tar compounds are measured after reformer, most of them are benzene [14]. The thermal stability of benzene is also higher than that of toluene or naphthalene [87]. The qualitative effect of the main gasification gas compounds on steam reforming of benzene was studied with a nickel catalyst in the presence of H_2S in Publication IV.

The stoichiometry of the steam reforming of benzene was investigated for modelling purposes. All products were measured at 900 °C for two different gas compositions, one with a gas mixture containing benzene and steam and the other containing H_2 in addition to the afore-mentioned compounds. The elemental balances were calculated for the stoichiometric ratios presented in Table 8. The ratios indicate that the main reaction was steam reforming with CO and H_2 as products (1). Without H_2 in the gas mixture, a small amount of CO_2 was also formed by reforming reaction (2) or by WGS (4). With a nickel catalyst, the product distribution obtained in this

study is typical [79, 78] whereas with a dolomite catalyst a quite different product distribution was obtained [80].

Table 8. Measured stoichiometry in steam reforming without and with hydrogen at 900 °C (mol formed/mol of benzene reacted) compared to the stoichiometry of the steam reforming reaction (1). Bz refers to benzene.

	Bz+H_2O	**Bz+H_2O+ +H_2**	**Steam reforming reaction (1)**
Benzene conversion, %	65	62	
CO/Bz	4.8	5.7	6
CO_2/Bz	0.7	0.0	0
H_2/Bz	9.7	10.8	9
H_2O/Bz	6.1	5.7	6
H_2/CO	2.0	1.9	1.5

The reforming of benzene at high temperatures may lead to thermal reactions as well. The thermal reactions were investigated by experiments with SiC instead of a nickel catalyst. However, the conversion of benzene on SiC was 3.7% at 900 °C and was considered negligible. With SiC, around 15 ppm of tar compounds calculated as benzene were formed, whereas with the nickel catalyst no hydrocarbon products were detected, indicating the activity of nickel in reforming possible intermediates formed by thermal cracking.

The reaction order was defined by fitting the results to a power law model (10). In addition to benzene and H_2O, the feed gas in all experiments contained 100 ppm of H_2S and N_2 for balance. The reaction order for benzene was close to one, which is the value typically used in literature [76–78]. For H_2O, the reaction order was close to zero, which is also typical for steam reforming at high temperature [73, 82, 90].

$$-r_{Bz} = k' c_{Bz}^{\alpha} c_{H_2O}^{\beta} \quad (10)$$

The effect of the main gasification gas compounds, i.e. H_2, CO and CO_2, on the steam reforming rate of benzene was studied qualitatively by investigating the effect of each compound on the benzene steam reforming rate. The rate expression was a first-order equation with respect to benzene and was fitted separately to the data sets of different gas mixtures. The clearest effect was caused by H_2 and CO_2, as can be seen from the estimates of reaction rate constant at the reference temperature and activation energy presented in Table 9. Hydrogen decreased the reaction rate, whereas CO_2 increased it. The first-order kinetics for the dry reforming reaction indicate that it is clearly slower than the steam reforming reaction. Thus, the increased reaction rate observed with the Bz+H_2O+CO_2 gas mixture could be due to a dual effect of H_2O and CO_2. Co-adsorption of CO_2 and H_2O on the catalyst surface may have some beneficial effect by bringing more oxygen to the surface, since in both reaction mechanisms the surface species O* and HO* react with adsorbed hydrocarbons [89,90]. The increased rate with CO_2 could not be explained by parallel steam and dry reforming reactions.

Table 9. Parameter estimates for first-order kinetics calculated by linearization for different gas compositions

	k_{ref} $m^3/(kg_{cat}*h)$	95% confidence limit	E_a kJ/mol	95% confidence limit	Correlation	RSS
Bz+H_2O	133	±7	230	±13	-0.65	$2.28*10^{-6}$
Bz+CO_2	34	±19	295	±36	-0.89	$1.79*10^{-7}$
Bz+H_2O +H_2	59	±24	378	±100	-0.939	$3.18*10^{-6}$
Bz+H_2O +CO	173	±58	206	±98	-0.58	$1.94*10^{-6}$
Bz+H_2O +CO_2	247	±12	169	±15	-0.204	$2.96*10^{-8}$
Gasification gas 1	103	±32	307	±73	-0.907	$4.83*10^{-6}$
Gasification gas 2	212	±46	272	±79	-0.348	$4.07*10^{-7}$

In addition to the effect of single compounds, two types of model gasification gases (Table 1) were also tested. Interestingly, the steam/O_2 gasification gas (Gasification gas 2) resulted in a higher reforming rate than the Bz+H_2O mixture and higher than the air gasification type of gas (Gasification gas 1). The benzene reforming rate with the air gasification type of gas was between Bz+H_2O and Bz+H_2O+H_2.

Compared to a study by Swierczynski et al. [77] without H_2S in the feed, the reaction rates were lower in this study. Interestingly, it was noticed in this study that the benzene steam reforming rate with different gas compositions were around the same at 900 °C. Only the dry reforming rate was still clearly lower than the steam reforming rate. Thus, the differences in benzene steam reforming rates with different gas composition could only be observed at lower temperatures. This is likely due to H_2S poisoning of the catalyst. According to Hepola [58], at temperatures above 900 °C, catalyst poisoning by H_2S can be avoided. However, if the surface coverage for sulfur is calculated according to equation (11) from Rostrup-Nielsen and Christiansen [71], at 900 °C with gas containing 10% of H_2 the surface coverage is 1 and at lower temperatures >1. The catalyst with the surface fully covered by sulfur should be completely deactivated, which was not the case in our experiments. This might be due to inaccuracy of the equation (11) close to full coverage, or due to sulfur being preferentially adsorbed on edges and corners leaving some facet sites free for reforming reaction to take place. Additionally, it is possible that sulfur was adsorbed in multi-layer or sub-surface form [91]. Although the gasification gas also contains compounds other than hydrogen, according to Rostrup-Nielsen and Christiansen [71], steam and carbon does not compete with sulfur adsorption.

$$\theta_S = 1.45 - 9.53 * 10^{-5} * T * \ln\left(\frac{p_{H_2S}}{p_{H_2}}\right) \quad (11)$$

Based on the first-order kinetics with different gas compositions, three Langmuir-Hinshelwood models were fitted with Bz+H_2O and Bz+H_2O+H_2 gas compositions. The models and the parameter estimates are presented in Table 10. The models

differed in the adsorption term. Model A was taken from the study of Simell et al. In model B, benzene adsorption was assumed to take place on a single site and hydrogen adsorption to be dissociative. Compared to model B, model C assumed dual site benzene adsorption. The models were tested for gasification gases; all of the tested models represented the air gasification gas reasonably well, whereas the O_2/H_2O gasification gas was not well described solely by retarding effect of H_2 in the denominator, likely due to higher product concentrations in the gas and the rate enhancing effect of CO_2. The estimated adsorption enthalpy was clearly higher than reported in the literature [59,92], which may be due to high correlation of the parameter or to H_2S poisoning of the catalyst.

Table 10. Parameter estimates with 95% confidence intervals, the RSS for models fitted with data sets Bz+H_2O and Bz+H_2O+H_2 and the RSS for simulation with gasification gases.

Model	**A**	**B**	**C**
Model equation	$\frac{k' * c_{bz}}{1 + K_{H_2} c_{H_2}}$	$\frac{k' * c_{bz}}{1 + \sqrt{K_{H_2} * c_{H_2}}}$	$\frac{k' * c_{bz}}{\left(1 + \sqrt{K_{H_2} * c_{H_2}}\right)^2}$
k_{ref}	142.5±15.95	172.5± 43.18	165.9±31.06
E_a	226±29.72	212.2±63.49	217±49.01
$K_{ref}(H_2)$	0.896±0.5023	1.343±1.832	0.2023±0.1996
ΔH_{H2}	-336.6±178.5	-455.2±370.8	-415.5±287.8
RSS	$6.1437*10^{-6}$	$6.6255*10^{-6}$	$6.5151*10^{-6}$
RSS for gasification gas 1	$1.6000*10^{-5}$	$1.6187*10^{-5}$	$1.6366*10^{-5}$
RSS for gasification gas 2	$4.8322*10^{-5}$	$3.7844*10^{-5}$	$4.0395*10^{-5}$

5. Conclusions

The main objective of this thesis was to study and develop the reforming technology for biomass gasification gas for synthesis use. A key parameter with respect to reformer operation is the tar load at the outlet of the gasifier. Catalytically active gasifier bed materials can be used to lower the tar content in the gas to protect the catalysts in the reformer from excessive tar load. Typical bed materials used in fluidized bed gasification are silica sand, dolomite, olivine and MgO. Dolomite and MgO were found to be highly active bed materials in tar decomposition at atmospheric pressure. Olivine/kaolin mixture was less active resulting about half of the amount of tar compared to silica sand in atmospheric gasification experiments. In contrast, pure olivine was inherently as inactive as silica sand. Compared to silica sand, the catalytically active bed materials also shifted the composition of tar towards lighter tar compounds.

Interestingly, the catalytic activity of dolomite and MgO dropped when the pressure was increased. At only 5 bar pressure, activity was almost completely lost dropping almost to the level of activity of silica sand and olivine, and at 10 bar, the total hydrocarbon conversion was the same for all bed materials. Dolomite has been reported to be highly active only in oxide form. When the CO_2 partial pressure increases, the calcium in dolomite changes to carbonate. However, the decrease in activity of dolomite could not be explained by the carbonation.

The gasification gas contains light hydrocarbons such as ethene, in addition to tar compounds. Ethene reacts at high temperatures forming more tar compounds. High temperature zones in the gasifier or reformer, for example in the oxygen inlet areas, may lead to tar formation by radical chain reactions from ethene. The conversion of ethene as well as the selectivity towards tar compounds increased with increasing pressure from 1 to 3 bar. With increasing pressure, the tar composition shifted towards heavier tar compounds. The tar formed by thermal reactions of ethene resembles high temperature gasification tar. Therefore, ethene can be used in gas cleaning studies to produce a tar mixture resembling real tar.

Combined together, the decreasing activity of bed materials and increasing amount of tar formed from ethene with increasing pressure make steam reforming in pressurized conditions challenging. An acceptably low inlet tar content for a steam reforming reactor seems difficult to achieve. Both studies were performed with model gas compositions. Further experiments in a real biomass gasifier are required to confirm the trends observed in this study.

The level of methane conversion can be affected in addition to temperature by catalyst choice. The desired level of methane conversion depends on the process concept and the end product. For FT synthesis, high methane conversion leads to lower production costs, thus a highly active catalyst for methane reforming combined with high reforming temperatures achieved by autothermal reforming would be a suitable combination. Conversely, for SNG or H_2 production by steam gasifi-

cation, low methane conversion is desired. Thus, an indirectly heated steam reformer and a catalyst with high activity towards tar but lower methane reforming activity would be a suitable combination.

Methane conversion activity of several precious metal catalysts and a nickel catalyst was compared. Significant differences between the catalysts were observed. One of the precious metal catalysts proved highly active in methane conversion, whereas the activity of the other tested precious metal catalysts was at the same level as the nickel catalyst. With precious metal catalysts, the steam and autothermal reforming modes were tested. The reforming mode did not affect methane conversion but did affect naphthalene conversion: oxygen addition slightly increased the conversion compared to results without oxygen, especially at temperatures around 800 °C. In a real gasification process, however, oxygen can be used to increase the reformer temperature leading to higher methane conversion.

A pressurized oxygen-blown gasification process with hot gas filtration and an autothermally operated staged reformer has been demonstrated to work for FT-liquids production. However, steam gasification followed by hot gas filtration and reformer has been less studied. The steam gasification concept is more suitable for a smaller scale of around 100 MW and low-pressure synthesis products, such as SNG, or H_2. For this concept, steam reforming instead of autothermal reforming would be beneficial due to lower investment costs as the oxygen plant would not be required.

The technical feasibility of steam reforming of biomass gasification tar compared to autothermal reforming was studied in extended experiments of around 500 h. The deactivation rate was found to be lower in autothermal mode than in steam reforming mode. With a nickel catalyst, lowering the hydrocarbon content of the gasification gas before the reformer allows operation in steam reforming mode with the same deactivation rate as with the higher hydrocarbon content gas in autothermal mode. With a precious metal catalyst, the decrease in total hydrocarbon conversion was approximately the same irrespective of the hydrocarbon content in the gas in steam reforming mode.

Based on the long-term reforming catalyst stability studies, the concentration of hydrocarbons in the gas needs to be low enough to avoid carbon formation and subsequent catalyst deactivation and plugging of the reactor. An H_2O/C_{HC} ratio above 4 and O/C_{HC} ratio above 8 are recommended for gasification gas reforming. Low enough tar content could also enable steam reforming of gasification gas without oxygen addition.

For SNG or H_2 production by steam gasification where preserving methane in the gas is desired, the kinetics of benzene reforming could be used as the basis of design of the reformer. The gas composition affects the kinetics of benzene steam reforming; high CO_2 concentration had a beneficial effect, whereas H_2 had a rate decreasing effect. Interestingly, it was also found that the steam reforming rate of benzene was roughly the same at 900 °C and the effect of gas compounds could be seen only at lower temperatures, where H_2S poisoning of the nickel catalyst is more severe. Further research is required to present the qualitative observations as a kinetic model encompassing the gasification gas compositions from air to steam

gasification gases and describing, in particular, the effect of CO_2. However, benzene reforming can modelled with a simple first-order power law kinetic model if the parameters are fitted for a certain gasification gas composition.

References

[1] Climate Change 2014, Synthesis Report, Summary for Policymakers. 2014. https://www.ipcc.ch/pdf/assessment-report/ar5/syr/AR5_SYR_FINAL_SPM.pdfm (accessed December 28, 2016)

[2] World Energy Outlook 2016. Paris: 2016. doi:http://dx.doi.org/10.1787/weo-2016-en.

[3] Forests and Agriculture n.d. https://ec.europa.eu/clima/policies/forests/index_en.htm (accessed November 19, 2016).

[4] Searle S, Malins C. Availability of cellulosic residues and wastes in the EU. Washington: 2013.

[5] Hannula I. Synthetic fuels and light olefins from biomass residues, carbon dioxide and electricity. Performance and cost analysis. Doctoral dissertation, Aalto University, 2015.

[6] McKeough P, Kurkela E. Process evaluations and design studies in the UCG project 2004-2007. VTT Research notes 2434. 2008.

[7] Kara M, Helynen S, Mattila L, Viinikainen S, Ohlström M, Lahnalammi M, editors. Energian käytön ja tuotannon teknologiset näkymät. Energ. Suomessa. 3rd ed., Helsinki: Edita Prima Oy; 2004, p. 244–5.

[8] Rabou LPLM, Zwart RWR, Vreugdenhil BJ, Bos L. Tar in Biomass Producer Gas, the Energy research Centre of The Netherlands (ECN) Experience: An Enduring Challenge. Energy & Fuels 2009;23:6189–98.

[9] Stefan Koppatz, Christoph Varga, Christoph Pfeifer MK. Report on long term test and comparison with existing gas cleaning. UNIQUE, Deliverable 4.2, 2010.

[10] Leppälahti J, Simell P, Kurkela E. Catalytic conversion of nitrogen compounds in gasification gas. Fuel Process Technol 1991;29:43–56.

[11] Kurkela E, Ståhlberg P, Laatikainen J. Pressurized fluidized-bed gasification experiments with wood, peat and coal at VTT in 1991-1992 Part 1. Test facilities and gasification experiments with sawdust, VTT publications 161. 1993.

[12] Hannula I, Kurkela E. Liquid transportation fuels via large-scale fluidised-bed gasification of lignocellulosic biomass. VTT Technology 91. Espoo:

VTT; 2013.

[13] Jokela V. NSE Biofuels Oy, Wood Based BTL Diesel Development 2007-2011. IEA Workshp, Piteå: 19.10.2011.

[14] Kurkela E, Kurkela M, Hiltunen I. Steam-oxygen gasification of forest residues and bark followed by hot gas filtration and catalytic reforming of tars: Results of an extended time test. Fuel Process Technol 2016;141:148–58.

[15] Kurkela E, Kurkela M, Hiltunen I. The effects of wood particle size and different process variables on the performance of steam-oxygen blown circulating fluidized-bed gasifier. Environ Prog Sustain Energy 2014;33:681–7.

[16] Hannula I. Reforming options for H_2 and SNG manufacture via steam gasification. Vetaani Final Seminar, Helsinki: 9.4.2014.

[17] Kurkela E, Simell P, McKeough P, Kurkela M. Synteesikaasun ja puhtaan polttokaasun valmistus, VTT publications 682. 2008.

[18] Pfeifer C, Hofbauer H. Development of catalytic tar decomposition downstream from a dual fluidized bed biomass steam gasifier. Powder Technol 2008;180:9–16.

[19] Kirnbauer F. State of the art biomass gasification for CHP production. Regatec, Barcelona: 8.5.2015.

[20] Hedenskog M. The GoBiGas-project. Regatec, Barcelona: 8.5.2015.

[21] Wolfesberger U, Aigner I, Hofbauer H. Tar Content and Composition in Producer Gas of Fluidized Bed Gasification of Wood - Influence of Temperature and Pressure. Environ Prog Sustain Energy 2009;28:372–9.

[22] Milne TA, Evans RJ, Abatzoglou N. Biomass Gasifier “Tars”: Their Nature, Formation, and Conversion, NREL/TP-570-25357. 1998.

[23] Evans RJ, Milne TA. Chemistry of Tar Formation and Maturation in the Thermochemical Conversion of Biomass. Dev. Thermochem. Biomass Convers., 1997, p. 803–16.

[24] Han J, Kim H. The reduction and control technology of tar during biomass gasification/pyrolysis: An overview. Renew Sustain Energy Rev 2008;12:397–416.

[25] Kiel JHA, van Paasen JPA, Neeft JPA, Devi L, Ptasinski KJ, Janssen FJJG, Meijer R, Berends RH, Temmink HMG, Brem G, Padban N, Bramer EA.

Primary measures to reduce tar formation in fluidised-bed biomass gasifiers. Final report SDE project P1999-012. ECN-C--04-014. 2004.

[26] Maniatis K, Beenackers AACM. Tar Protocols . IEA Bioenergy Gasification Task. Biomass and Bioenergy 2000;18:1–4.

[27] Jarvis MW, Haas TJ, Donohoe BS, Daily JW, Gaston KR, Frederick WJ, Nimlos MR. Elucidation of Biomass Pyrolysis Products Using a Laminar Entrained Flow Reactor and Char Particle Imaging. Energy & Fuels 2011;25:324–36.

[28] Trimm DL. Fundamental Aspects of the Formation and Gasification of Coke. In: Albright LF, Crynes BL, Corcoran WH, editors. Pyrolysis Theory Ind. Pract., New York: Academic Press; 1983, p. 203–32.

[29] Shukla B, Koshi M. A novel route for PAH growth in HACA based mechanisms. Combust Flame 2012;159:3589–96.

[30] Shukla B, Koshi M. Comparative study on the growth mechanisms of PAHs. Combust Flame 2011;158:369–75.

[31] Mayerhofer M, Mitsakis P, Meng X, de Jong W, Spliethoff H, Gaderer M. Influence of pressure, temperature and steam on tar and gas in allothermal fluidized bed gasification. Fuel 2012;99:204–9.

[32] Knight RA. Experience with raw gas analysis from pressurized gasification of biomass. Biomass and Bioenergy 2000;18:67–77.

[33] Brage C, Qizhuang Y, Sjöström K. Characterisation of tars from coal-biomass gasification. 3rd Int. Symp. Coal Combust., Beijing, China: 1995.

[34] Valin S, Ravel S, Guillaudeau J, Thiery S. Comprehensive study of the influence of total pressure on products yields in fluidized bed gasification of wood sawdust. Fuel Process Technol 2010;91:1222–8.

[35] Tuomi S, Kurkela E, Simell P, Kaisalo N. Gasification concept testing for dual fluidized-bed based SNG process. ICPS2013, Vienna, Austria: 2013.

[36] Abu El-Rub Z, Bramer E a., Brem G. Review of Catalysts for Tar Elimination in Biomass Gasification Processes. Ind Eng Chem Res 2004;43:6911–9. doi:10.1021/ie0498403.

[37] Sutton D, Kelleher B, Ross JRH. Review of literature on catalysts for biomass gasification. Fuel Process Technol 2001;73:155–73.

[38] Dayton D. A Review of the Literature on Catalytic Biomass Tar Destruction Milestone Completion Report, NREL/TP-510-32815. 2002.

[39] Shen Y, Yoshikawa K. Recent progresses in catalytic tar elimination during biomass gasification or pyrolysis—A review. Renew Sustain Energy Rev 2013;21:371–92.

[40] First-of-its-kind at Skive n.d. http://spectrum.andritz.com/index/iss_20/art_20_16.htm (accessed April 9, 2015).

[41] Simell PA, Leppälahti JK, Kurkela EK. Tar decomposing activity of carbonate rocks under high CO_2 partial pressure. Fuel 1995;74:938–45.

[42] Orìo A, Corella J, Narvàez I. Performance of Different Dolomites on Hot Raw Gas Cleaning from Biomass Gasification with Air. Ind Eng Chem Res 1997;36:3800–8.

[43] Tuomi S, Kurkela E, Simell P, Reinikainen M. Behaviour of tars on the filter in high temperature filtration of biomass-based gasification gas. Fuel 2015;139:220–31.

[44] Rapagnà S, Jand N, Kiennemann A, Foscolo PU. Steam-gasification of biomass in a fluidised-bed of olivine particles. Biomass and Bioenergy 2000;19:187–97.

[45] Devi L, Ptasinski KJ, Janssen FJJG, van Paasen SVB, Bergman PCA, Kiel JHA. Catalytic decomposition of biomass tars: use of dolomite and untreated olivine. Renew Energy 2005;30:565–87.

[46] Miccio F, Piriou B, Ruoppolo G, Chirone R. Biomass gasification in a catalytic fluidized reactor with beds of different materials. Chem Eng J 2009;154:369–74.

[47] Abu El-Rub Z, Bramer E a., Brem G. Experimental comparison of biomass chars with other catalysts for tar reduction. Fuel 2008;87:2243–52.

[48] Corella J, Toledo JM, Padilla R. Olivine or Dolomite as In-Bed Additive in Biomass Gasification with Air in a Fluidized Bed : Which Is Better ? 2004;2000:713–20.

[49] Hofbauer H, Rauch R, Bosch K, Koch R, Aichernig C. Biomass CHP Plant Güssing – A Success Story. Expert Meeting on Pyrolysis and Gasification of Biomass and Waste; October 2002, Strasbourg, France.

[50] Kirnbauer F, Wilk V, Kitzler H, Kern S, Hofbauer H. The positive effects of bed material coating on tar reduction in a dual fluidized bed gasifier. Fuel 2012;95:553–62.

[51] Kirnbauer F, Hofbauer H. Investigations on Bed Material Changes in a Dual

Fluidized Bed Steam Gasification Plant in Güssing , Austria. Energy&Fuels 2011;25:3793–8.

[52] Marinkovic J, Thunman H, Knutsson P, Seemann M. Characteristics of olivine as a bed material in an indirect biomass gasifier. Chem Eng J 2015;279:555–66.

[53] Devi L, Craje M, Thüne P, Ptasinski KJ, Janssen FJJG. Olivine as tar removal catalyst for biomass gasifiers: Catalyst characterization. Appl Catal A Gen 2005;294:68–79.

[54] Devi L, Ptasinski KJ, Janssen FJJG. Pretreated olivine as tar removal catalyst for biomass gasifiers: investigation using naphthalene as model biomass tar. Fuel Process Technol 2005;86:707–30.

[55] Kurkela E, Ståhlberg P, Simell P. Method and process for cleaning a product gas of a gasification reactor. EP 1165727 B1, 2005.

[56] Yung MM, Jablonski WS, Magrini-Bair K a. Review of Catalytic Conditioning of Biomass-Derived Syngas. Energy & Fuels 2009;23:1874–87.

[57] Kaufman Rechulski MD, Schildhauer TJ, Biollaz SMA, Ludwig C. Sulfur containing organic compounds in the raw producer gas of wood and grass gasification. Fuel 2014;128:330–9.

[58] Hepola J. Sulfur transformations in catalytic hot-gas cleaning of gasification gas. VTT Publications 425. Espoo: 2000.

[59] Xu J, Froment GF. Methane steam reforming, methanation and water-gas shift: I. Intrinsic kinetics. AIChE J 1989;35:88–96.

[60] Anis S, Zainal Z a. Tar reduction in biomass producer gas via mechanical, catalytic and thermal methods: A review. Renew Sustain Energy Rev 2011;15:2355–77.

[61] Xu C (Charles), Donald J, Byambajav E, Ohtsuka Y. Recent advances in catalysts for hot-gas removal of tar and NH_3 from biomass gasification. Fuel 2010;89:1784–95.

[62] Rönkkönen H, Simell P, Reinikainen M, Krause O, Niemelä MV. Catalytic clean-up of gasification gas with precious metal catalysts – A novel catalytic reformer development. Fuel 2010;89:3272–7.

[63] Rhyner U, Edinger P, Schildhauer TJ, Biollaz SM a. Experimental study on high temperature catalytic conversion of tars and organic sulfur compounds. Int J Hydrogen Energy 2014;39:4926–37.

[64] Kurkela E, Kurkela M. Advanced Biomass Gasification for High-Efficiency Power, Publishable Final activity Report of BiGPower Project. Espoo: 2009.

[65] Rhyner U. Reactive Hot Gas Filter for Biomass Gasification. Dissertation, ETH Zurich, 2013.

[66] Simell P, Kurkela E, Hiltunen I. Method of Reforming Gasification Gas. WO11107661A, 2011.

[67] Simell P, Kurkela E. Multiple stage method of reforming a gas containing tarry impurities employing a zirconium-based catalyst. WO2007/116121A1, 2007.

[68] Simell P, Kurkela E. Method for the purification of gasification gas. EP1404785 B1, 2007.

[69] Rostrup-Nielsen JR. Catalytic steam reforming. Berlin: Springer-Verlag; 1984.

[70] Rostrup-Nielsen JR, Christensen TS, Dybkjær I. Steam Reforming of Liquid Hydrocarbons. Stud Surface Sci Catal 1998;113:81–95.

[71] Rostrup-Nielsen JR, Christiansen LJ. Concepts in Syngas Manufacture. London: Imperial College Press; 2011.

[72] Rostrup-Nielsen JR. Steam reforming catalysts. Teknisk Forlag a/s; 1975.

[73] Rostrup-Nielsen JR. Coking of nickel catalysts for steam reforming of hydrocarbons. J Catal 1974;33:184–201.

[74] Font Palma C. Modelling of tar formation and evolution for biomass gasification: A review. Appl Energy 2013;111:129–41.

[75] Depner H, Jess A. Kinetics of nickel-catalyzed purification of tarry fuel gases from gasification and pyrolysis of solid fuels. Fuel 1999;78:1369–77.

[76] Jess A. Catalytic upgrading of tarry fuel gases: A kinetic study with model components. Chem Eng Process Process Intensif 1996;35:487–94.

[77] Swierczynski D, Courson C, Kiennemann A. Study of steam reforming of toluene used as model compound of tar produced by biomass gasification. Chem Eng Process Process Intensif 2008;47:508–13.

[78] Corella J, Caballero MA, Aznar M-P, Brage C. Two Advanced Models for the Kinetics of the Variation of the Tar Composition in Its Catalytic Elimination in Biomass Gasification. Ind Eng Chem Res 2003;42:3001–11.

[79] Devi L, Ptasinski KJ, Janssen FJJG. Decomposition of Naphthalene as a Biomass Tar over Pretreated Olivine: Effect of Gas Composition, Kinetic Approach, and Reaction Scheme. Ind Eng Chem Res 2005;44:9096–104.

[80] Simell PA, Hirvensalo EK, Smolander VT. Steam Reforming of Gasification Gas Tar over Dolomite with Benzene as a Model Compound. Ind Eng Chem Res 1999;38:1250–7.

[81] Simell PA, Hakala NAK, Haario HE, Krause AOI. Catalytic decomposition of gasification gas tar with benzene as the model compound. Ind Eng Chem Res 1997;36:42–51. doi:10.1016/S0140-6701(97)84319-6.

[82] Rhyner U, Edinger P, Schildhauer TJ, Biollaz SMA. Applied kinetics for modeling of reactive hot gas filters. Appl Energy 2014;113:766–80.

[83] Tuomi S, Kaisalo N, Koskinen-Soivi M-L, Simell P. Producing simulated tar-laden gasification gas by ethene pyrolysis. TCS2014, Sept. 2.-5., Denver, Colorado: 2014.

[84] Kurkela E. Formation and removal of biomass-derived contaminants in fluidized-bed gasification processes, VTT 287. 1996.

[85] Rostrup-Nielsen JR, Skov A, Christiansen LJ. Deactivation in pseudo-adiabatic reactors. Appl Catal 1986;22:71–83.

[86] Rostrup-Nielsen JR, Hojlund Nielsen PE. Catalyst Deactivation in Synthesis Gas Production, and Important Syntheses. In: Oudar J, Wise H, editors. Deactiv. Poisoning Catal., New York: Marcel Dekker Inc.; 1985.

[87] Jess A. Mechanisms and kinetics of thermal reactions of aromatic hydrocarbons from pyrolysis of solid fuels. Fuel 1996;75:1441–8.

[88] Świerczyński D, Libs S, Courson C, Kiennemann A. Steam reforming of tar from a biomass gasification process over Ni/olivine catalyst using toluene as a model compound. Appl Catal B Environ 2007;74:211–22.

[89] Mortensen PM, Dybkjær I. Industrial Scale Experience on Steam Reforming of CO_2-Rich Gas. Appl Catal A Gen 2015;495:141–51.

[90] Wei J, Iglesia E. Isotopic and kinetic assessment of the mechanism of reactions of CH_4 with CO_2 or H_2O to form synthesis gas and carbon on nickel catalysts. J Catal 2004;224:370–83.

[91] Hepola J, McCarty J, Krishnan G, Wong V. Elucidation of behavior of sulfur on nickel-based hot gas cleaning catalysts. Appl Catal B Environ 1999;20:191–203.

[92] Hou K, Hughes R. The kinetics of methane steam reforming over a Ni/α-Al_2O_3 catalyst. Chem Eng J 2001;82:311–28.

I

Kaisalo, N., Koskinen-Soivi M.-L., Simell P., Lehtonen J., (2015) Effect of process conditions on tar formation from thermal reactions of ethylene. *Fuel* ***153***, 118-127.

Fuel 153 (2015) 118–127

Contents lists available at ScienceDirect

Fuel

journal homepage: www.elsevier.com/locate/fuel

Effect of process conditions on tar formation from thermal reactions of ethylene

Noora K. Kaisalo [a,*], Mari-Leena Koskinen-Soivi [a], Pekka A. Simell [a], Juha Lehtonen [b]

[a] VTT Technical Research Centre of Finland, P.O. Box 1000, FI-02044 VTT, Finland
[b] Department of Biotechnology and Chemical Technology, Aalto University, P.O. Box 16100, FI-00076 Aalto, Finland

HIGHLIGHTS

- A mixture of tar compounds can be produced by thermal reactions of ethene.
- The amount of tar increases when pressure is increased from 1 to 3.5 bar.
- Also, the fraction of heavier tar compounds increased with pressure.
- Tar-laden product gas can be used in biomass gasification gas cleaning studies.

ARTICLE INFO

Article history:
Received 11 September 2014
Received in revised form 29 November 2014
Accepted 19 February 2015
Available online 9 March 2015

Keywords:
Biomass gasification
Tar
Gas chromatography
Ethylene

ABSTRACT

Thermal reactions of ethylene were studied to understand better the effect of process conditions on tar formation in biomass gasification. The effects of pressure, residence time and temperature on thermal reactions of ethylene were studied. The analysis of products from methane up to pyrene was performed by the novel online GC method. Ethylene conversion increased linearly as a function of pressure and residence time. Tar formation increased exponentially in the pressure range 1–3.5 bar and linearly with the residence time. The fraction of heavier tar compounds was found to increase with temperature and pressure. The tar composition was compared with different biomass gasification tar compositions, and the compositions were found to resemble each other. The obtained tar-laden product gas could be used as a realistic tar model when the cleaning of biomass gasification gas is studied.

1. Introduction

Gasification of biomass is an efficient and versatile way to convert biomass into energy, fuels or chemicals. Biomass gasification is thereby one solution to help fulfil the renewable energy requirements set by various countries and reduce the dependency on fossil fuels. In order to be able to use biomass gasification gas in catalytic downstream processes or engines, the gas must be cleaned from impurities such as tar and particulates. Tar formation in the gasifier and purification of gasification gas from tar are a major concern because tar causes problems in downstream units through fouling, and soot and coke formation.

Gasification literature presents various definitions of tar and many ways to classify the tar compounds. One of the definitions is that tar is a biomass gasification product that is condensable downstream of the gasifier, and the compounds in tar are generally assumed to be primarily aromatic [1]. This definition is not very exact, thus, in the tar protocol [2], tar is defined as aromatic compounds that are heavier than benzene. This definition will be used in this study. Tar compounds can be classified by formation temperature into primary, secondary and tertiary tar, as has been done by, for example, Milne [1]. Primary tar consists of decomposition products of biomass, which are mostly oxygenated compounds [3,4]. Secondary and tertiary tars are formed by the reactions of primary tar and combinations of fragments of tar compounds [3]. Secondary tar consists of alkylated aromatic one- and two-ring compounds, including heteroaromatics [4]. Tertiary tar consists of aromatic hydrocarbons, such as benzene, naphthalene, phenanthrene, and other polyaromatic hydrocarbons (PAH) [1]. These compounds cannot be found from the source biomass. In tertiary

Abbreviations: PAH, polyaromatic hydrocarbons; HAVA, hydrogen abstraction and vinyl radical addition; HACA, hydrogen abstraction acetylene addition; PAC, phenyl addition and cyclization; MAC, methyl addition and cyclization; CFB, circulating fluidised bed; BFB, bubbling fluidised bed.

* Corresponding author. Tel.: +358 40 685 7095.
E-mail address: noora.kaisalo@vtt.fi (N.K. Kaisalo).

http://dx.doi.org/10.1016/j.fuel.2015.02.085
0016-2361/

tar, the product range is also wide, from benzene to heavy aromatics [1]. Thus, other classifications have been used, such as classification based on the physical properties of tar compounds [5] or on the number of rings in a tar compound [3,6].

Gasification of biomass begins with pyrolysis vapour formation, and during gasification, oxygen in the molecules of woody biomass is released as CO and CO_2, and at the same time, radicals and small molecules are formed, reacting further to form aromatics [7]. Part of the oxygen in biomass is also bound to oxygenates, such as phenols. Few studies have been made of the thermal reactions of the primary tars formed in the pyrolysis phase. Lignin, the only part of the wood containing aromatic structures, has been believed to be responsible for tar formation [8]. However, Norinaga et al. [8] showed that tar can also be formed from cellulose even though cellulose does not contain aromatic structures. They studied secondary thermal reactions of primary pyrolysis products of cellulose in the temperature range 700–800 °C. Ethylene, benzene and toluene were formed, among other products. According to Palma [9], PAH compounds are formed by a direct combination of aromatic rings from lignin decomposition, by hydrogen abstraction acetylene addition (HACA) or by abstraction of CO from phenol forming a cyclopentadienyl radical, which reacts further to form PAH. Ledesma et al. [10] studied pyrolysis of eugenol, which represents primary tar formed from lignin. The major hydrocarbons formed in the pyrolysis of eugenol were ethylene and acetylene, and their yield increased with temperature. In addition, the influence of olefins and C_2–C_5 radicals on the formation of tar compounds in gasification is discussed in literature [1,11].

Reactions of hydrocarbon radicals are also discussed in studies related to combustion. These studies have concentrated on PAH and soot formation in flames [12]. There are also many studies related to chemical vapour deposition of carbon. Most of these studies have concentrated on carbon formation by pyrolysis of light hydrocarbons, and the initial reaction steps up to benzene have been modelled in detail [13–15]. Studies related to chemical vapour deposition of carbon have been conducted in conditions below atmospheric pressure. Fewer studies have concentrated on formation pathways for heavier aromatic compounds [16–18]. Shukla and Koshi [17,18] presented different radical mechanisms explaining radical aromatic growth: HACA (hydrogen abstraction and acetylene addition), HAVA (hydrogen abstraction and vinyl radical addition) mechanism, PAC (phenyl addition and cyclization) and MAC (methyl addition and cyclization).

High temperature zones do exist in gasification processes, for example the air/oxygen feed inlet areas in tar reformers (900–1100 °C), downdraft gasifier combustion zones (approx. 1200 °C), fluid bed gasifier freeboards (800–900 °C), etc. Reactor design and development for gasification applications therefore require deep understanding of tar and soot formation in these conditions as well as expertise in the effects of temperature and pressure. Considering tar and other hydrocarbons present in gasification, ethylene is the most abundant compound after methane, usually detected in the range 0.2–4 vol-% in dry gas [19–21]. Ethylene may form soot and tar compounds during hot gas cleaning steps, filtration and reforming.

Syntheses, such as Fischer–Tropsch and methanation, are usually pressurized, thus, pressurizing the gasification process would improve the economics of the whole concept. In biomass gasification literature, pressurised gasifier studies are available, although the effect of pressure on tar formation has not been studied systematically and the results are somewhat contradictory [4,22–25]. In addition, light hydrocarbon pyrolysis studies have been limited to atmospheric or below atmospheric pressure [15–18].

Consequently, the motivations of this study are twofold: (1) What role do the light hydrocarbons play in gasification conditions; can, for example, the residual PAH present in certain conditions in catalytic reforming be explained as being reaction products of the light hydrocarbons? (2) Can we produce proper model tar by thermal reactions of ethylene so that the product can be used as feed in, for example, filter-clogging studies?

2. Materials and methods

2.1. Experimental set-up

The experiments were conducted in a pressurised plug flow reactor system with a quartz reactor. The experimental set-up is illustrated in Fig. 1. The quartz reactor was sealed in a steel reactor that was in a three-zone furnace. The inner diameter of the quartz reactor was 1 or 1.5 cm, depending on the experimental conditions, with a thermocouple pocket of 0.4 cm in diameter in the centre of the reactor. The total length of the reactor was 45 cm. The thermocouple pocket was made of quartz and spanned from the top of the reactor to the bottom and covered the thermocouple completely. The temperature profile of the reactor was measured with a K-type thermocouple under nitrogen flow with an oven temperature of 950 °C. During the experiments, the temperature was measured from a single point, which was the maximum temperature point in the temperature profile measured under N_2.

The residence time was calculated according to the inlet volumetric flow rate at the measured reaction temperature for each experimental condition. The residence time was calculated for the length of the reactor where the temperature was over 900 °C in the temperature profile measured under N_2 flow. The length of the reactor used in the residence time calculation was 27 cm. This was chosen because at 900 °C the conversion of ethylene started to be significant also with short residence times. The temperature used in the result and residence time calculations is the measured reactor temperature.

During the experiments, the H_2 and CH_4 concentrations were followed with a continuous gas analyser. After the concentrations were stabilized, at least two samples with an online gas chromatograph were taken from each experimental condition. For some of the conditions, five samples were taken to check the stability of the system and the repeatability of the analysis. Typically, each experimental condition was maintained for 2–3 h. From time to time, the reactor and the lines were cleaned with a mixture of isopropanol and toluene, after any carbon formed on the quartz reactor walls was burned by air at 850 °C.

The gases were fed to the reactor by mass flow controllers. In all the experiments, the feed gas contained 5 vol-% of ethylene (Aga, 99.95%) in N_2 (Aga, 99.999%). According to Norinaga and Deutschmann [14], small amounts of impurities are important in the initiation of reactions. The impurities in ethylene were analysed to be 1 ppm of methane and 9 ppm of ethane.

2.2. Analysis of products

An online analysis of hydrocarbons from methane up to pyrene was made using an Agilent 7890A gas chromatograph equipped with one injector, two flame ionization detectors (FID) and three columns. The columns were Agilent GS – GASPRO (30 m × 0.32 mm ID, 0 μm film), HP – 5 (30 m × 0.32 mm ID, 0.25 μm film) and a restrictor column (3 m × 0.18 mm). The GS-GASPRO column was used to separate the hydrocarbons that elute before benzene, whereas the HP-5 was used for benzene and other aromatics. The gas was led to a sample loop of 0.25 ml in a six-port valve. From there, it was led to the HP-5 column and after that to the GS-GASPRO column and a FID. Just before benzene and heavier hydrocarbons were eluted from the HP-5 column, the direction of the gas flow was switched into the restrictor column instead of the

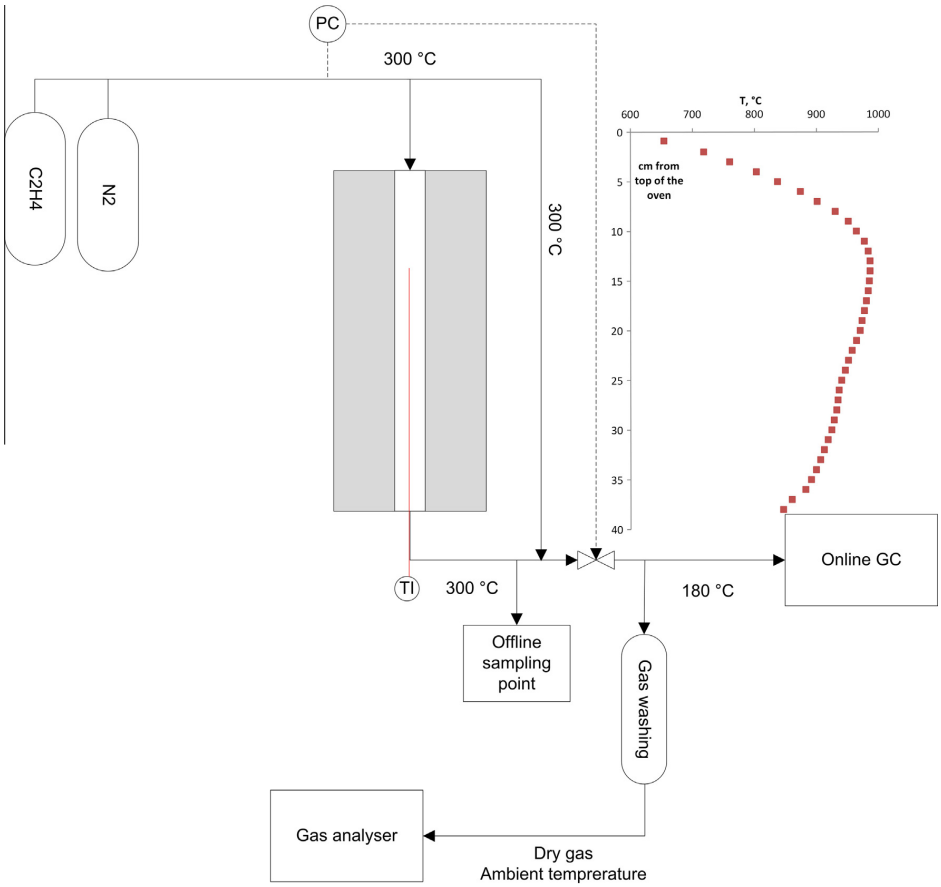

Fig. 1. Experimental set-up and temperature profile of the oven.

GS-GASPRO column and from there to the other FID. The carrier gas was helium. The initial temperature was 100 °C. An oven programme of 100 °C – 9.2 min – 20 °C/min – 270 °C – 42 min was set for the gas chromatograph and the total run-time was 60 min. Hydrogen was measured by the online gas analyser for dry gases (ABB AO2020) by a thermal conductivity detector (TCD). The calibration of hydrocarbons heavier than benzene was based on the results of liquid sampling.

In addition to online analysis, gas bags and liquid tar samples were taken from some of the set points and analysed by offline gas chromatography. The liquid sampling was modified from the tar sampling system described in detail in [26]. The liquid tar samples were taken using four impinger bottles, of which the two first were at room temperature and the two last in an ice bath. The absorbent used was isopropanol. All the bottles contained glass pearls to improve gas–liquid contact. The gas volume passed through the impinger bottles was about 10 dm^3. The gas bags were analysed by the Hewlett Packard 5890 series II GC with the HP Plot Al_2O_3 column and with FID, and hydrogen by the Agilent 490 micro GC equipped with TCD. A GC–MS (Agilent 6890 N GC, DB-1 column, with Agilent 5973 mass selective detector) was used to identify the unknown products from the gas bag samples and liquid samples.

2.3. Calculation of results

In the calculation of elemental balances, it was assumed that all formed H_2, and hydrogen bound to hydrocarbons could be analysed. Thus, the molar flow of hydrogen atoms in the inlet was equal to the outlet molar flow. Based on the molar flow of hydrogen calculated by Eq. (1), the volumetric outlet flow was calculated (Eq. (2)) and used to calculate the molar carbon outlet flow and molar outlet flows of the analysed compounds (3).

$$n_{H_{IN}} = N^{H}_{C2H4} * \frac{x_{C2H4_{IN}} * Q_{IN}}{V_m} \quad (1)$$

$$Q_{OUT} = n_{H_{IN}} * \frac{V_m}{\sum_{i=1}^{k} (N_i^H * x_i)} \quad (2)$$

$$n_{i_{OUT}} = x_i * \frac{Q_{OUT}}{V_m} \quad (3)$$

where x_i is the volume fraction of compound i, n_i is the molar flow of compound i, Q is the volumetric flow rate at normal conditions, N_i^H is the number of hydrogen atoms in compound i and V_m is the molar volume of an ideal gas. This approach was chosen because almost all hydrogen containing products could be analysed, in contrast to carbon-containing products such as soot or very heavy tars, which

contain mainly carbon and only very little hydrogen. The outlet flow rate was calculated because there was not a measured flow rate for every experimental condition. For the product concentration, the average of the online GC results was used.

The molar selectivity (S%) of the products was calculated by the following equation:

$$S\% = \frac{n_i}{n_{C2H4_{IN}} - n_{C2H4_{OUT}}} * 100\% \quad (4)$$

3. Results

3.1. Analysed products

In this study, the analysis of all the hydrocarbons from methane to heavy tar compounds was done with an online gas chromatograph. Typically, heavier compounds have been collected in a cold trap or impinger bottles for offline analysis [10,15]. The online gas chromatography for all the hydrocarbons including tar compounds was a novel method tested in this study. The products of all the experimental conditions were analysed by online gas chromatography; the conditions in which gas bag samples or liquid samples were taken in addition to online analysis are indicated in Table 1.

The chromatogram of light hydrocarbons analysed by online GC can be found in Supplementary Information linked to this paper. The products were recognised by the retention time matching with calibration gas, except vinylacetylene and 3-penten-1-yne, which were recognised by mass spectrometry analysis of a gas bag sample. In online gas chromatography, ethane and ethylene could not be separated from each other. However, it was possible to check the level of ethane by offline gas chromatography from the gas bag samples. The amount of ethane was between 14 and 83 ppm in all gas bag samples. The concentration was considered so low that it did not affect the calculation of ethylene conversion significantly. Thus, it was not taken into consideration in the further result calculations.

The main C_2 hydrocarbon formed from ethylene was acetylene. The most abundant C_3 compounds in this study were propene and propadiene. Propane was formed in very small concentrations in a few experimental conditions. More C_4 hydrocarbons than C_3 compounds were formed. The most abundant C_4 compounds were 1,3-butadiene (300–660 ppm) and vinylacetylene (50–350 ppm). The most abundant C_5 compound was 3-penten-1-yne (40–220 ppm). The total of the other, unknown, C_5 compounds was 5–20 ppm. The C_6 compounds were formed in small amounts; the total was between 4 and 9 ppm. None of the C_6 compounds was recognized.

Cyclopentadiene has been reported in many studies to be an important precursor for PAH formation [27–29]. However, it could not be detected in this study. The most abundant C_5 hydrocarbon in this study was 3-penten-1-yne, which in turn has not been reported as a product of ethylene conversion in other studies.

The chromatogram of the aromatic hydrocarbons that were analysed by online GC is presented in Supplementary Information linked to this paper. The benzene was the most abundant aromatic compound. The main one-ring tar compounds were toluene, styrene and ethynylbenzene and the most abundant two-ring compounds were naphthalene and indene. The main compounds of the three-ring group were, in turn, acenaphthylene,

Table 1
Experimental conditions and amount of tar.

P (bar)	T (°C)	Residence time (s)	Error in C balance (%)	Tar amount (mg/m^3_n)	1-ring (mg/m^3_n)	2-ring (mg/m^3_n)	3-ring (mg/m^3_n)	4-ring (mg/m^3_n)
1[a]	787	0.3	0.1	0	0	0	0	0
1	844	0.3	0.4	2	1	1	0	0
1	901	0.3	0.8	39	26	13	0	0
1	954	0.3	1.6	549	310	216	18	5
1[a,b]	955	0.3	−0.8	558	274	256	21	6
1	955	0.3	0.1	357	192	151	12	3
1	974	0.3	1.7	987	490	419	55	23
1[a,b]	978	0.3	0.1	682	326	313	38	5
1	947	0.1	−2.3	19	12	6	0	0
1	962	0.1	−2.3	81	56	25	0	0
1	960	0.1	−2.1	80	53	27	1	0
1	956	0.1	−2.4	77	53	24	0	0
1[a,b]	956	0.5	0.7	826	377	387	54	9
1	954	0.7	1.6	1401	648	613	93	47
1[a,b]	954	0.9	0.3	2083	878	934	174	98
2	949	0.1	−1.7	176	113	60	3	0
2	953	0.1	−2.3	214	130	80	4	0
2	952	0.1	−1.0	213	130	79	4	0
2	945	0.1	−0.8	277	163	106	7	1
2	955	0.2	−1.2	348	196	142	10	1
2	961	0.2	−2.8	813	389	372	45	7
2	956	0.2	−2.1	700	343	314	36	6
2	954	0.3	0.1	843	397	390	49	7
2	951	0.5	0.4	1148	509	545	81	13
2	954	0.7	−2.8	2299	849	1162	233	56
2	954	0.7	−0.6	2171	814	1096	218	42
2	954	0.7	1.8	2056	900	918	153	85
2[b]	956	0.9	−1.8	3115	1033	1629	359	94
3[a,b]	952	0.1	−1.4	835	406	373	50	7
3[b]	954	0.7	−0.1	3076	1274	1415	231	156
3[b]	956	0.9	−1.6	3865	1504	1818	323	219
3.5	956	0.1	−0.2	1505	686	665	66	87
3.5	952	0.7	0.5	4386	1341	1787	472	787
3.5	953	0.9	1.5	7213	1603	2433	763	2415
6[b]	961	2.0	−40.4	6901	1311	3728	798	1065
6[b]	954	2.0	−20.9	5706	876	3666	838	326

[a] Gas bag samples taken in addition to online GC sampling.
[b] Liquid tar samples taken in addition to online GC sampling.

fluorene, phenanthrene and anthracene, of which the latter two elute together. Of the four-ring group, fluoranthene and pyrene were the main compounds. Considering the total tar composition, the main compounds were toluene, ethynylbenzene, styrene, indene and naphthalene. Liquid samples and gas bags were taken to verify the online results and calibrate the online system. The identification percentage for tar compounds was between 84 and 98 depending on the experimental condition. The amount of unknown compounds in online analysis was calculated based on the response factor of the previous known compound.

3.2. Carbon balances and ethylene conversion

As can be seen from Table 1, the errors in the carbon balances were generally small, a maximum of 2.8%, except at the two experimental points with the highest pressure and longest residence time, when the error in the carbon balance was large. The large error at these two experimental points is most likely to have been due to the formation of soot or very heavy hydrocarbons in the reactor. In most of the experimental conditions, slightly less carbon was analysed than was in the inlet feed. This is most probably due to soot formation. The amount of soot deposited on the reactor surfaces was not analysed in this study. However, when the reactor was opened between some of the experiments, a soot layer was observed on the quartz reactor. It was assumed that the soot layer did not have an effect. After the two experimental points with the highest pressure, the reactor and the pipelines were cleaned.

Ethylene conversion increased with temperature pressure and residence time. The conversion was exponentially dependent on temperature, Fig. 2. Further experiments, in which the effect of pressure and residence time were studied, were carried out in the temperature range 945–962 °C, with an average temperature of 954 °C. This temperature was chosen because ethylene conversion was significant, enabling easier analysing of the products. As can be seen from Figs. 3 and 4, the conversion increased almost linearly with pressure and residence time.

3.3. Selectivities of the products

The main products were hydrogen, methane, acetylene and 1,3-butadiene. The order of the compounds depends on the experimental conditions. The selectivities of light hydrocarbons are presented in Figs. 5 and 6. According to literature, 1,3-butadiene is formed by a combination of two vinylradicals formed from ethylene [14]. Acetylene, one of the main products, is mainly formed from vinylacetylene, which in turn is formed from 1,3-butadiene [14]. Methane is produced from methyl radicals by abstraction of hydrogen from either hydrogen molecules, ethylene or some product hydrocarbons [10,14]. C_3 compounds may be formed by vinyl and methyl radical fusion or by decomposition of C_4 compounds [15].

In the presentation of aromatic compounds, the compounds are divided in lumps according to the number of rings (Fig. 7). As benzene is not usually classified as a tar compound, it is not included in the one-ring compounds. Benzene may be formed from 1,3-butadiene by the addition of vinylradical or from vinylacetylene by the addition of vinylradical or acetylene [14]. The product is a C_6 compound that either forms benzene by isomerization and hydrogen abstraction or by isomerization only [14]. Benzene has also been presented as forming directly by the reaction of two C_3 species or by C_2 and C_4 species [12,29]. The molecular mass and number of rings in the tar compound increase in steps, the size of the step depending on the mechanism: HAVA, HACA, MAC or PAC [17,18]. In general, the selectivity towards tar increases with pressure and residence time. The selectivity of four- and three-ring compounds increases especially at the highest pressure, 3.5 bar.

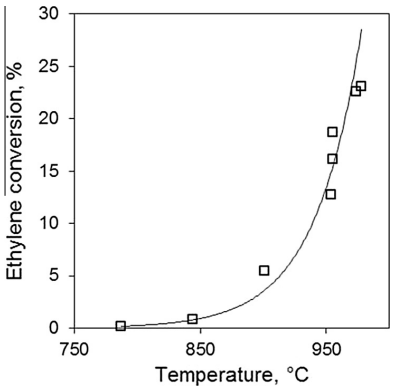

Fig. 2. Conversion of ethylene at 1 bar with residence time 0.3 s.

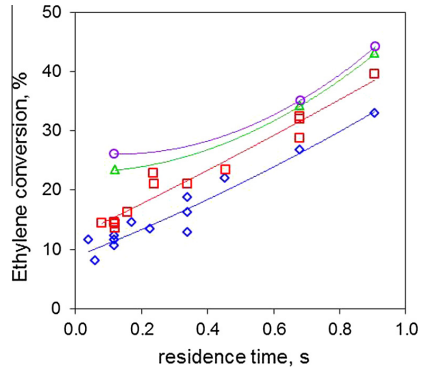

Fig. 3. Conversion of ethylene at 954 °C, at pressures of 1 bar (◇), 2 bar (□), 3 bar (Δ) and 3.5 bar (○).

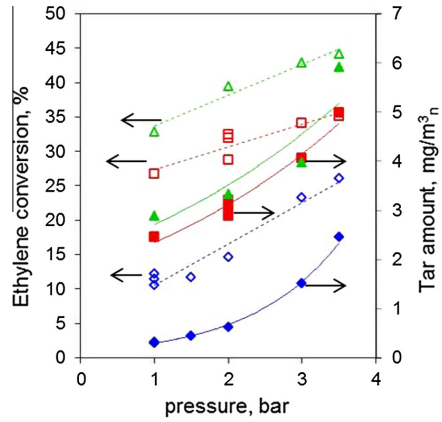

Fig. 4. Conversion of ethylene as a function of pressure at 954 °C marked with empty symbols and the tar amount with filled symbols at residence times of 0.1 s (◇), 0.7 s (□) and 0.9 s (Δ).

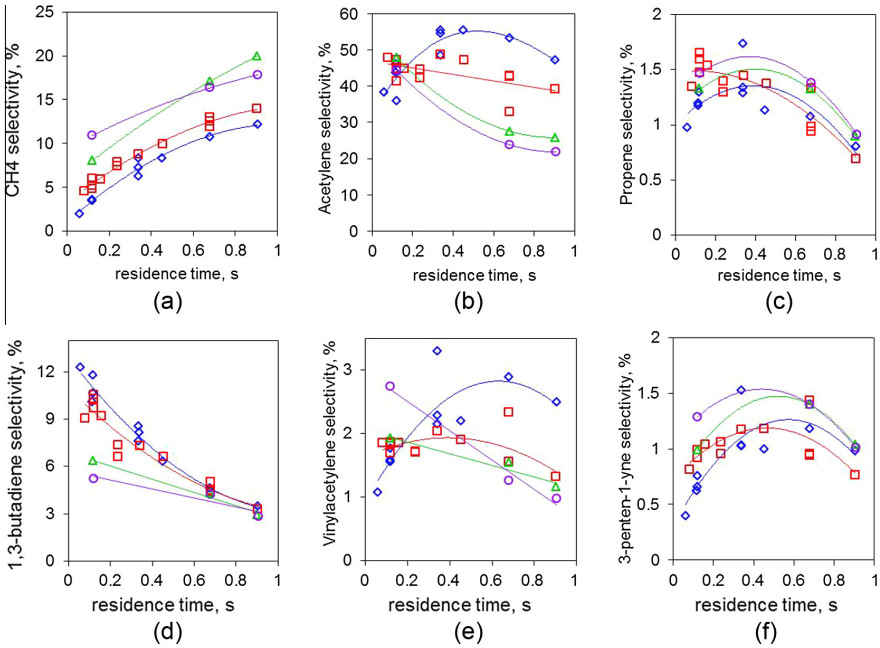

Fig. 5. Selectivity of light hydrocarbons as a function of residence time at 954 °C, at pressures of 1 bar (◇), 2 bar (□), 3 bar (Δ) and 3.5 bar (○), (a) methane, (b) acetylene, (c) propene, (d) 1,3-butadiene, (e) vinylacetylene and (f) 3-penten-1-yne.

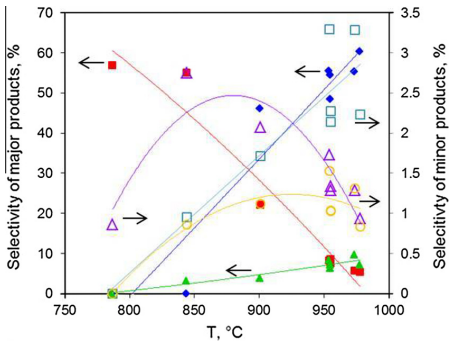

Fig. 6. Selectivity of light hydrocarbons as a function of temperature, major products on primary axis with filled symbols (methane Δ, acetylene ◇, 1,3-butadiene □) and minor products on secondary axis with empty symbols (propene Δ, vinylacetylene □, 3-penten-1-yne ○).

3.4. Effect of process conditions on tar formation and composition

The amount of tar compounds increased exponentially with temperature. At 787 °C, no tar compounds were detected, and at 844 °C the total tar concentration was only 2.2 mg/m^3_n. This was understandable since the ethylene conversion was also under 1% at these temperatures, leading to small amounts of products. The heavier tar compounds are formed relatively slowly from the primary reaction products and thus they were observed only in very small amounts. The tar consisted mainly of one- and two-ring compounds in all experimental conditions. The shares of three- and four-ring compounds increased slightly from zero to a few per cent above 950 °C.

The total amount of tar increased exponentially with pressure and relatively linearly with residence time. Tar formation with increasing pressure behaved differently to ethylene conversion, which increased linearly, as can be seen from Fig. 4.

The amounts of different tar groups relative to the total amount of tar say more about the changes in tar composition due to operation conditions, Fig. 8. The amount of benzene is considered relative to the total amount of tar. The absolute mg/m^3_n values for different classes of tar compounds can be found from Table 1.

4. Discussion

4.1. Products of thermal reactions of ethylene compared with the gasification results

A mixture of light hydrocarbons and tar compounds was formed from thermal reactions of ethylene. The light hydrocarbons formed in gasification are usually not reported in detail because they are not considered as problematic as tar. The major light hydrocarbons are typically methane and ethylene [19,20]. For example, in indirect gasification of biomass, the product gas may contain ethylene up to 4 vol-% in dry gas [19], although in air- or oxygen-blown gasification, the ethylene content is lower 0.2–1.2 vol-% in dry gas [20,30]. In this study, the main light hydrocarbons were methane, ethylene and acetylene, although, especially with short residence times or at low temperature, 1,3-butadiene also had quite high selectivity, Fig. 5.

The amount of tar in gasification depends on the gasifier type. As a rough approximation, gas from an updraft gasifier contains 100 g/m^3_n tar, from a fluidised bed gasifier 10 g/m^3_n and from a downdraft gasifier 1 g/m^3_n [1]. The amount of tar obtained in the conditions of this study was always below 10 g/m^3_n, Table 1. A longer residence time and different starting material may explain

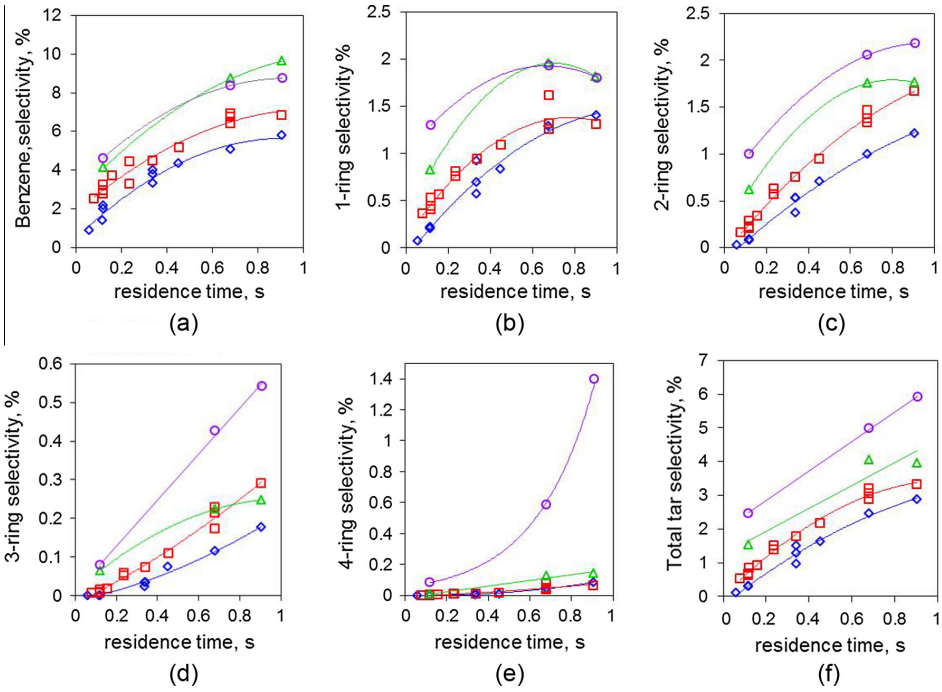

Fig. 7. Selectivity of aromatic compounds as a function of residence time at 954 °C, at pressures of 1 bar (◇), 2 bar (□), 3 bar (Δ) and 3.5 bar (○), (a) benzene, (b) one-ring compounds, (c) two-ring compounds, (d) three-ring compounds, (e) four-ring compounds and (f) total tar.

the differences in the tar amount in gasification and in this study. In fluidised bed gasifiers, the residence time in the freeboard is in the order of seconds [31], thus clearly longer than at the experimental points in this study. In addition, in the gasification process, small hydrocarbons have time to form tar and soot in hot gas filtration and catalytic cleaning. In this study, all the aromatic compounds are initially formed from a C_2 hydrocarbon, whereas in gasification, the gas already contains initially heavier hydrocarbons as a result of biomass decomposition, which can then react further. For example, the lignin fraction of the wood contains aromatic structures as such [9], which may be liberated during gasification and grow by reacting further with light radicals.

Not only the total amount but also the composition of tar needs to be compared. The gasification process affects the composition of tar. Exemplary gasification tar compositions have been collected in Table 2, including few examples from this study. The absolute tar amounts obtained in this study are presented in Table 1 and the change in composition with a change in pressure or residence time is presented in Fig. 8. Tar from the updraft gasifier can be characterised as primary tar, downdraft gasifier tar as tertiary and fluidised bed as secondary and tertiary [3].

The clearest difference in the composition of tar is the understandable lack of heterocyclic compounds in tar formed by thermal reactions of ethylene compared with gasification tar. Thus, the tar from thermal reactions of ethylene is not a good representation of the tar from the fixed bed Novel gasifier [32], which contains 25.6% heterocyclic compounds (Table 2). The smallest share of heterocyclic compounds is formed in high temperature CFB air gasification. However, there the share of four-ring compounds is highest and clearly higher than was obtained in the experiments in this study. The results from steam gasification have about 10% heterocyclic compounds, but the major group is two-ring compounds, and the one-ring compounds have the second largest share, as is the case in this study. The steam gasification results show large differences in the total amount of tar depending on the bed material. With sand as the bed material, the amount of tar was 20 g/m^3_n and that high concentration of tar could not be produced in this study. If dolomite was used as the bed material, the tar concentration was only 4.7 g/m^3_n, which is more in the order of the tar amounts that were produced in this study. With dolomite, the tar levels were lower than with sand because dolomite is catalytically active in decomposing tars [33]. In the downdraft gasification, the largest share of tar comprised one-ring compounds, the second largest being two-ring compounds. This kind of composition can also be produced by ethylene at high temperature, for example, by shortening the residence time, which increases the share of one-ring compounds, Fig. 8.

The most abundant aromatic compound in gasification gas is always benzene, which was also the case in this work. The most abundant compounds in gasification tar depend on the process. In the gasification experiments presented in Table 2, the two most common among the one-ring compounds were always toluene and styrene. In this study, the two most common one-ring compounds were the same, but the third major compound was ethynylbenzene, and in some of the gasification experiments it was not formed at all. The most common two-ring compounds in gasification were indene and naphthalene, as was the case in this work. The same was observed with three-ring compounds: the most common being acenaphthylene and phenanthrene in both the gasification and the experiments in this study. The most common

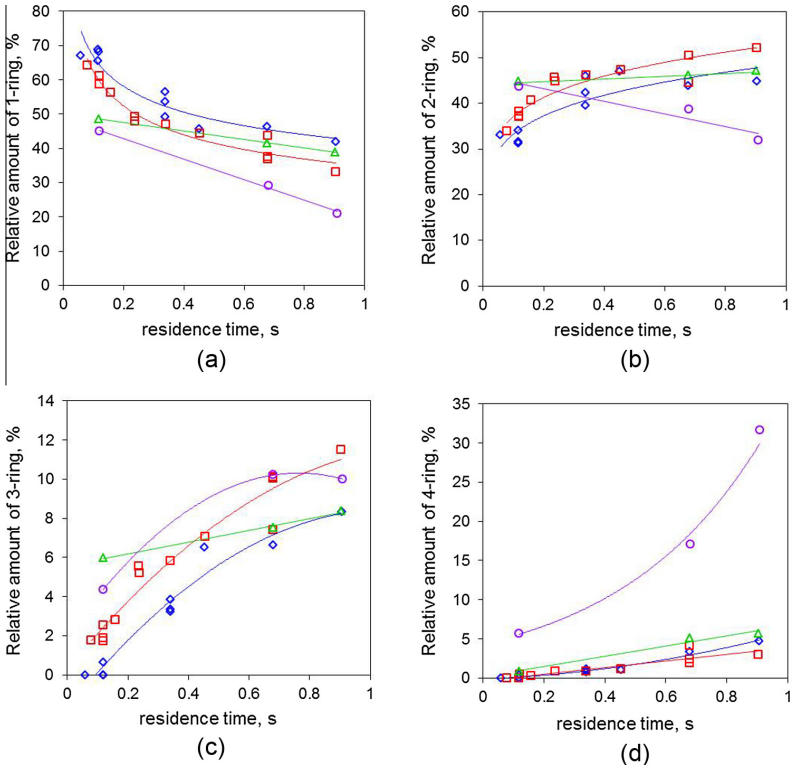

Fig. 8. Relative amount (mg/m^3_n based) of tar groups to total tar at 954 °C, at pressures of 1 bar (◇), 2 bar (□), 3 bar (Δ) and 3.5 bar (○), (a) one-ring compounds, (b) two-ring compounds, (c) three-ring compounds and (d) four-ring compounds.

Table 2
Tar product distribution in different type of gasification experiments and selected results of this study for comparison.

	P (bar)	*T* (°C)	Residence time (s)	1-ring[a] (%)	2-ring (%)	3-ring (%)	4-ring (%)	Heterocyclic (%)	Tot (%)	Total tar (g/m^3_n)
CFB, air, sawdust, sand [31]	5	940	4	5.9	48.9	28.9	14	2.3	100	4.3
BFB, H_2O, wood, sand [21]	1	800	6	20.4	28.6	13.8	2.3	10.7	76	20.5[b]
BFB, H_2O, wood, dolomite [21]	1	800	6	31.9	37.7	11.8	2.4	7	91	4.7[b]
Downdraft gasifier, wood [32]	1	1050–1160	seconds	38.8	32.9	12.2	4.3	11.7	100	1.2
Fixed bed, Novel gasifier, forest residue [32]	1	730	seconds	19.5	37.8	13.2	3.9	25.6	100	4.7
Results of this study	1	954	0.9	42	45	8	5	0	100	2.1
Results of this study	3	956	0.9	39	47	8	6	0	100	3.9
Results of this study	6	954	2.0	19	54	12	15	0	100	6.9

[a] Benzene is not included in 1-ring compounds.
[b] Unidentified tar compounds included in total amount of tar.

four-ring compounds were fluoranthene and pyrene in both cases. Thus, the major gasification tar compounds are also formed as the major aromatic products in thermal reactions of ethylene.

4.2. Effect of temperature on ethylene conversion and product formation

Ethylene conversion increases with temperature, leading to an increase in the formation of products. Selectivity towards light intermediate products decreased (1,3-butadiene) or had a maximum as a function of temperature, such as propene, and 1-penten-3-yne, (Fig. 6), whereas the selectivity towards tar compounds increased with temperature. This indicates that light compounds are intermediate compounds forming heavier tar compounds when temperature, residence time or pressure increases.

In gasification, the tar composition changes with a temperature increase. Tar contains less oxygen containing compounds, such as phenols, and more PAH and naphthalene when the temperature is increased [4]. It has been reported that at gasification temperatures of 850–900 °C, only more stable aromatic compounds are left, instead of oxygenated tar compounds [31]. Thus, the tar produced in this study represents better a tar from gasification at higher temperature because of the lack of heterocyclic compounds. Also, the share of heavier three- and four-ring compounds increased

with temperature as well as in gasification [4]. As in gasification, an increase in the share of naphthalene of the total tar was observed in this study. Styrene and indene of the aromatic compounds have been reported to decrease in gasification experiments with a temperature increase [4], and the same was observed in the experiments in this study. In gasification, the temperature increase favours the formation of aromatics without substituent groups [9].

The ethylene and other light hydrocarbons in gasification gas also cause problems at the reforming stage by giving rise to soot formation. In the staged-reformer concept described by Simell et al. [34], ZrO_2 catalysts can be used as a pre-reforming catalyst to decompose tar followed by a precious metal and/or nickel catalyst layer. However, ZrO_2 catalysts do not convert light olefinic hydrocarbons, such as ethylene and butadiene, into syngas, and these light hydrocarbons may cause soot or coke formation at the subsequent nickel catalyst stage [35]. In this study, it was seen that ethylene produces PAH and soot.

4.3. Effect of pressure on ethylene conversion and product formation

Increase of the pressure increased the ethylene conversion. The same was noticed by Norinaga and Deutschmann [14] who studied the effect of pressure on ethylene pyrolysis on the total pressure of 5–15 kPa, which corresponds to the partial pressure of ethylene in this study. Interestingly, the ethylene conversion increased almost linearly with the pressure whereas the tar amount increased exponentially in the pressure range 1–3.5 bar, Fig. 4. If the results of two experiments at 6 bar and with 2 s residence time are compared with the experiments at lower pressure, it can be seen that the amount of tar did not increase significantly any more from 3.5 to 6 bar pressure. This could be due to soot formation reactions. Moreover, the large error in the elemental carbon balance gives support to this assumption. With high pressure and long residence time, the aromatics have time to react to soot. The soot formation may also be enhanced with increasing pressure, which may cause problems. Especially, if it is formed in the reformer, it may plug the front face of the catalyst. Becker and Hüttinger [36] report that the carbon deposition rate increases exponentially with residence time in the ethylene pyrolysis. According to them, acetylene and ethylene may also deposit carbon directly, but, compounds that form carbon more actively are formed with increasing residence time. Because the amount of soot formed during the experiments was not analysed in this study it is not possible to see the effect of pressure on soot formation.

In this study, increasing the pressure increased the amount of tar exponentially; however, the effect of pressure on tar formation in gasification is not clear. Based on gasification literature, no clear effect of pressure on the tar amount can be found. In addition, finding an explanation for the contradictory results in gasification studies is not easy; no reason can be found from gasification media, bed material, and temperature or pressure range when comparing the literature results.

Even though the effect of pressure on the total amount of biomass gasification tar is not clear based on literature, the increase in pressure seems to change the composition of tar to shift more towards heavier compounds [4,22,24]. The same observation was made in this study.

5. Conclusions

The formation of light hydrocarbon and tar compounds from ethylene was studied. The tar formation was found to increase exponentially in a pressure range of 1–3.5 bar, which indicates that pressurised gasification and gas cleaning may be difficult due to enhanced tar and soot formation. In reformers, it may cause catalyst deactivation and clogging. However, this study was only conducted with ethylene, whereas gasification gas contains compounds, such as water, which may steam reform the hydrocarbons and thus inhibit tar formation. Nevertheless, with increasing pressure, the tar composition shifts towards more refractory and difficult-to-handle polyaromatics. The carbon formation, especially at 6 bar pressure, was significant.

The tar produced by thermal reactions of ethylene is a fairly good representation of biomass gasification tar. Thus, ethylene could be used to produce biomass gasification tar for filtration or reforming studies. Nowadays, a single model compound or mixture of only a few compounds is used. Thus, products of thermal reactions of ethylene would provide a more realistic tar composition. Furthermore, other light hydrocarbons, present in biomass gasification gas, were also observed in this study produced by thermal reactions of ethylene. The product composition from thermal reactions of ethylene can be changed by modifying the operation conditions.

Acknowledgments

The research was carried out as part of the VETAANI project. The authors would like to acknowledge Tekes (The Finnish Funding Agency for Technology and Innovation), Gasum, Neste Oil, Metso Power, Helsingin Energia, Huoltovarmuuskeskus, Outotec and SGC (Swedish Gas Centre) for the financial support in the project.

Appendix A. Supplementary material

Supplementary data associated with this article can be found, in the online version, at http://dx.doi.org/10.1016/j.fuel.2015.02.085.

References

[1] Milne TA, Evans RJ, Abatzoglou N. Biomass gasifier "tars": their nature, formation, and conversion. NREL/TP-570-25357; 1998.
[2] Maniatis K, Beenackers AACM. Tar protocols. IEA bioenergy gasification task. Biomass Bioenergy 2000;18:1–4.
[3] Rabou LPLM, Zwart RWR, Vreugdenhil BJ, Bos L. Tar in biomass producer gas, the energy research centre of The Netherlands (ECN) experience. An enduring challenge. Energy Fuels 2009;23:6189–98.
[4] Wolfesberger U, Aigner I, Hofbauer H. Tar content and composition in producer gas of fluidized bed gasification of wood – influence of temperature and pressure. Environ Prog Sust Energy 2009;28:372–9.
[5] Kiel JHA, van Paasen SVB, Neeft JPA, Devi L, Ptasinski KJ, Janssen FJJ, et al. Primary measures to reduce tar formation in fluidised-bed biomass gasifiers; 2004.
[6] Han J, Kim H. The reduction and control technology of tar during biomass gasification/pyrolysis: an overview. Renew Sust Energy Rev 2008;12:397–416.
[7] Jarvis MW, Haas TJ, Donohoe BS, Daily JW, Gaston KR, Frederick WJ, et al. Elucidation of biomass pyrolysis products using a laminar entrained flow reactor and char particle imaging. Energy Fuels 2011;25:324–36.
[8] Norinaga K, Shoji T, Kudo S, Hayashi J. Detailed chemical kinetic modelling of vapour-phase cracking of multi-component molecular mixtures derived from the fast pyrolysis of cellulose. Fuel 2013;103:141–50.
[9] Font Palma C. Modelling of tar formation and evolution for biomass gasification: a review. Appl Energy 2013;111:129–41.
[10] Ledesma EB, Hoang JN, Nguyen Q, Hernandez V, Nguyen MP, Batamo S, et al. Unimolecular decomposition pathway for the vapor-phase cracking of eugenol, a biomass tar compound. Energy Fuels 2013;27:6839–46.
[11] Dufour a, Masson E, Girods P, Rogaume Y, Zoulalian a. Evolution of aromatic tar composition in relation to methane and ethylene from biomass pyrolysis-gasification. Energy Fuels 2011;25:4182–9.
[12] Richter H, Howard J. Formation of polycyclic aromatic hydrocarbons and their growth to soot – a review of chemical reaction pathways. Prog Energy Combust Sci 2000.
[13] Norinaga K, Janardhanan VM, Deutschmann O. Detailed chemical kinetic modeling of pyrolysis of ethylene, acetylene and propylene at 1073–1373 K with a plug-flow reactor model. Int J Chem Kinet 2008:199–208.
[14] Norinaga K, Deutschmann O. Detailed kinetic modeling of gas-phase reactions in the chemical vapor deposition of carbon from light hydrocarbons. Ind Eng Chem Res 2007;46:3547–57.

[15] Norinaga K, Deutschmann O, Hüttinger KJ. Analysis of gas phase compounds in chemical vapor deposition of carbon from light hydrocarbons. Carbon 2006;44:1790–800 (NY).
[16] Norinaga K, Deutschmann O, Saegusa N, Hayashi J. Analysis of pyrolysis products from light hydrocarbons and kinetic modeling for growth of polycyclic aromatic hydrocarbons with detailed chemistry. J Anal Appl Pyrolysis 2009;86:148–60.
[17] Shukla B, Koshi M. A novel route for PAH growth in HACA based mechanisms. Combust Flame 2012;159:3589–96.
[18] Shukla B, Koshi M. Comparative study on the growth mechanisms of PAHs. Combust Flame 2011;158:369–75.
[19] Tuomi S, Kurkela E, Simell P, Kaisalo N. Gasification concept testing for dual fluidized-bed based SNG process. ICPS2013, Vienna, Austria; 2013.
[20] Kurkela E, Kurkela M, Hiltunen I. The effects of wood particle size and different process variables on the performance of steam-oxygen blown circulating fluidised-bed gasifier. Environ Prog Sustain Energy 2014.
[21] Tuomi S, Kurkela E, Simell P, Reinikainen M. Behaviour of tars on the filter in high temperature filtration of biomass-based gasification gas. Fuel 2015;139:220–31.
[22] Mayerhofer M, Mitsakis P, Meng X, de Jong W, Spliethoff H, Gaderer M. Influence of pressure, temperature and steam on tar and gas in allothermal fluidized bed gasification. Fuel 2012;99:204–9.
[23] Brage C, Qizhuang Y, Sjöström K. Characterisation of tars from coal-biomass gasification. In: 3rd Int symp coal combust. Beijing, China; 1995.
[24] Knight RA. Experience with raw gas analysis from pressurized gasification of biomass. Biomass Bioenergy 2000;18:67–77.
[25] Valin S, Ravel S, Guillaudeau J, Thiery S. Comprehensive study of the influence of total pressure on products yields in fluidized bed gasification of wood sawdust. Fuel Process Technol 2010;91:1222–8.
[26] Simell P, Ståhlberg P, Kurkela E, Albrecht J, Deutsch S, Sjöström K. Provisional protocol for the sampling and analysis of tar and particulates in the gas from large-scale biomass gasifiers. Version 1998. Biomass Bioenergy 2000;18:19–38.
[27] Dong GL, Huttinger KJ. Consideration of reaction mechanisms leading to pyrolytic carbon of different textures. Carbon 2002;40:2515–28 (NY).
[28] Wang D, Violi A, Kim DH, Mullholland Ja. Formation of naphthalene, indene, and benzene from cyclopentadiene pyrolysis: a DFT study. J Phys Chem A 2006;110:4719–25.
[29] Yu H, Zhang Z, Li Z, Chen D. Characteristics of tar formation during cellulose, hemicellulose and lignin gasification. Fuel 2014;118:250–6.
[30] Kurkela E, Ståhlberg P, Laatikainen J. Pressurized fluidized-bed gasification experiments with wood, peat and coal at VTT in 1991–1992. Part 1. Test facilities and gasification experiments with sawdust, VTT publications 161. 1993.
[31] Kurkela E. Formation and removal of biomass-derived contaminants in fluidized-bed gasification processes. VTT 287; 1996.
[32] Kurkela E, Simell P, Ståhlberg P, Berna G, Barbagli F, Haavisto I. Development of novel fixed-bed gasification for biomass residues and agrobiofuels. VTT research notes 2059; 2000.
[33] Simell PA, Leppälahti JK, Bredenberg JB. Catalytic purification of tarry fuel gas with carbonate rocks and ferrous materials. Fuel 1992;71:211–8.
[34] Simell P, Hannula I, Tuomi S, Nieminen M, Kurkela E, Hiltunen I, et al. Clean syngas from biomass – process development and concept assessment. Biomass Convers Biorefinery 2014.
[35] Simell P, Kurkela E. Method for the purification of gasification gas. EP1404785 B1; 2007.
[36] Becker A, Huttinger KJ. Chemistry and kinetics of chemical deposition of pyrocarbon – II pyrocarbon deposition from ethylene, acetylene in the low temperature regime. Carbon 1998;36:177–99 (NY).

II

Tuomi, S., Kaisalo, N., Simell, P., Kurkela, E. (2015) Effect of pressure on tar decomposition activity of different bed materials in biomass gasification conditions. *Fuel* ***158***, 293-305.

Fuel 158 (2015) 293–305

Contents lists available at ScienceDirect

Fuel

journal homepage: www.elsevier.com/locate/fuel

Effect of pressure on tar decomposition activity of different bed materials in biomass gasification conditions

Sanna Tuomi, Noora Kaisalo *, Pekka Simell, Esa Kurkela

VTT Technical Research Centre of Finland, P.O. Box 1000, FI-02044 VTT, Finland

HIGHLIGHTS

- The tested bed materials were sand, dolomite, MgO, olivine and olivine/kaolin.
- Dolomite and MgO had the highest tar decomposing activities.
- The catalytic activities of dolomite and MgO reduced with increasing pressure.
- Pure olivine was inactive and behaved similarly to sand in laboratory-scale tests.

ARTICLE INFO

Article history:
Received 22 December 2014
Received in revised form 10 April 2015
Accepted 19 May 2015
Available online 29 May 2015

Keywords:
Biomass gasification
Tar
Bed materials
Pressure
Tar decomposition

ABSTRACT

The objective of this study was to compare the tar decomposing activity of different bed materials and to investigate the effect of pressure on their activity at pressures up to 10 bar. Gasification experiments were first conducted in an atmospheric pressure bubbling fluidised-bed gasifier, while the influence of pressure was studied in a laboratory-scale fixed-bed reactor with simulated gasification gas. The tested bed materials were sand, dolomite, MgO, olivine A and a 50/50 wt.% mixture of olivine B and kaolin. At atmospheric pressure both in gasification and laboratory-scale experiments, dolomite and MgO were the most active bed materials. In air/steam-blown fluidised-bed gasification conditions, all the studied bed materials were capable of reducing the tar content in reference to the base case sand; the reductions amounted to 87%, 83% and 54% with dolomite, MgO and olivine B/kaolin mixture, respectively. Increasing pressure decreased the tar decomposing activities of dolomite and MgO. On the other hand, higher pressure enhanced thermal tar decomposition reactions over sand and olivine A. In pressurised conditions at 5 bar, the carbonate and oxide forms of dolomite (calcium either as $CaCO_3$ or CaO) had similar activities implying that the observed loss in activity at higher pressures was more attributed to the pressure rather than the calcination.

1. Introduction

Gasification of biomass converts solid biomass to gas containing mainly syngas compounds, CO and H_2, but also impurities, such as tar compounds. Tars have been identified as the main challenge in biomass-based gasification processes causing blocking and fouling of downstream units. One possibility to cut down the tar content in biomass-derived gasification gas is to use catalytically active bed materials already in the gasifier. Lower tar concentration in the gas at gasifier outlet facilitates the further clean-up and end-use of the gas, for example by preventing blinding of the hot gas filter or inhibiting coke formation in the reformer. In-situ tar control in the gasifier with catalytic bed materials is often combined with secondary tar removal methods, such as catalytic reforming or scrubbing, to ensure an effective tar reduction for applications that are less tolerant to tars.

Different catalysts to be incorporated in a fluidised-bed gasifier for tar decomposition have been extensively screened by a number of researchers, and the main findings have been summarised in reviews provided by e.g. Abu El-Rub et al. [1], Sutton et al. [2], Dayton [3] and Shen and Yoshikawa [4]. Low cost natural minerals, which include e.g. dolomite, limestone, magnesite and olivine, are typically employed as bed materials – either alone or mixed with

Abbreviations: CFB, circulating fluidised-bed; FID, flame ionization detector; FT, Fischer–Tropsch; FTIR, Fourier transformation infrared spectrometer; GC, gas chromatograph; GC–MS, gas chromatograph–mass spectrometry; TC, thermal conductivity.

* Corresponding author. Tel.: +358 406857095; fax: +358 207227048.
E-mail address: noora.kaisalo@vtt.fi (N. Kaisalo).

http://dx.doi.org/10.1016/j.fuel.2015.05.051
0016-2361/

sand. Among these, dolomite ($CaCO_3{\cdot}MgCO_3$) is favoured because of its high efficiency in tar removal, which has been demonstrated both in gasifier conditions, in a secondary reactor and in laboratory-scale studies with tar model compounds, as outlined in [1–4]. The disadvantage of dolomite is related to its fragile nature due to which it is easily elutriated from the gasifier bed [5]. This in turn leads to higher consumption of make-up bed material and increased costs. However, attrition problem does not prevent using dolomite even in commercial scale gasifier in Skive, Denmark [6]. Another drawback associated with dolomite is that it has been reported to be catalytically active only in calcined form [7], which has been suggested to limit its use to relatively low pressures (close to atmospheric) in biomass gasification processes [3,8]. Under typical conditions prevailing in a fluidised-bed gasifier at atmospheric pressure, at ca. 800–900 °C, both $CaCO_3$ and $MgCO_3$ are calcined into their oxide forms (CaO and MgO) releasing the CO_2 [9]. When the pressure is raised, the partial pressure of CO_2 increases and when it exceeds the calcium calcination/carbonation equilibrium, calcium is converted to carbonate while magnesium still usually occurs as oxide. Simell et al. [7] found that in pressurised conditions, the catalytic tar reforming activity of dolomite is almost completely lost when the calcium is carbonated. Only in the so-called transition region, where the CO_2 partial pressure was close to the calcination/carbonation equilibrium, were the calcium-based bed materials (including dolomite) still found to exhibit some catalytic activity over the inert reference SiC.

In order to maintain the oxide state of dolomite in pressurised conditions, the gasification temperature should be increased which, in practice, is often restricted by ash melting and bed sintering which start to occur at elevated temperatures [8]. In pressurised process development-scale gasification experiments with a CFB gasifier in steam/oxygen-blown mode [8], dolomite was found to be a suitable catalytic bed material when operated at pressures up to 4 bar. Above 4 bar, bed sintering and agglomerate formation were encountered with sand/dolomite mixtures, and they had to be replaced by MgO or MgO/dolomite mixtures. The addition of MgO in the gasifier bed inhibited ash-related issues, and stable operation was achieved even at pressures above 4 bar.

One bed material option, which has been gaining more attention, is olivine. Olivine is a silicate mineral containing magnesium and iron: $(Mg,Fe)_2SiO_4$. It is employed as a bed material, for example, in the demonstration-scale CHP plant in Güssing, Austria, which is based on steam gasification of woody biomass [10]. The clear advantage of olivine compared to dolomite is its high resistance to attrition, which is comparable to that of sand [11]. However, its activity is generally somewhat lower than that of dolomite [5,11–15]. The tar decomposing activity of olivine is related to its MgO and Fe_2O_3 contents [4] and to the coating effect of the olivine particles in fluidised-bed gasification conditions [16,17]. Kirnbauer et al. [16,17] discovered that when olivine was used as a bed material in a dual fluidised-bed gasifier in steam gasification conditions, a calcium-rich layer was formed on top of the olivine particles as they interacted with biomass ash components and possible other additives, such as dolomite. This coating enhanced tar conversion and resulted in an 80% reduction in tars (detected by GC–MS) compared to unused olivine. The formation of coating layer has been explained in detail in [18]. Calcination of olivine may improve its activity. Devi et al. [19,20] discovered that when olivine was calcined at 900 °C in air, its activity towards naphthalene conversion improved. This was suggested to originate from the segregation of iron to the surface of the olivine particles and also from the iron(III) phases formed during calcination. However, high calcination temperature 1500 °C may decrease the porosity and the activity [5].

The catalytic nature of different bed materials at atmospheric pressure has been well covered in earlier studies, but their activity in pressurised gasification conditions is not well known. Systematic comparison of bed material activities in pressurised conditions is lacking, although some publications feature studies performed with one single bed material at a few pressure levels, for example with olivine [21,22]. Pressurised gasification becomes relevant in process concepts where the final steps of the process chain operate at high pressures, such as the FT-synthesis for producing FT-liquids. In those cases, the costs caused by the final compression of the product gas to the synthesis pressure could be reduced by elevating the pressure in the front-end gasification process i.e. in gasification and gas cleaning. As an example, the cost saving potential for a methanol production process based on oxygen/steam-blown gasification of biomass was estimated at around 3–4% reduction in the methanol production costs when the gasification pressure was elevated from 1 bar to 5 bar [23]. Thus, it is of great interest to consider the bed material activities also at higher pressures and to study whether they pose technical challenges to the gasification process operating in pressurised conditions.

In this work, the effect of pressure on the tar decomposition activity of different bed materials was evaluated in biomass gasification conditions. Experiments were divided into two parts. The studies were initiated by bench-scale fluidised-bed gasification experiments at atmospheric pressure with bark pellets as feedstock. After that, laboratory-scale tests using a fixed-bed reactor were carried out with simulated gasification gas in the pressure range of 1–10 bar. A gas composition resembling that obtained in the gasification tests was used as feed gas; the aim was to compare the activity of bed materials as a function of pressure in easily controllable laboratory conditions, not to compare the two reactor technologies.

2. Experimental

2.1. Fluidised-bed gasification tests at atmospheric pressure

2.1.1. Experimental conditions and test procedure

The fluidised-bed gasification tests with different bed materials were carried out in a bench-scale atmospheric pressure bubbling fluidised-bed gasifier (AFB60) with a bed and freeboard diameter of 63 mm and 102 mm, respectively. A more detailed description and a schematic diagram of the used test rig is given in [24]. The experiments were performed in air/steam gasification conditions (75/25 vol.% air/steam) where the air/steam mixture was fed as primary fluidising gas and no secondary or tertiary air was used. Bark pellets (Table 1), which were crushed and sieved to 0.5–1.0 mm particle size, were used as feedstock. Bed materials were

Table 1
Feedstock composition.

Feedstock	Bark pellets
Moisture content, wt.%	8.6
LHV, MJ/kg (dry)	19.9
Proximate analysis, wt.% (d.b.)	
Volatile matter	70.8
Fixed carbon	25.3
Ash	3.98
Ultimate analysis, wt.% (d.b.)	
C	53.2
H	5.5
N	0.3
S	0.04
O (as difference)	37.1
Ash	3.9

d.b. = dry basis

tested under constant gasification conditions during 6–7-h tests: gasification temperature 850 °C, fluidising velocity 0.30 m/s, air ratio 0.22, gas residence time in the gasifier 7 s and in the gasifier bed 0.5 s (calculated based on static bed height).

The bed volume was the same in each experiment; the static bed height was approximately 15–16 cm. Bed material was inserted as a batch at the beginning of the test, and no make-up bed material was added during the experiment, although some material was carried over to the filter over time as a result of attrition in the gasifier. The product gas was filtered at 800 °C by ceramic filter candles (Dia-Schumalith 10–20 KK by Pall Corporation). After each experiment, the gasifier and the filter were oxidised in a mixture of air/nitrogen at 850 °C and 700 °C, respectively, in order to determine the residual carbon content in the gasifier bed and on the filter.

The product gas composition was measured after the gasifier (upstream the filter unit) with an online gas analyser (ABB AO2020) as well as a micro GC (Varian CP-4900 equipped with a TC detector) which sampled every 15 min. The continuous gas analyser, which was mainly applied for monitoring the process stability during the experiments, measured the CO, CO_2, H_2, CH_4 and O_2 content in dry gas. The micro GC was used for analysing CO, CO_2, H_2, CH_4, O_2, N_2 and C_2–C_5 hydrocarbons. Tars were measured after the gasifier (upstream the filter unit) according to the European Tar Protocol [25] and samples were taken in isopropanol. The samples were analysed for benzene and 52 tar compounds up to coronene with a GC equipped with a FID detector (Agilent 6890A, column: Agilent 19091B-112 Ultra 2). A GC with a TC detector (HP 5890 series II, column: PoraPLOT U) was used for quantifying the water content from tar samples. The used sampling and analytical methods are explained in more detail in [24].

2.1.2. Tested bed materials

Four different bed materials were selected for the fluidised-bed gasification tests: sand (Maxit hiekkatuote, Finland), dolomite (Myanit D, Sweden), MgO (M85, Slovakia) and a 50/50 wt.% olivine B/kaolin mixture. The bed material properties are given in Table 2. Silica sand was used as a reference point in the experiments as it has no catalytic effect with respect to tar reduction. All bed materials were sieved to 0.1–0.25 mm particle size except for the olivine B/kaolin mixture which was used as received (around 80 wt.% of the particles below 0.5 mm). Dolomite was calcined in-situ in nitrogen atmosphere before start-up. No pre-treatment was applied for the other bed materials in gasification experiments.

Table 2
Properties of the used bed materials.

Bed material	Sand	Dolomite (Myanit D)	MgO (M85)	Olivine A	Olivine B/ kaolin mixture
BET surface area[a], m^2/g	3.1	5.2[b]	16.2	3.5	4.9
Element, wt.% (XRF)					
Na	2.1	–	–	–	0.02
Mg	0.56	12	50	29	24
Al	6.7	0.44	0.14	0.52	2
Si	35	2.3	0.42	19	18
P	0.07	–	0.02	–	–
S	–	–	0.05		0.01
Cl	0.01	–	0.06		0.01
K	2.8	0.08	0.02	0.04	0.06
Ca	2.2	21	4.1	0.08	2.1
Ti	0.14	0.01	0.01	–	0.08
V	–	–	–	–	–
Cr	–	–	–	0.19	0.3
Mn	0.03	0.07	0.40	0.09	0.11
Fe	1.8	0.4	6.0	6.4	7.2
Co	–	–	–	0.02	0.02
Ni	–	–	–	0.44	0.49
Cu	0.01	–	–		–
Zn	–	–	–		–
Rb	0.01	–	–	–	–
Sr	0.04	–	–	–	–
Zr	0.01	–	–	–	–
Ba	0.09	–	–	–	–

"–" = below detection limit (<0.01 wt.%).
[a] Determined from unused bed material samples.
[b] Determined from the carbonate form ($CaCO_3$·$MgCO_3$).

The same bed materials were later tested in laboratory-scale experiments except for the olivine B/kaolin mixture. This mixture was replaced by pure olivine A (Table 2) because it contained too fine particles which would have passed through the quartz sinter on top of which the bed material was packed. Sand, dolomite, MgO and olivine A were sieved to the particle size of 0.25–0.56 mm for the laboratory-scale tests.

2.2. Laboratory-scale tests in a fixed-bed reactor at pressurised conditions

2.2.1. Experimental setup and sampling

The laboratory-scale tests were conducted in a pressurised plug-flow reactor (PPFR, Fig. 1). The reactor itself was a quartz tube reactor which was placed inside a pressure vessel made of MA325 steel. The pressure vessel was equipped with a three-zone furnace which was used to heat up the reactor to the target operation temperature. Prior to the experiments, the axial temperature profile inside the reactor was determined with 2 l/min nitrogen flow while the furnace was set to 900 °C. Based on the defined temperature profile, the catalyst bed was placed in the hottest region of the reactor. The bed material was packed on top of a quartz sinter inside the tube reactor. Temperature was measured by a K-type thermocouple located inside a thermocouple pocket in the centre of the reactor.

All gases, which included CO, CO_2, H_2, CH_4, N_2, C_2H_4, H_2S and NH_3 in this study, were mass flow controlled and fed from gas cylinders (supplied by AGA). The gas purities were as follows: CO 99.97%, CO_2 99.99%, H_2 99.999%, CH_4 99.995%, N_2 99.999%, C_2H_4 99.95%, H_2S 0.500 mol.% in N_2, NH_3 5 mol.% in N_2. Gases were preheated to 300 °C. Water was fed by an isocratic pump to an evaporator and the generated steam was mixed with the dry gas components. Tar model compound mixture was fed by an isocratic pump through a capillary tube into the preheated gas stream where it evaporated. The feed gas mixture entered the reactor from the top. The operation pressure was adjusted by a pressure-control valve located downstream the reactor.

All hydrocarbons were analysed by an online GC Agilent 7890A equipped with two FID detectors. Light hydrocarbons C_1–C_5 were separated with GS-GASPRO column (30 m, 0.32 mm ID, film 20 μm) and tar compounds with HP-5 column (30 m, 0.32 mm ID, film 25 μm). The peaks of tar compounds present in the feed gas (benzene, toluene and naphthalene) were identified. The amounts of other GC-eluable tars were calculated based on the response factor of naphthalene. The response factor of naphthalene was chosen because the unidentified compounds were both lighter and heavier than naphthalene. FTIR (Calcmet 2388) was applied for measuring the water vapour and the NH_3 content in the gas. A continuous gas analyser (ABB AO2020) was used to analyse the CO, CO_2, H_2 and O_2 content in dry gas. CO and CO_2 measurement was based on non-dispersive infrared absorption, H_2 on thermal conductivity and O_2 on an oxygen cell detector. In order to check that a correct gas composition was fed to the reactor, also the inlet gas was measured for each set point by taking it through a bypass line.

2.2.2. Experimental conditions and test procedure

The feed gas composition used in the laboratory-scale bed material tests (Table 3) was derived from the fluidised-bed

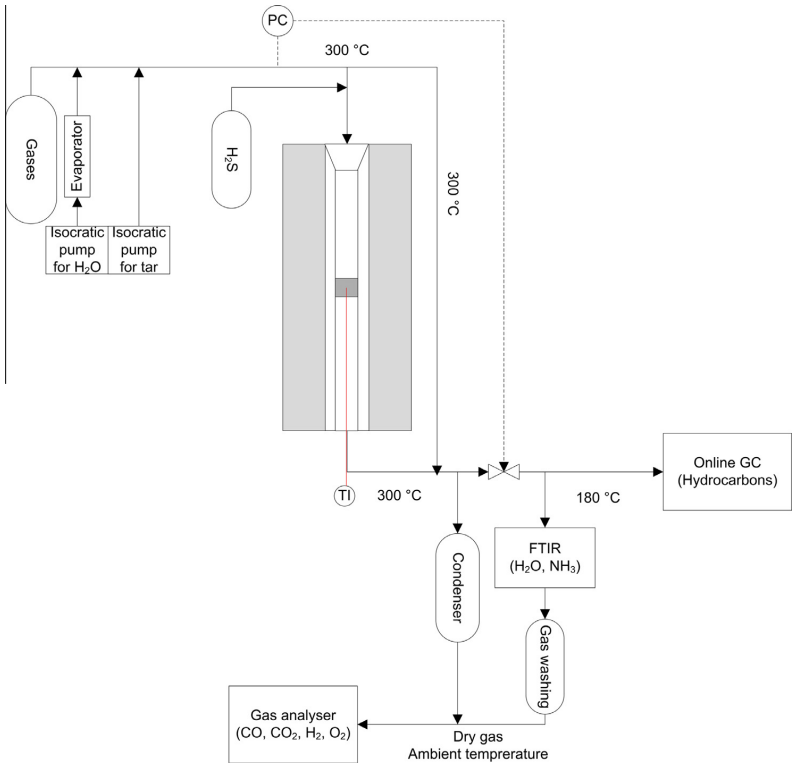

Fig. 1. Pressurised plug-flow reactor (PPFR) used in laboratory-scale tests.

Table 3
Feed gas composition used in bed material tests.

Dry gas composition									(wet basis)
CO vol.%	CO_2 vol.%	H_2 vol.%	CH_4 vol.%	N_2 vol.%	C_2H_4 vol.%	NH_3 ppm-v	H_2S ppm-v	Tar + benzene g/m^{3}n	H_2O vol.%
15.0	15.0	20.0	3.4	45.4	1.0	2000	100	10.0	12.0

experiments. A gas composition (measured after the gasifier) close to that obtained during air/steam gasification of crushed bark pellets in the presence of sand was selected. The tar model compound mixture consisted of 10 wt.% benzene (Merck, >99.7%), 80 wt.% toluene (Merck, ⩾99.9%) and 10 wt.% naphthalene (Merck, ⩾99%). The combined tar and benzene content was 10 g/m^{3}n (in dry gas). The feed gas also contained hydrogen sulphide and ammonia which are commonly present in biomass-based gasification gas. Their contents were not measured in bench-scale gasification tests with bark but typical concentrations [26,27] were chosen for the laboratory-scale tests.

The bed material tests were carried out at temperatures 850 °C and 900 °C and pressures 1, 5 and 10 bar(a). The temperature was measured from the middle of the catalyst bed. Dolomite was also tested in an additional pressure point of 2.5 bar(a) both at 850 °C and 900 °C. The residence time in the catalyst bed was kept constant at 0.1 s. In order to achieve the target residence time at all pressure levels, two different quartz tube reactors with inner diameters of 1.60 cm and 2.66 cm (equipped with a 0.4 cm thermocouple pocket) were used in the experiments. The gas flow rate varied between 1.4 and 7.2 l/min. The catalyst bed height was 2.5 cm or 3.8 cm depending on the conditions and the reactor diameter.

Because the form of calcium ($CaO/CaCO_3$) has been shown to affect the catalytic activity of dolomite [7], the test conditions were selected in a way to bring forth the impact of pressure both in calcined and carbonate states of dolomite (Fig. 2). At 850 °C, the 5 bar and 10 bar set points were in the carbonate region and the 2.5 bar and 1 bar set points in the calcining region, respectively. Whereas at 900 °C, only the 10 bar set point was in the carbonate region and the others in the calcining region. The differences in the catalytic activity between the oxide and carbonate forms of dolomite were further investigated in pressurised conditions at 5 bar and 850 °C. The CO_2 partial pressure in the feed gas was varied so that the calcium occurred either as oxide (25.7 kPa, 5.14 vol.% CO_2) or as carbonate (75.0 kPa, 15.0 vol.% CO_2). The total gas flow was kept constant by increasing the N_2 content in the same proportion.

The bed material tests were conducted in series where each test condition was maintained for around 2 h. Some set points were repeated in order to check whether the bed material had deactivated during the experiment e.g. due to carbon formation. The dolomite tests where the calcium was in calcined form were performed

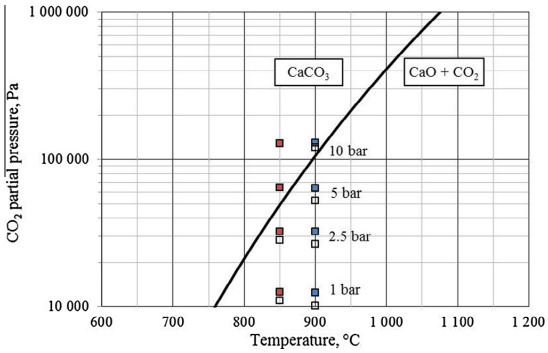

Fig. 2. Equilibrium decomposition curve of $CaCO_3$ in relation to the partial pressures of CO_2 in dolomite test conditions. Filled symbols represent CO_2 partial pressures measured at catalyst bed inlet and open symbols those measured at catalyst bed outlet.

separately from those where the calcium was as carbonate. Before the dolomite tests in calcined state, the fresh dolomite was treated in-situ at 900 °C and atmospheric pressure in constant nitrogen flow for 1 h in order to calcine the whole catalyst bed. The other bed materials, except for sand, were pre-treated similarly although no actual calcination was required. In the dolomite tests in carbonate state, the calcination procedure was not performed and the conditions were kept in the carbonate region at all times, even when moving from one set point to the next. This approach was taken because the calcium calcination/re-carbonation cycles have been reported to influence the tar decomposition activity of dolomite [7]. Magnesium was present as MgO in all tests with dolomite.

2.3. Calculation methods

2.3.1. Fluidised-bed gasification experiments

Mass balances (C, H, N, O, ash) were calculated for every test run using average values of the measured data. The gas composition obtained from the GC measurements was used in mass balance calculations instead of the online gas analyser data. The dry gas flow rate, which could not be measured during the experiments, was determined from nitrogen balance, and the content of water vapour in the gas was calculated from hydrogen balance. The calculated water vapour contents corresponded well with the values analysed from tar samples.

2.3.2. Laboratory-scale experiments

Several GC samples were taken of the inlet and outlet gas during steady-state conditions and an average was calculated. The elemental balances (C, H, N, O) were determined based on the measured inlet and outlet gas compositions. The dry gas flow rate at the reactor outlet was calculated from the carbon balance, while the dry gas flow rate at the reactor inlet was determined from the mass flow meters.

The form of calcium ($CaCO_3$/CaO) in dolomite tests was defined based on the feed gas composition by comparing the partial pressure of CO_2 with the calcium calcination/carbonation equilibrium in the test conditions. The equilibrium decomposition curve of $CaCO_3$ was determined from the following equation [28]:

$$\log_{10}K_1 \approx \log_{10}(p_{CO2}) = -8799.7/T_k + 7.521, \quad (1)$$

where K_1 is the equilibrium constant for the calcination/carbonation reaction, p_{CO2} is the equilibrium partial pressure of CO_2 (atm) and T_k is the temperature (K).

For the laboratory scale experiments, the possibility of carbon formation according to thermodynamic equilibrium was calculated by HSC Chemistry 8, Outotec simulation program.

The tar decomposition activity of the studied bed materials was evaluated based on the molar conversions of which were calculated from the inlet and outlet molar flows according to Eq. (2):

$$\text{Conversion, } \% = (n_{i,\text{in}} - n_{i,\text{out}})/n_{i,\text{in}} * 100\%, \quad (2)$$

where n_i represents molar flow of a compound i in mmol/s.

The total tar conversions were calculated taking into account toluene, naphthalene and tars that were formed in the catalyst bed. Benzene was excluded from the calculation because it is firstly not defined as "tar" and secondly, it is not considered as a harmful or challenging compound in downstream equipment, such as in filtration. The total hydrocarbon conversion was calculated based on the sum of the carbon moles of all the hydrocarbons.

Benzene was formed in all test conditions and therefore, benzene yield was determined (Eq. (3)):

$$\text{Yield} = n_{i,\text{out}}/n_{i,\text{in}}. \quad (3)$$

The selectivity of benzene from toluene was calculated by Eq. (4):

$$\text{Selectivity}_{\text{benzene}}, \ \% = n_{c\ \text{in benzene,out}}/(n_{c\ \text{in toluene,in}} - n_{c\ \text{in toluene,out}}) \quad (4)$$

For comparing the results from fluidised-bed and laboratory-scale tests at atmospheric pressure, the tar decomposing activity of the bed materials was determined in reference to sand from Eq. (5):

$$\text{Tar decomposing activity in reference to sand, } \% = (c_{\text{out,sand}} - c_{\text{out},x})/c_{\text{out,sand}} * 100\%, \quad (5)$$

where $c_{\text{out},x}$ denotes the tar concentration in mg/m^{3}n (dry basis) at the reactor/gasifier outlet for bed material x (dolomite, MgO, olivine A or olivine B/kaolin). The unidentified tar compounds that were formed in the catalyst bed in laboratory-scale tests were calculated as naphthalene.

3. Results

3.1. Elemental balances in experiments

In the fluidised-bed gasification experiments, the carbon and oxygen balances (out/in) ranged between 97–101% and 99–100%, respectively. The ash balances, 35–73%, remained incomplete in each test run most likely because the produced fly ash could not be fully retrieved from the filter unit. Carbon conversions to gas and tars are given in Table 4. In the laboratory-scale tests, the hydrogen, nitrogen and oxygen balances were within acceptable range: 95–105%. The molar flows for the compounds in laboratory experiments are given in the Appendix A.

3.2. Fluidised-bed gasification experiments

3.2.1. Gas composition

The gas compositions (after the gasifier) measured with the different bed materials are presented in Table 5. The results have been calculated as an average for the steady-state gasification

Table 4
Carbon conversions to gas and tars (%) in fluidised-bed gasification experiments.

Sand	Dolomite	Olivine B/kaolin	MgO
92.6	91.4	93.7	91.5

Table 5
Gas composition (purge N_2-free) measured after the gasifier in air/steam fluidised-bed gasification experiments with bark.

Gas composition (dry basis), vol.%	Sand	Dolomite	Olivine B/kaolin	MgO
CO	16.1	17.8	16.8	18.0
CO_2	15.9	14.5	15.6	14.9
H_2	20.2	25.8	24.2	25.9
N_2	42.7	38.4	39.0	37.6
CH_4	3.8	3.0	3.4	3.0
C_2H_2	0.02	0.00	0.00	0.00
C_2H_4	1.18	0.47	0.86	0.58
C_2H_6	0.07	0.04	0.07	0.05
C_3–C_5 hydrocarbons	0.00	0.00	0.00	0.01
Benzene, g/m^{3}n (per dry gas)	7.06	3.44	5.13	3.56
Toluene, g/m^{3}n (per dry gas)	0.56	0.14	0.32	0.16
Naphthalene, g/m^{3}n (per dry gas)	1.68	0.27	0.92	0.38
Tars in total, g/m^{3}n (per dry gas)	3.63	0.48	1.67	0.63
H_2O, vol.% (wet basis)	18.2	13.5	13.6	12.7

conditions based on the micro-GC data from which the diluting effect of purge nitrogen has been extracted. The use of dolomite, MgO and olivine B/kaolin mixture resulted in a distinct increase in hydrogen content (20–28%) and a small increase in carbon monoxide content (4–12%) compared to sand. The carbon dioxide content, on the other hand, was slightly reduced (2–9%). The largest changes in the gas composition occurred with bed materials with the highest catalytic activity for tar conversion, namely dolomite and MgO (see Section 3.2.2).

3.2.2. Tars

Fig. 3 shows the tar contents (in dry gas) obtained with the different bed materials, while the relative tar composition is given in Table 6. The GC-eluable tar compounds have been categorised according to the number of rings; GC-unidentified tars are included as the "unknown" group. The results represent an average of 3–5 tar measurements.

The activity of the studied bed materials decreased in the following order (Fig. 3): dolomite > MgO > olivine B/kaolin > sand. Compared to the reference case sand, the total tar concentration in the gas was reduced by 87%, 83% and 54% when dolomite, MgO and olivine B/kaolin were used, respectively. Also a shift towards lighter tars was observed, especially with the highly active dolomite and MgO (Table 6).

With all the studied bed materials, the two dominant tar groups were the 2-ring and 1-ring compounds which, as combined, represented more than 77 wt.% of the total tar content. Also the two most abundant tar compounds were found in these groups: naphthalene (2-ring) and toluene (1-ring) which amounted to

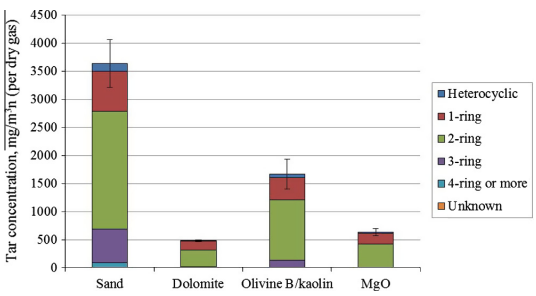

Fig. 3. Tar concentration (in dry gas) in fluidised-bed experiments. Error bars represent the standard deviations of total tar concentrations.

Table 6
Tar composition obtained with different bed materials in fluidised-bed gasification tests.

Tar composition, wt.%	Sand	Dolomite	Olivine B/kaolin	MgO
Heterocyclic	3.6	1.9	3.9	3.3
1-ring	19.8	33.9	23.6	30.2
2-ring	57.6	60.5	64.4	65.0
3-ring	16.7	0.0	8.1	1.5
4-ring or more	2.2	0.0	0.0	0.0
Unknown	0.2	3.7	0.0	0.0
SUM (unidentified incl.)	100.0	100.0	100.0	100.0

46–59 wt.% and 15–28 wt.% of total tars, respectively. With sand, tar comprised a wide spectrum of compounds ranging from pyridine (heterocyclic compound) up to pyrene (4-ring compound). Altogether 23 different tar compounds were detected with GC: indene, acenaphthylene, phenanthrene, styrene and fluorine being the five most abundant compounds after naphthalene and toluene. When dolomite was applied, only five different tar compounds could be detected: 1H-pyrrole, toluene, styrene, indene and naphthalene. The concentration of tars decreased in all tar groups, while tars with 3 or more rings were completely eliminated. Consequently, the relative share of heterocyclic tars was reduced by 47%, whereas the relative share of 1 to 2-ring compounds increased in comparison to sand. Similar changes in the tar composition were obtained with MgO but in addition to the five tar compounds reported for dolomite, also 3-ring compounds were present in trace amounts (acenaphthylene and acenaphthene, 10 mg/m^{3}n in total). The tar composition obtained with the olivine B/kaolin mixture was the closest to that of sand. However, the use of olivine B/kaolin resulted in a 78 wt.% reduction in the amount of 3-ring compounds and tars with 4 or more rings were fully eliminated. The heaviest tar compound in this case was phenanthrene.

3.3. Laboratory-scale experiments

3.3.1. Form of calcium in dolomite tests

As can be observed from Fig. 2, the changes in the CO_2 content over the dolomite bed did not cause the calcium to shift from carbonate to oxide or vice versa in any of the set points. Thereby, the dolomite bed was either in fully carbonate or oxide state during the experiments.

To separate the impacts of pressure and the state of calcium in dolomite tests, the activities of oxide and carbonate forms of dolomite were studied at one pressure level (5 bar and 850 °C) by varying the CO2 partial pressure (Table 7). Interestingly, there was no clear difference between the two cases.

3.3.2. Tar conversion over the tested bed materials

The impact of pressure on tar conversion over dolomite, MgO and olivine A was studied in the range of 1–10 bar and compared with sand. Ethene, toluene, naphthalene and total tar conversions are illustrated in Fig. 4. Fig. 5 shows the benzene yield and concentration of tar compounds produced on the catalyst bed (other than benzene, toluene and naphthalene). The concentrations represent a

Table 7
Benzene and tar conversions in tests with dolomite (5 bar and 850 °C) where the CO_2 content in the feed gas was varied.

Form of calcium	Oxide	Carbonate
CO_2 partial pressure, kPa	25.7	75.0
Toluene, %	92	99
Naphthalene, %	14	13
Total tars (excl. benzene), %	81	88

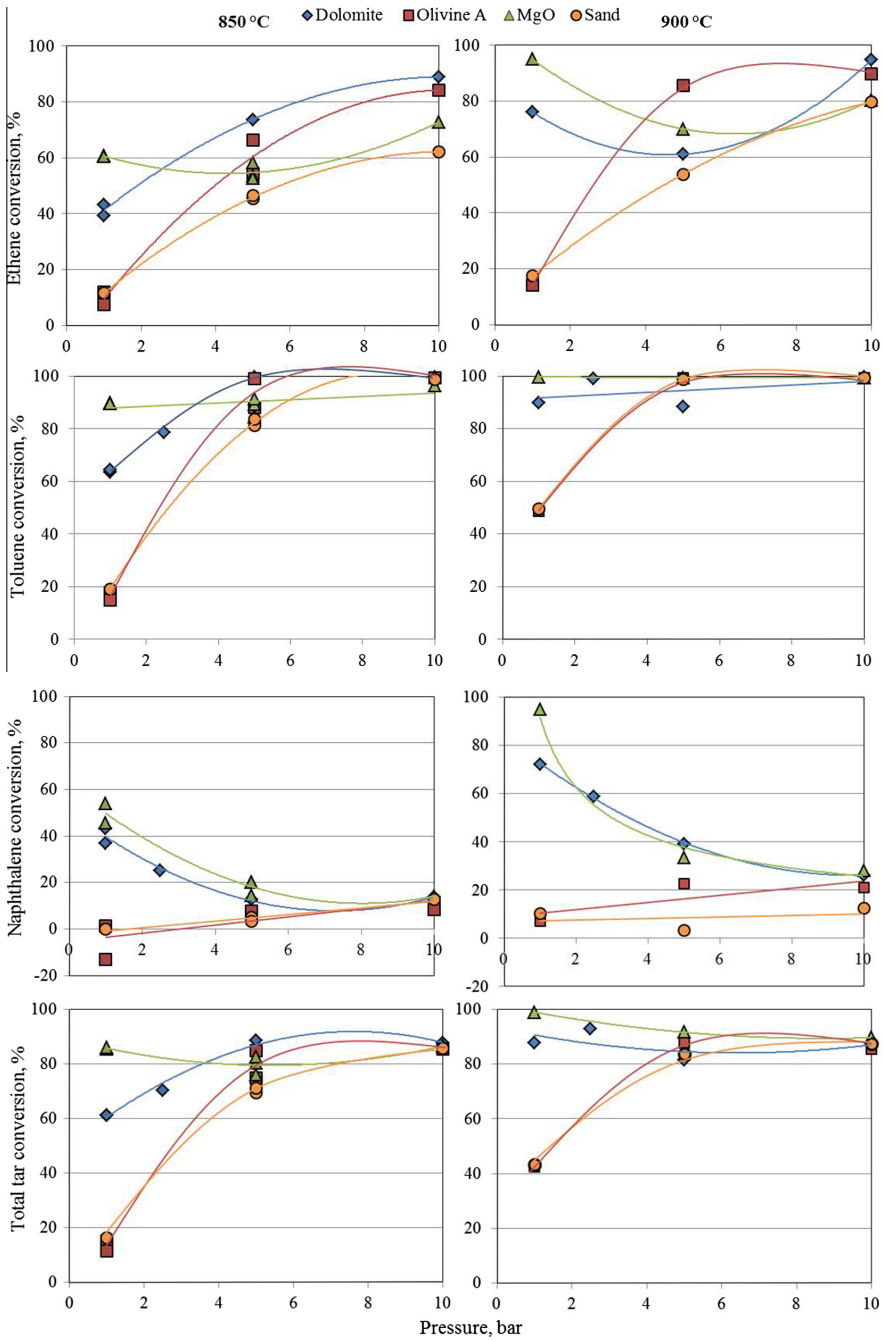

Fig. 4. Ethene, toluene, naphthalene and total tar conversion at 850 °C (left) and 900 °C (right). Note that the trend lines in figures are solely for eye guidance.

sum of tars as the individual compounds were not identified. In Fig. 4, it should be noted that the toluene conversions of sand and olivine A completely overlap at 900 °C. Furthermore, the toluene conversions of MgO overlap with those of sand and olivine A at the 5 bar and 10 bar points at 900 °C.

Among the tested bed materials, dolomite and MgO exhibited the highest activity towards tar elimination. The highest total tar conversions were obtained at 1 bar with MgO: 85% and 99% at 850 and 900 °C, respectively. Quite expectedly, tar conversions were enhanced by increasing the temperature. As can be seen from

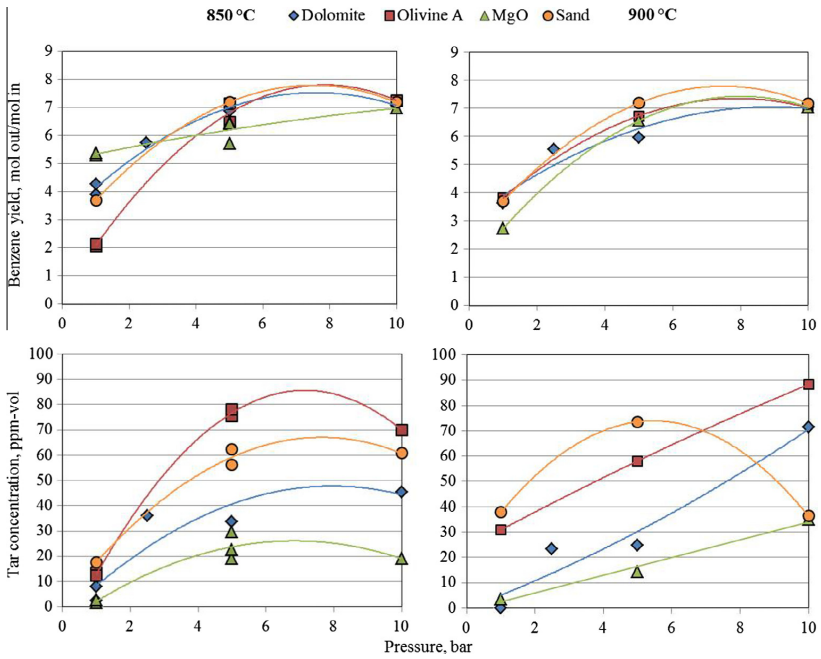

Fig. 5. Benzene yield and concentration of tar compounds formed on the bed material (excluding benzene, toluene and naphthalene) at 850 °C (left) and 900 °C (right). Note that the trend lines in figures are solely for eye guidance.

Fig. 4, dolomite and MgO had quite similar activities. Olivine A, on the other hand, was found to behave in many respects similarly to sand, although studies by others [5,11–15,29,30] have suggested at least moderate catalytic activity towards tar decomposition. Thus, based on the laboratory-scale experiments, the studied bed materials can be divided into two categories:

(1) Catalytically active bed materials, dolomite and MgO, which generally achieved higher tar conversions compared to inert sand.
(2) Inert bed materials, sand and olivine A, in the presence of which tars are only affected by thermal reactions.

These two categories showed a different behaviour with respect to tar conversion as a function of pressure. With sand and olivine A, the total tar conversion increased with pressure at both temperatures. This is mostly due to the steeply increasing toluene conversion. A small increase was also observed for naphthalene conversion, but since naphthalene is thermally more stable than toluene, the effect remained clearly minor. With dolomite and MgO, the effect of pressure on the total tar conversion was not as pronounced as with sand and olivine A; the total tar conversions remained in the same range or slightly reduced at higher pressures. Likewise with sand and olivine A, pressure enhanced toluene conversion over dolomite, although the effect was not as significant. With MgO, the toluene conversion was almost constant in the studied pressure range due to the high conversions obtained already at 1 bar. As for naphthalene, pressure had an adverse effect on naphthalene conversion with dolomite and MgO compared to sand and olivine A. A declining trend was observed with increasing pressure at both temperatures when dolomite or MgO was used. This explains to large extent the slightly reduced total tar conversions obtained at higher pressures.

Benzene was formed in all tested conditions and higher pressure promoted its formation (Fig. 5). Simultaneous decomposition of toluene and formation of benzene suggests that benzene was mostly produced by demethylation of toluene. The selectivity of benzene from toluene (Fig. 6) was close to 100% except at 850 °C, 1 bar with olivine where it was clearly larger and at 900 °C, 1 and 2.5 bar with dolomite and MgO where it was lower. The lower selectivity with MgO and dolomite can be explained by their high steam reforming activity.

It is worth noting that at elevated pressures toluene decomposition dominated the total tar conversion and thereby, high conversions were obtained even in the case of sand at 5 bar and 10 bar. Thus, naphthalene conversions were considered to best represent the tar decomposing activity of dolomite and MgO due to the thermal stability of naphthalene. As can be seen from the naphthalene conversions in Fig. 4, dolomite and MgO were highly active at 1 bar while at 5 bar and 10 bar, the conversions approached those obtained with sand. The tar decomposing activity of MgO and dolomite was, thus, clearly reduced at higher pressures. With dolomite, the conversions dropped both in calcined and carbonate forms.

Ethene was converted with all the bed materials either by steam reforming to syngas compounds or by thermal reactions producing tars or carbon (Fig. 4). In an earlier study of thermal formation of tar from ethene [31] it was observed that ethene forms light hydrocarbons and tar compounds and the share of heavier tar compounds increases when the pressure increases. In this study, more unidentified tar compounds were formed with increasing pressure with all the bed materials. The unidentified compounds were both lighter and heavier than naphthalene, but with increasing pressure the share of heavier compounds increased. This indicates that also polymerisation reactions of tars took place or more tars were formed from light hydrocarbons.

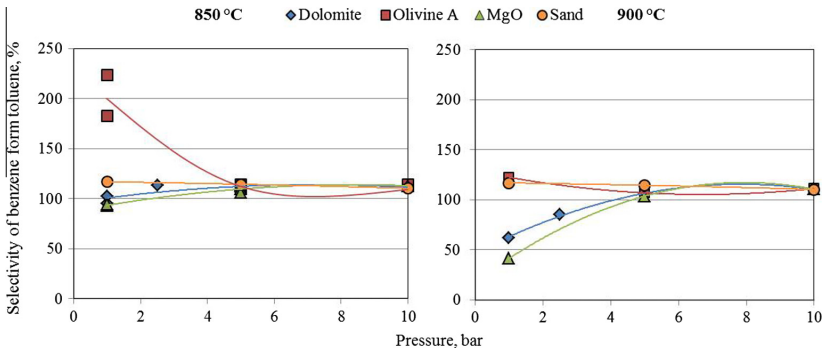

Fig. 6. Selectivity of benzene from toluene at 850 °C (left) and 900 °C (right). Note that the trend lines in figures are solely for eye guidance.

Total conversion of hydrocarbons to gases or carbon (Fig. 7) was calculated based on the number of carbon moles in hydrocarbons. This was done to clarify if hydrocarbons just convert to each other's or if they are converted to gases. In addition to steam reforming, it is possible that part of the carbon in the hydrocarbons end up forming carbon in the bed. In the steam reforming reactions, more gas molecules are formed. According to the Le Châtelier's principle, the increase of pressure in this case would push the reaction on the side of starting materials, which would hinder the reforming of hydrocarbons. From total hydrocarbon conversion, it can be seen that at both temperatures with all the bed materials, the total hydrocarbon conversion ends up to around 5% at 10 bar.

According to thermodynamic equilibrium calculations made, carbon should not be formed in the conditions of the experiments. However, some carbon was visually observed on the quartz reactor and in the bed after the experiments, but the amount was not measurable by weighting the bed nor did it deactivate the bed material during the experiments.

4. Discussion

4.1. Comparison between fluidised-bed gasification tests and laboratory-scale test

In this study, the selected bed materials were first tested in fluidised-bed gasification conditions at atmospheric pressure. The influence of pressure on their catalytic activity was then investigated in laboratory-scale tests where gasifier conditions were simulated. However, the difficulty in creating representative conditions such as in the gasifier bed is that in a fluidised-bed gasifier, the bed material is exposed to nascent tars whereas more mature tar compounds (toluene and naphthalene) were used in laboratory-scale tests. These two types of tars may have a different response to catalytic bed materials which can come across as differences in tar conversions between the two test series. It has been proposed that tars present in the gasifier bed may be more easily decomposed over catalytic materials as they have not yet been polymerised into heavier compounds [32]. The selection of toluene and naphthalene to model tar in the laboratory-scale tests was, however, justified as they were the two most abundant tar compounds present in the gas in the fluidised-bed tests.

Table 8
Comparison of fluidised-bed gasification tests and laboratory-scale tests at atmospheric pressure: tar decomposing activity in reference to sand,%.

Fluidised-bed gasification tests, 850 °C	Dolomite	MgO	Olivine B/kaolin
Toluene, %	75	72	43
Naphthalene, %	84	78	45
Total tars (excl. benzene), %	87	83	54
Lab-scale tests, 850 °C	Dolomite	MgO	Olivine A
Toluene, %	57	88	2
Naphthalene, %	40	56	1
Total tars (excl. benzene), %	55	83	2
Lab-scale tests, 900 °C	Dolomite	MgO	Olivine A
Toluene, %	81	99	2
Naphthalene, %	71	95	1
Total tars (excl. benzene), %	80	98	2

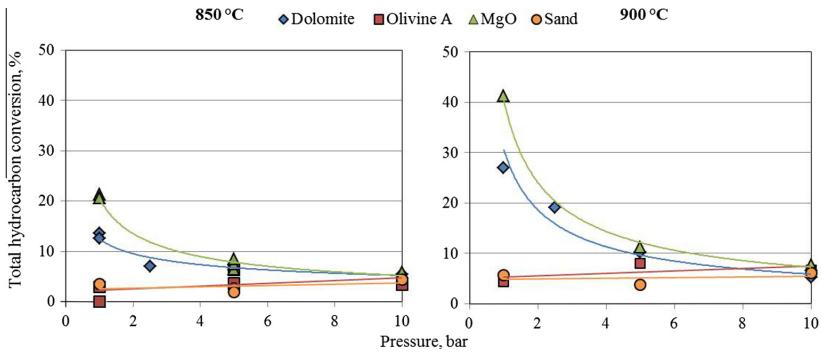

Fig. 7. Total conversion of hydrocarbons based on carbon moles at 850 °C (left) and 900 °C (right). Note that the trend lines in figures are solely for eye guidance.

Table 8 summarises the results from the fluidised-bed and laboratory-scale tests at atmospheric pressure expressed in terms of tar decomposing activity in reference to sand, as is explained in 2.3. Clearly, dolomite was more active in the fluidised-bed gasification tests than in the laboratory-scale tests at 850 °C. When the temperature was increased to 900 °C, the tar conversions were of the same order as obtained in the fluidised-bed gasification tests already at 850 °C. MgO, on the other hand, showed a similar activity in both tests at 850 °C, although the conversions of individual compounds (toluene and naphthalene) were not the same. Hence, it seems that dolomite may be more sensitive to the nature of tars and is more efficient in converting less mature tar compounds when used as in-bed catalyst in the gasifier bed. On the contrary, the catalytic activity of MgO appears to be less dependent on the tar composition than with dolomite.

Also other factors may explain the differences observed for dolomite. Firstly, in the fixed bed experiments the bed is not isothermal and the temperature was measured only from the middle of the bed thus the part of the bed might be colder than the measured temperature. Secondly, two different types of reactors were used; the gasifier was a bubbling fluidised-bed reactor and a fixed-bed reactor was employed for the laboratory-scale tests. The residence time in the fluidised-bed reactor was around 0.5 s in the gasifier bed whereas it was only 0.1 s in the laboratory-scale fixed-bed reactor. In addition, the particle size of the bed materials was smaller in the fluidised-bed experiments, leading to higher surface area which may also explain the higher activity.

The largest differences between the two test series were obtained in tests with olivines. The obvious explanation for this discrepancy is that different materials were used in the experiments: a 50/50 wt.% mixture of olivine B and kaolin compared to pure olivine A. In fluidised-bed conditions with the olivine B/kaolin mixture, the total tar content was reduced by 54% in comparison to sand but in laboratory-scale tests, the pure olivine A was inactive and behaved like sand. Kaolin, which is a clay mineral composed of aluminium silicate, may have participated in tar conversion in the fluidised-bed gasification test as it has been reported to have some catalytic effects towards tar decomposition [1,33,34], although not as significant as e.g. with dolomite [34].

Based on our experiment in the gasifier, it is not clear whether the catalytic activity of kaolin could have dominated tar conversion test while olivine B was inert or if olivine B also acted as a catalyst. In addition to the possible activity of kaolin, also formation of calcium rich layer on olivine particles as reported by Kirnbauer [16,17] in fluidised bed conditions may have affected the conversions. In this study, the gasifier bed was oxidised after the experiment. Therefore, the bed material sample was no longer representative and the possible coating effect could not be examined in order to verify if coating had occurred and whether it could explain the activity. Obviously, this type of coating could not take place in laboratory-scale tests where the bed material was exposed to simulated gasification gas instead of biomass feedstock.

In addition, olivine A and olivine B used in the mixture had different origins. Even though their elemental composition is relatively similar (Table 2), they may still exhibit different activities towards tar decomposition due to pre-treatments applied by the manufacturer. However, the BET surface areas determined for the unused olivine A and the olivine B/kaolin mixture were very similar (Table 2) indicating that at least the porosity of the material could not explain the differences in their catalytic activity.

The low activity in laboratory-scale tests could also be explained by the same factors as already presented for dolomite: different tar composition, reactor type, particle size and residence time. It is, however, unlikely that these differences would have caused olivine to completely lose its activity in laboratory-scale tests.

4.2. Catalytic activity of the studied bed materials

Both in the fluidised-bed gasification tests and in the fixed-bed tests carried out with simulated gasification gas, dolomite and MgO had the highest activity in tar conversion among the tested bed materials. In both test conditions, the catalytic activity of MgO was comparable to that of dolomite. This is in good agreement with studies by Delgado et al. [35,36] where calcined dolomite, magnesite and calcite were applied as tar removal catalysts in a secondary reactor located downstream the gasifier. Tar conversions of the same order were obtained with dolomite and magnesite, especially above 850 °C, while treating gas derived from steam gasification of pine sawdust.

In the fluidised-bed experiments at atmospheric pressure, particularly the heaviest tar fraction (tars with 3 or more rings) was efficiently eliminated in the presence of dolomite and MgO, and the amount of heterocyclic compounds was considerably reduced. Similar observations were made by Simell et al. [37] when gas originating from an industrial-scale updraft gasifier was treated over a dolomite bed at 900 °C. The selective removal of heavy tars could be explained by two ways: either the formation of heavy tars is inhibited over dolomite and MgO bed or these materials particularly catalyse their decomposition. The use of highly active bed materials also influenced the gas composition by yielding more hydrogen and carbon monoxide in relation to the base case sand. This is likely to be caused by the reforming reactions of tars and light hydrocarbons.

In the laboratory-scale tests, dolomite and MgO exhibited the highest activity towards tar conversion at 1 bar, while their catalytic activity reduced at higher pressures. The naphthalene conversions decreased progressively until 10 bar, where the conversions were close to those of sand. Although dolomite and MgO were not particularly active with respect to naphthalene conversion at higher pressures, they still seemed to inhibit tar formation as slightly less unidentified tars were formed compared to inert materials (Fig. 5). With inert sand, the toluene and naphthalene conversions increased with pressure which indicated that higher pressures, on the other hand, enhanced thermal decomposition of tars. However, at 10 bar the total conversion of hydrocarbons was the same with all the bed materials (Fig. 7).

Based on the literature [7], the deactivation of dolomite at higher pressures was assumed to be caused by the increasing CO_2 partial pressure due to which CaO is converted into $CaCO_3$ – the less active form. Therefore, a clear difference in the activity between the carbonated and the calcined dolomite was expected. However, the results did not agree with this assumption. When the pressure was increased from 1 bar to 5 bar, the activity decreased both at 850 °C (carbonate form) and 900 °C (oxide form) (Fig. 4). In order to separate the effect of pressure from that of the form of dolomite, an additional test was conducted at 5 bar, where the shift between carbonate/oxide was realised by changing the CO_2 partial pressure in the feed gas. Surprisingly, the conversions obtained with the two different CO_2 partial pressures were similar indicating that the carbonate form was as active as the oxide form (Table 7). Hence, it was concluded that the observed loss in the activity of dolomite in pressurised conditions was mostly caused by the increasing pressure instead of the transition between $CaO/CaCO_3$. The contradictory results between this work and the study by Simell et al. [7] could be related to the used feed gas composition. Simell et al. [7] used toluene as tar model compound in a simplified gas mixture which consisted of N_2, CO_2 and H_2O. In this study, a gas mixture resembling real biomass gasification gas with benzene, toluene and naphthalene as tar model compounds was employed. Also ethene was present in the feed gas which is likely to influence the tar conversions as it may be converted to tars or carbon [31] in the catalyst bed. In addition, Simell et al. [7]

conducted the experiments at higher pressure, at 20 bar, while the pressure range was 1–10 bar in this study.

The results concerning the catalytic activity of olivine were twofold. In the fluidised-bed gasification test at atmospheric pressure, a moderate tar conversion was obtained with the olivine B/kaolin mixture. Its catalytic activity towards tar decomposition was of the same order as reported for olivine in steam gasification conditions [29]. In the laboratory-scale tests, the pure olivine A

Table A1
Molar flows of the compounds in the laboratory scale experiments with sand.

Temperature	850 °C					900 °C			
P, bar	1	1	2.5	5	10	1	2.5	5	10
Inlet, mol/s $*10^{-6}$									
CO	153.2	170.8	170.8	338.2	148.7	165.9	335.9	153.2	170.8
CO_2	142.9	165.1	165.1	327.0	136.9	164.8	324.7	142.9	165.1
H_2	191.3	219.1	221.3	436.7	184.3	210.0	438.9	191.3	219.1
N_2	442.5	513.4	511.4	1026.2	423.7	482.8	1026.2	442.5	513.4
H_2O	143.6	173.8	173.8	364.6	146.2	169.5	358.5	143.6	173.8
CH_4	33.33	37.79	37.64	76.79	32.09	36.83	78.23	33.33	37.79
C_2H_4	10.58	11.70	11.80	23.33	10.05	11.54	24.01	10.58	11.70
C_2H_6	0	0	0	0	0	0	0	0	0
Other light hydrocarbons	0	0	0	0	0	0	0	0	0
Benzene	0.292	0.315	0.327	0.655	0.275	0.305	0.653	0.292	0.315
Toluene	1.869	2.107	2.083	4.232	1.767	1.969	4.309	1.869	2.107
Naphthalene	0.214	0.269	0.263	0.540	0.216	0.248	0.539	0.214	0.269
Unidentified tar compounds	0	0	0	0	0	0	0	0	0
Outlet, mol/s $*10^{-6}$									
CO	155.4	172.1	173.8	343.2	149.0	171.2	347.2	155.4	172.1
CO_2	143.1	165.3	163.6	327.5	140.6	161.5	322.5	143.1	165.3
H_2	192.1	215.9	214.4	417.3	182.0	207.0	409.9	192.1	215.9
N_2	447.9	514.6	519.1	1036.5	425.3	487.4	1037.3	447.9	514.6
H_2O	141.3	177.0	176.1	347.1	140.8	173.5	367.7	141.3	177.0
CH_4	33.08	41.41	42.42	92.48	31.98	43.55	101.1	33.08	41.41
C_2H_4	9.385	6.482	6.324	8.939	8.292	5.326	4.888	9.385	6.482
C_2H_6	0.252	3.059	3.095	6.244	0.251	2.240	5.657	0.252	3.059
Other light hydrocarbons	0.087	0.143	0.144	0.089	0.313	0.166	0.074	0.087	0.143
Benzene	0.572	2.013	2.050	4.491	1.024	2.225	4.720	0.572	2.013
Toluene	1.510	0.398	0.343	0.051	0.891	0.025	0.028	1.510	0.398
Naphthalene	0.215	0.259	0.254	0.478	0.195	0.243	0.476	0.215	0.259
Unidentified tar compounds	0.020	0.004	0.004	0.005	0.041	0.005	0.005	0.020	0.004

Table A2
Molar flows of the compounds in the laboratory scale experiments with dolomite.

Temperature	850 °C					900 °C			
P, bar	1	1	2.5	5	10	1	2.5	5	10
Inlet, mol/s $*10^{-6}$									
CO	156.3	156.3	343.5	179.0	351.0	152.7	339.2	747.3	337.2
CO_2	141.5	141.5	322.0	164.5	327.3	132.7	322.0	681.9	313.6
H_2	191.6	191.6	418.6	221.4	434.1	184.9	416.4	907.7	417.7
N_2	441.8	442.1	954.7	502.4	1013.0	425.1	959.3	2140.2	974.1
H_2O	145.4	133.6	332.2	155.5	323.7	126.6	340.8	636.7	272.1
CH_4	33.25	32.91	75.20	38.48	75.61	31.15	75.01	157.81	72.30
C_2H_4	9.995	9.891	21.74	12.03	22.43	9.80	22.15	47.74	21.46
C_2H_6	0	0	0	0	0	0	0	0	0
Other light hydrocarbons	0	0	0	0	0	0	0	0	0
Benzene	0.275	0.273	0.638	0.342	0.631	0.252	0.609	1.300	0.622
Toluene	1.780	1.761	4.140	2.201	4.053	1.633	4.022	8.354	4.005
Naphthalene	0.213	0.211	0.556	0.264	0.497	0.201	0.519	1.025	0.493
Unidentified tar compounds	0	0	0	0	0	0	0	0	0
Outlet, mol/s $*10^{-6}$									
CO	184.4	181.3	397.5	182.2	362.9	194.1	427.3	894.1	360.3
CO_2	122.9	125.2	279.1	167.3	323.9	109.0	263.6	568.7	298.5
H_2	180.8	181.9	380.6	214.9	409.0	176.8	382.6	816.0	379.3
N_2	437.3	438.8	949.2	523.1	1025.8	414.7	945.2	2112.7	978.9
H_2O	144.2	141.0	352.8	156.8	294.3	137.0	363.4	808.9	336.8
CH_4	35.76	34.59	82.11	45.77	93.72	35.74	89.33	188.28	104.45
C_2H_4	5.693	5.998	12.14	3.186	2.506	2.358	5.702	18.65	1.124
C_2H_6	0.233	0.285	2.778	3.743	8.805	0.104	1.031	3.913	2.647
Other light hydrocarbons	0.062	0.058	0.207	0.031	0.022	0.045	0.212	0.760	0.013
Benzene	1.075	1.163	3.687	2.370	4.510	0.911	3.384	7.789	4.397
Toluene	0.651	0.625	0.893	0.011	0.019	0.168	0.042	0.979	0.020
Naphthalene	0.121	0.134	0.419	0.232	0.433	0.056	0.215	0.626	0.365
Unidentified tar compounds	0.002	0.009	0.089	0.044	0.115	0.000	0.058	0.135	0.176

acted like inert sand. Similarly to sand, higher pressure increased its activity only by promoting thermal decomposition of toluene and naphthalene. The possible causes for the observed differences between the fluidised-bed and laboratory-scale tests with olivines were already discussed in 4.1.

5. Conclusions

The tar decomposition activity of sand, dolomite, MgO and olivine A or olivine B/kaolin mixture was investigated in biomass gasification conditions in a bubbling fluidised-bed gasifier

Table A3
Molar flows of the compounds in the laboratory scale experiments with olivine.

Temperature	850 °C					900 °C		
P, bar	1	1	5	5	10	1	5	10
Inlet, mol/s $*10^{-6}$								
CO	154.9	154.9	170.8	170.8	335.9	148.1	170.0	322.3
CO_2	146.2	146.2	166.3	164.0	331.4	139.3	156.4	313.7
H_2	191.1	191.1	219.1	220.2	438.9	183.4	210.1	419.0
N_2	439.9	440.7	511.3	512.3	1020.9	424.0	487.4	985.8
H_2O	130.6	130.6	173.8	173.8	352.5	125.1	147.8	332.5
CH_4	32.65	32.17	38.20	38.20	77.47	31.49	36.22	74.24
C_2H_4	0.285	0.269	0.331	0.331	0.667	0.266	0.315	0.622
C_2H_6	0	0	0	0	0	0	0	0
Other light hydrocarbons	0	0	0	0	0	0	0	0
Benzene	0.285	0.269	0.331	0.331	0.667	0.266	0.315	0.622
Toluene	1.836	1.716	2.171	2.171	4.327	1.717	2.025	4.022
Naphthalene	0.222	0.186	0.274	0.274	0.542	0.209	0.249	0.521
Unidentified tar compounds	0	0	0	0	0	0	0	0
Outlet, mol/s $*10^{-6}$								
CO	155.9	153.5	173.5	175.1	342.2	152.1	178.9	335.1
CO_2	147.1	147.5	165.6	164.9	328.8	138.2	153.7	309.1
H_2	189.5	188.6	213.0	213.5	413.8	180.4	202.7	391.3
N_2	453.7	450.6	516.5	518.1	1030.1	432.4	498.7	1007.9
H_2O	133.7	133.0	174.3	170.3	361.1	127.0	152.6	343.2
CH_4	32.77	32.56	43.38	43.98	96.74	31.67	49.55	99.44
C_2H_4	9.069	9.371	5.632	4.067	3.725	8.434	1.678	2.333
C_2H_6	0.223	0.240	3.390	4.042	9.526	0.228	1.494	5.439
Other light hydrocarbons	0.054	0.058	0.112	0.045	0.044	0.139	0.022	0.026
Benzene	0.589	0.573	2.185	2.356	4.903	1.022	2.149	4.442
Toluene	1.513	1.460	0.259	0.019	0.025	0.882	0.013	0.023
Naphthalene	0.219	0.211	0.258	0.252	0.503	0.195	0.195	0.419
Unidentified tar compounds	0.015	0.014	0.004	0.003	0.005	0.033	0.072	0.004

Table A4
Molar flows of the compounds in the laboratory scale experiments with MgO.

Temperature	850 °C						900 °C		
P, bar	1	1	5	5	5	10	1	5	10
Inlet, mol/s $*10^{-6}$									
CO	154.0	154.0	178.7	177.7	177.7	337.3	148.6	171.4	352.2
CO_2	143.4	143.4	157.6	157.6	157.6	304.2	137.4	151.0	317.2
H_2	191.8	191.8	222.2	222.2	222.2	423.1	183.9	212.1	441.6
N_2	443.1	443.1	509.6	510.7	510.6	978.3	425.2	490.4	1019.6
H_2O	133.2	133.2	152.9	152.9	152.9	315.4	128.1	155.3	325.7
CH_4	32.25	32.25	37.95	37.95	37.95	73.43	30.98	36.18	76.12
C_2H_4	0.270	0.270	0.332	0.332	0.332	0.617	0.262	0.301	0.633
C_2H_6	0	0	0	0	0	0	0	0	0
Other light hydrocarbons	0	0	0	0	0	0	0	0	0
Benzene	0.270	0.270	0.332	0.332	0.332	0.617	0.262	0.301	0.633
Toluene	1.720	1.720	2.133	2.133	2.133	3.979	1.729	1.923	4.089
Naphthalene	0.186	0.186	0.260	0.260	0.260	0.476	0.209	0.223	0.503
Unidentified tar compounds	0	0	0	0	0	0	0	0	0
Outlet, mol/s $*10^{-6}$									
CO	192.4	191.5	203.0	201.0	199.8	378.3	209.1	205.0	410.4
CO_2	119.6	119.9	138.6	140.4	142.5	272.4	104.2	125.8	271.2
H_2	184.1	183.3	198.0	195.1	196.7	366.0	187.2	185.6	370.4
N_2	439.9	440.3	519.8	510.0	511.2	958.8	418.8	483.1	1014.5
H_2O	144.8	144.7	162.4	174.8	189.3	361.3	134.6	175.1	390.9
CH_4	34.07	34.47	41.25	40.70	42.29	83.99	33.23	43.80	95.32
C_2H_4	3.972	4.006	5.576	5.677	5.017	6.005	0.499	3.308	4.519
C_2H_6	0.259	0.264	3.230	3.214	2.768	8.400	0.054	1.528	5.554
Other light hydrocarbons	0.044	0.051	0.094	0.105	0.091	0.082	0.015	0.088	0.074
Benzene	1.428	1.451	2.150	2.139	1.908	4.325	0.714	1.980	4.489
Toluene	0.177	0.180	0.228	0.185	0.332	0.150	0.005	0.012	0.026
Naphthalene	0.101	0.086	0.224	0.209	0.209	0.411	0.011	0.149	0.359
Unidentified tar compounds	0.002	0.003	0.024	0.029	0.038	0.047	0.004	0.018	0.090

operating at atmospheric pressure, and later in pressurised conditions in a laboratory-scale fixed-bed reactor with simulated gasification gas. Among the tested bed materials, dolomite and MgO exhibited the highest catalytic activity in both test conditions. They had similar tar decomposing activities. However, pressure seems to be challenging from the tar reduction point of view; both dolomite and MgO were sensitive to pressure and partly lost their catalytic activity at higher pressures. With dolomite, the loss of activity in pressurised conditions was found to be mostly associated with the increasing pressure rather than the form of calcium present in dolomite ($CaO/CaCO_3$).

Olivine B/kaolin mixture showed a moderate catalytic activity in fluidised-bed gasification conditions at atmospheric pressure, while pure olivine A was inactive in fixed-bed tests and performed similarly to inert sand. This contradiction could be related to the differences between the test conditions (gasifier/simulated gasification gas in laboratory) or different pre-treatments/origin of the two olivines but also to the possible catalytic activity of kaolin in the fluidised-bed test.

Of all the tested bed materials, MgO is an attractive alternative which could replace calcium-based bed materials in pressurised gasification conditions. Its activity is comparable to that of dolomite, but it is not as prone to cause bed sintering [8]. However, this study showed that the in-situ tar reduction in the gasifier by using catalytic bed materials becomes more difficult at higher pressures and thus, secondary tar removal methods will have a bigger role in pressurised gasification processes.

Acknowledgements

This research was carried out as a part of the 2G2020 project. The authors would like to acknowledge Tekes (The Finnish Funding Agency for Technology and Innovation), UPM-Kymmene, Metso Power, Foster Wheeler Energia, Fortum Power and Heat, Carbona and NSE Biofuels for the financial support in the project.

Appendix A

The calculated molar flows of compounds of the laboratory experiments are presented in the Tables A1–A4.

References

[1] Abu El-Rub Z, Bramer EA, Brem G. Review of catalysts for tar elimination in biomass gasification processes. Ind Eng Chem Res 2004;43:6911–9.
[2] Sutton D, Kelleher B, Ross JRH. Review of literature on catalysts for biomass gasification. Fuel Process Technol 2001;73:155–73.
[3] Dayton D. A review of the literature on catalytic biomass tar destruction milestone completion report, NREL/TP-510-32815; 2002.
[4] Shen Y, Yoshikawa K. Recent progresses in catalytic tar elimination during biomass gasification or pyrolysis—a review. Renew Sustain Energy Rev 2013;21:371–92.
[5] Corella J, Toledo JM, Padilla R. Olivine or dolomite as in-bed additive in biomass gasification with air in a fluidized bed: which is better? 2004;2000:713–20
[6] http://spectrum.andritz.com/index/iss_20/art_20_16.htm [accessed 09.04.15].
[7] Simell PA, Leppälahti JK, Kurkela EK. Tar decomposing activity of carbonate rocks under high CO2 partial pressure. Fuel 1995;74:938–45.
[8] Kurkela E, Kurkela M, Hiltunen I. The effects of wood particle size and different process variables on the performance of steam-oxygen blown circulating fluidized-bed gasifier. Environ Prog Sustain Energy 2014;33:681–7.
[9] Simell P. Catalytic hot gas cleaning of gasification gas. VTT Publications 330. VTT Technical Research Centre of Finland; 1997.
[10] Hofbaue H, Rauch R, Bosch K, Koch R, Aichernig C. Biomass CHP plant Güssing – a success story. Expert Meeting on Pyrolysis and Gasification of Biomass and Waste. Strasbourg, France; October 2002.
[11] Rapagnà S, Jand N, Kiennemann A, Foscolo PU. Steam-gasification of biomass in a fluidised-bed of olivine particles. Biomass Bioenergy 2000;19:187–97.
[12] Devi L, Ptasinski KJ, Janssen FJJG, van Paasen SVB, Bergman PCA, Kiel JHA. Catalytic decomposition of biomass tars: use of dolomite and untreated olivine. Renew Energy 2005;30:565–87.
[13] Miccio F, Piriou B, Ruoppolo G, Chirone R. Biomass gasification in a catalytic fluidized reactor with beds of different materials. Chem Eng J 2009;154:369–74.
[14] Abu El-Rub Z, Bramer EA, Brem G. Experimental comparison of biomass chars with other catalysts for tar reduction. Fuel 2008;87:2243–52.
[15] Kiel JHA, van Paasen JPA, Neeft JPA, Devi L, Ptasinski KJ, Janssen FJJG, et al. Primary measures to reduce tar formation in fluidised-bed biomass gasifiers. Final report SDE project P1999-012. ECN-C-04-014; 2004.
[16] Kirnbauer F, Wilk V, Kitzler H, Kern S, Hofbauer H. The positive effects of bed material coating on tar reduction in a dual fluidized bed gasifier. Fuel 2012;95:553–62.
[17] Kirnbauer F, Hofbauer H. Investigations on bed material changes in a dual fluidized bed steam gasification plant in Güssing, Austria. Energy Fuels 2011;25:3793–8.
[18] Kirnbauer F, Hofbauer H. The mechanism of bed material coating in dual fluidized bed biomass steam gasification plants and its impact on plant optimization. Powder Technol 2013;245:94–104.
[19] Devi L, Craje M, Thüne P, Ptasinski KJ, Janssen FJJG. Olivine as tar removal catalyst for biomass gasifiers: catalyst characterization. Appl Catal A Gen 2005;294:68–79.
[20] Devi L, Ptasinski KJ, Janssen FJJG. Pretreated olivine as tar removal catalyst for biomass gasifiers: investigation using naphthalene as model biomass tar. Fuel Process Technol 2005;86:707–30.
[21] Mayerhofer M, Mitsakis P, Meng X, de Jong W, Spliethoff H, Gaderer M. Influence of pressure, temperature and steam on tar and gas in allothermal fluidized bed gasification. Fuel 2012;99:204–9.
[22] Wolfesberger U, Aigner I, Hofbauer H. Tar content and composition in producer gas of fluidized bed gasification of wood – influence of temperature and pressure. Environ Prog Sustain Energy 2009;28:372–9.
[23] McKeough P, Kurkela E. Process evaluations and design studis in the UCG project 2004–2007. VTT Research notes 2434; 2008.
[24] Tuomi S, Kurkela E, Simell P, Reinikainen M. Behaviour of tars on the filter in high temperature filtration of biomass-based gasification gas. Fuel 2015;139:220–31.
[25] Biomass Gasification – Tar and Particles in Product Gases – Sampling and Analysis. TC BT/TF 143 WI CSC 03002.4. Technical Specification; 2004.
[26] Hepola J, Simell P. Sulphur poisoning of nickel-based hot gas cleaning catalysts in synthetic gasification gas II. Chemisorption of hydrogen sulphide. Appl Catal B Environ 1997;14:305–21.
[27] Leppälahti J, Simell P, Kurkela E. Catalytic conversion of nitrogen compounds in gasification gas. Fuel Process Technol 1991;29:43–56.
[28] Bryan BG, Goyal A, Patel JG, Ghate MR. Results of in-situ desulfurization tests in the U-gas coal gasification process. CONF-880915-1. Chicago, Illinois, USA: Institute of Gas Technology; 1988.
[29] Koppatz S, Pfeifer C, Hofbauer H. Comparison of the performance behaviour of silica sand and olivine in a dual fluidised bed reactor system for steam gasification of biomass at pilot plant scale. Chem Eng J 2011;175:468–83.
[30] Pfeifer C, Koppatz S, Hofbauer H. Catalysts for dual fluidised bed biomass gasification—an experimental study at the pilot plant scale. Biomass Convers Biorefinery 2011;1:63–74.
[31] Kaisalo NK, Koskinen-Soivi M-L, Simell PA, Lehtonen J. Effect of process conditions on tar formation from thermal reactions of ethylene. Fuel 2015;153:118–27.
[32] Corella J, Aznar M-P, Gil J, Caballero MA. Biomass gasification in fluidized bed: where to locate the dolomite to improve gasification? Energy Fuels 1999;13:1122–7.
[33] Wen WY, Cain E. Catalytic pyrolysis of a coal tar in a fixed-bed reactor. Ind Eng Chem Process Des Dev 1984;23:627–37.
[34] Simell P, Bredenberg JB. Catalytic purification of tarry fuel gas. Fuel 1990;69:1219–25.
[35] Delgado J, Aznar MP, Corella J. Calcined dolomite, magnesite, and calcite for cleaning hot gas from a fluidized bed biomass gasifier with steam: life and usefulness. Ind Eng Chem Res 1996;35:3637–43.
[36] Delgado J, Aznar MP, Corella J. Biomass gasification with steam in fluidized bed: effectiveness of CaO, MgO, and CaO – MgO for hot raw gas cleaning. Ind Eng Chem Res 1997;36:1535–43.
[37] Simell PA, Leppälahti JK, Bredenberg JB. Catalytic purification of tarry fuel gas with carbonate rocks and ferrous materials. Fuel 1992;71:211–8.

III

Kaisalo, N., Kihlman, J., Hannula, I., Simell, P. (2015) Reforming solutions for biomass-derived gasification gas – Experimental results and concept assessment. *Fuel* ***147***, 208-220.

Fuel 147 (2015) 208–220

Contents lists available at ScienceDirect

Fuel

journal homepage: www.elsevier.com/locate/fuel

Reforming solutions for biomass-derived gasification gas – Experimental results and concept assessment

Noora Kaisalo *, Johanna Kihlman, Ilkka Hannula, Pekka Simell

VTT Technical Research Centre of Finland, P.O. Box 1000, FI-02044 VTT, Finland

HIGHLIGHTS

- Biomass gasification gas could be reformed for around 500 h.
- Both steam and autothermal reforming are feasible depending on gas composition.
- To avoid carbon formation $H_2O/C_{REF} > 4$ and $O/C_{REF} > 8$ are recommended.
- Selection of reforming approach has only limited impact to the overall efficiency.

ARTICLE INFO

Article history:
Received 3 November 2014
Received in revised form 16 January 2015
Accepted 20 January 2015
Available online 31 January 2015

Keywords:
Biomass gasification
Steam reforming
Autothermal reforming
Performance analysis

ABSTRACT

Reforming is a key enabling technology for the production of tar and hydrocarbon free synthesis gas from biomass. In this work, two different reforming concepts, steam and autothermal reforming, were studied for cleaning of biomass-derived gasification gas. Long-term laboratory scale experiments (around 500 h) were carried out with two model biomass gasification gas compositions with low and medium hydrocarbon loads. The experiments were made using nickel and precious metal catalysts at atmospheric pressure and at temperatures around 900–950 °C. The deactivation of the catalysts was followed. Gas with low hydrocarbon content could be steam reformed with nickel and precious metal catalyst. Both autothermal and steam reforming modes were studied for gas with medium hydrocarbon content. In steam reforming mode, the catalysts deactivated more than in autothermal mode. Based on the experiments H_2O/C_{REF} molar ratio above 4 and O/C_{REF} molar ratio above 8 are recommended. A concept assessment was carried out to examine plant level impacts of the reforming approaches to synthesis gas production. The results showed that the choice of reforming concept has only limited impact to the overall efficiency of synthetic biofuel production.

1. Introduction

Fluidized bed gasification is an efficient way to convert woody biomass to synthesis gas (syngas), which can be further upgraded to renewable gaseous or liquid fuels or chemicals. However, in addition to synthesis gas components ($CO + H_2$), biomass gasification gas contains hydrocarbon remains, such as tar, methane and ethylene, which must be either removed or converted to CO and H_2 before the catalytic fuel synthesis can take place. Also other impurities, for example H_2S and ammonia, are present in the gas. There are two main approaches for cleaning tar from the gas: scrubbing with organic solvents or catalytic reforming. For synthetic fuels production, reforming of the remaining hydrocarbons can be used to (a) increase syngas yield and (b) reduce the coking tendency of fuel synthesis catalysts.

Reforming reactor design for this kind of application is challenging as the reactor is easily clogged by carbon formation from hydrocarbons. Also, deactivation of catalyst by H_2S affects the process. Several types of catalysts have been studied for the reforming of hydrocarbons in biomass gasification gas [1–9]. Transition metal catalysts are highly active in steam reforming of tar and light hydrocarbons. Typically, steam reforming type catalysts with nickel or precious metal as active component have been studied. Nickel catalysts are widely researched due to their high activity

Abbreviations: AH, autothermal reforming concept used for hydrogen production; AM, autothermal reforming concept used for methane production; DH, district heat; HH, high hydrocarbon content; LH, low hydrocarbon content; MH, medium hydrocarbon content; PM, precious metal catalyst; PSA, pressure swing adsorption; SH, steam reforming concept used for hydrogen production; SNG, synthetic natural gas; SM, steam reforming concept used for methane production.

* Corresponding author. Tel.: +358 40 685 7095.
E-mail address: noora.kaisalo@vtt.fi (N. Kaisalo).

http://dx.doi.org/10.1016/j.fuel.2015.01.056
0016-2361/

and lower price in comparison to precious metals. The downside of nickel is that it is more prone to coke formation than precious metal catalysts. In addition to steam reforming activity, nickel catalysts are efficient in ammonia conversion [10]. Precious metal catalysts for tar removal are less studied than nickel catalysts due to their higher price. Especially rhodium catalysts have been found to be more active and more resistant to coke formation and poisoning by H_2S than nickel catalysts [11].

Caballero et al. [12] reported a 50 h steam reforming experiment with almost 100% tar conversion with commercial nickel pellet catalyst. The feed gas was produced by air gasification using dolomite as bed material leading to the steam-to-reformable carbon (H_2O/C_{REF}) ratio between 2.2 and 3.1 and the tar content of 4.8–7.9 g/m^3_N. The gas was reformed at the temperature of 830–850 °C with GHSV of 3000–4000 h^{-1}. Wang et al. [13] tested nickel catalysts in a fluidized bed reformer for 100 h with air–steam gasification of pine sawdust. They obtained stable tar conversion for 100 h with NiO–MgO catalyst. However, they did not report the methane reforming activity in long term tests. The temperature in the reforming experiments was 780 °C, H_2O/C ratio was 2.2 and GHSV 15,000 h^{-1}. Wang et al. [14] also used NiO–MgO/γ-Al_2O_3/cordierite monolith catalysts in pilot scale autothermal reforming of gas from oxygen enriched air sawdust gasification. They reported 60 h test without blocking, but after reforming the gas contained 7–110 mg/m^3_N of tar.

Despite the extensive research done with different steam reforming catalysts, studies with long term reforming experiments using biomass gasification gas are rare. To be economically feasible reforming catalysts should retain their activity for 1–2 years [15]. For such a long operation time, coke formation should be completely avoided in the reformer. In the high temperatures (above 800 °C) present in the reformers for biomass gasification gas, the carbon growth begins as thermal formation of soot which settles on the walls and catalyst particles. In a steady state process the soot begins to accumulate on the catalyst bed and fills the voids between the catalyst particles finally forming solid graphite [16–18]. Eventually, the reactor will be blocked by the carbon. The main reactions affecting carbon formation at high operation temperatures (above 800 °C) are hydrocarbon decomposition (R1), (R2), methane decomposition (R3) and gasification of carbon (R4) [16]. In addition to coke formation, nickel catalysts are also poisoned by H_2S, even though poisoning can be overcome by operating at temperature of 900 °C or above [19].

$$C_nH_m \rightarrow nC + 0.5mH_2 \quad (R1)$$

$$C_nH_m \rightarrow \text{olefins} \rightarrow \text{coke} \quad (R2)$$

$$CH_4 \leftrightarrow C + 2H_2 \quad (R3)$$

$$C + H_2O \leftrightarrow CO + H_2 \quad (R4)$$

Reforming of unfiltered gasification gas by zirconia and nickel monolith catalysts has been successfully demonstrated over long periods in large scale demonstration CHP plants in Kokemäki, Finland [20,21] and Skive, Denmark [22]. However, filtering the gas before reforming simplifies construction and operation of the reformer as it allows the use of granular catalysts which are better available commercially. This has been the approach in the development of ultra clean syngas processes aiming for synthesis purposes. For this application, VTT has developed a staged reformer concept including oxidative ZrO_2 reforming stage and precious metal and nickel layers [23–26]. The staged reformer concept developed at VTT has been demonstrated to work for 500 h without problems of coke formation or deactivation in a 0.5 MW process design unit [15]. However, producing Fischer Tropsch liquids by oxygen blown gasification and with oxidative steam reforming requires large scales to alleviate the cost of cryogenic oxygen production.

Methane can be synthesised by hydrogenating carbon oxides over catalysts based on nickel and other metals (Ru, Rh, Pt, Fe and Co) [27] although all commercially available modern catalyst systems are based on nickel due to its favourable combination of selectivity, activity and price [28]. Conversion of synthesis gas to methane can be described with the following reactions:

$$CO + 3H_2 \leftrightarrow CH_4 + H_2O \quad \Delta H = -206\ \text{kJ/mol} \quad (R5)$$

$$CO_2 + 4H_2 \leftrightarrow CH_4 + 2H_2O \quad \Delta H = -165\ \text{kJ/mol} \quad (R6)$$

For hydrogen production, the hydrogen concentration is increased by water gas shift reaction (WGS, R7) after reforming of hydrocarbons from the gasification gas. After WGS the hydrogen rich gas is pressurized and hydrogen separated by pressure swing adsorption (PSA).

$$CO + H_2O \leftrightarrow H_2 + CO_2 \quad (R7)$$

This article concentrates on a concept where synthetic natural gas (SNG) or hydrogen is produced from biomass-derived synthesis gas by indirectly heated steam gasification coupled with hot filtration and either steam or autothermal reforming, see Fig. 1 for a schematic. The schematic presents a target process assuming that hot filtration at 820 °C is technically feasible. In steam gasification, the investment in oxygen plant may be avoided which makes it suitable for smaller scales. Additionally, the amount of byproduct heat from the process would also be smaller and easier to utilize fully as district heat. The dual reactor system is complicated to pressurize, making it more suitable for end products that can be produced at relatively low pressure. In addition, large steam input to the gasifier drives the water–gas shift reaction towards high H_2/CO ratios, needed in SNG and H_2 production. In this study, the target was to examine the technical feasibility of different reforming concepts by long-term reforming experiments with model biomass gasification gas and further to evaluate the efficiencies of two different reforming concepts for methane and hydrogen production.

2. Experimental methods

The experiments were made in a laboratory scale plug flow quartz reactor. The set-up was automated to enable running of the experiments continuously. The general design of the experimental set-up is presented in Fig. 2. All the experiments were made with a gas flow of 2 dm^3_N/min (at 0 °C and 1 atm). The inner diameter of the reactor was 27 mm and the length of the whole reactor 450–500 mm. The reactor was equipped with a thermocouple pocket (4 mm of diameter) and the temperature was measured from the bottom of the catalyst bed.

A continuous gas analyzer (ABB AO2020) was used to measure H_2 (thermal conductivity detector), O_2 (oxygen cell detector), CO, CO_2 and CH_4 (non-dispersive infra-red adsorption detector) from dry gas. Tars and light hydrocarbons were analyzed with HP5890

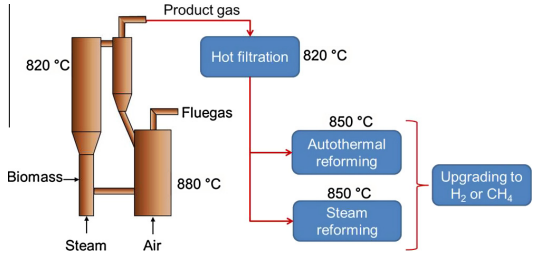

Fig. 1. Targeted process for the production of methane or hydrogen based on indirectly heated steam gasification of biomass followed by hot filtration and either autothermal or steam reforming of hydrocarbons and tar.

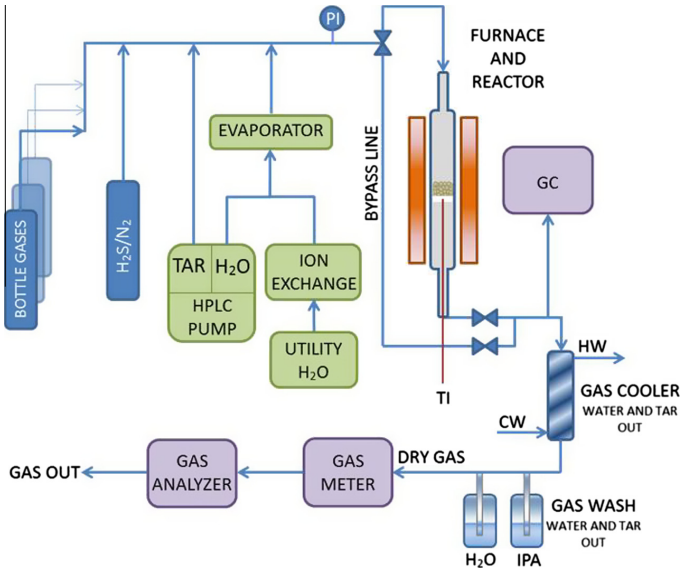

Fig. 2. General design of the experimental set-up.

series II or Agilent 7890A gas chromatograph (GC) depending on the reactor set-up. Both gas chromatographs were equipped with two FID detectors and two columns HP-PLOT/Q to analyze light hydrocarbons C_1–C_5 and HP-5 for tar compound analysis. The sample line from set-up to GC was heated.

The gas compositions used in the experiments are presented in Table 1. The gases were supplied by AGA with purities of CH_4 99.995%, C_2H_4 99.95%, CO 99.97%, CO_2 99.99%, H_2 99.999%, N_2 99.999%, O_2 99.999%, H_2S 0.500 mol.% in N_2, NH_3 5 mol.% in N_2. The model tar mixture consisted of benzene 10 wt.% (Merck, >99.7%), toluene 80 wt.% (Merck, ⩾99.9%) and naphthalene 10 wt.% (Merck, ⩾99%). The model compound mixture represents high temperature tar that contains mainly stable aromatic compounds. The gas having the lowest hydrocarbon content (LH) represents the steam gasification gas of wood with dolomite as bed material. Medium hydrocarbon content gas (MH) is between of the two previous gases in respect to hydrocarbon content. These gas compositions were studied operating the reactor in steam reforming mode. With MH also the addition of O_2 to the reformer was studied, which represented the autothermal operation mode. The total flow was kept always 2 dm^3_N/min whether the gas contained oxygen or not. The chosen oxygen concentration was based on practical knowledge of operating industrial size reformers.

The conditions of the experiments and the catalyst amounts are presented in Table 2. Catalysts were commercial precious metal catalysts of three different compositions (PM1, PM2 and PM3) and a commercial nickel catalyst. The catalyst particles were of the size of few millimeters, typically 3 × 3 mm cylinders. The surface area and bulk density of the catalysts are presented in Table 3. The GHSVs used are based on typical values used in the industry, 5000 h^{-1} for nickel catalyst and 10,000 h^{-1} for precious metal catalysts. The temperature profiles for steam and autothermal reforming experiments has been given in the Appendix A.

Elemental balances (C, H, N and O) were calculated based on the measured inlet and outlet gas compositions. The gas flow rate at the outlet was calculated from the carbon balance and water concentration in the outlet from the oxygen balance. Thus, carbon and oxygen balances were fitted to 100%.

The conversions of the compounds were calculated from the mass balances according to equation (1). In the results, the total tar conversion means the total conversion of benzene, toluene and naphthalene.

$$X_i = \frac{F_{i,IN} - F_{i,OUT}}{F_{i,IN}} * 100 \quad (1)$$

where X_i is the conversion of a compound i and F_i is the molar flow of the compound. For the total tar conversion, F_i is the sum of tar compounds.

The deactivation rate per 100 h was calculated from the slope of a line fitted to a product conversion versus time data. After about the first 100 h from the start of the experiment, the initial activity of the catalyst had stabilized and the decline in the activity of the catalysts became almost linear in all the experiments. Therefore, the deactivation rate was calculated from data from around 100 h onwards.

For the estimation of the carbon formation tendency of a gas two indicators were used: steam-to-reformable carbon molar ratio (H_2O/C_{REF}, Eq. (2)) and oxygen-to-reformable carbon molar ratio

Table 1
Simulated biomass gasification gas compositions presented as dry gas, except water concentration in wet gas.

	CO vol.%	CO_2 vol.%	H_2 vol.%	CH_4 vol.%	O_2 vol.%	N_2 vol.%	C_2H_4 vol.%	NH_3 ppmv	H_2S ppmv	Tar g/m^3_N	H_2O vol.%
LH	19.2	22.7	50.6	6.3	0	0	1	2000	100	10.27	30
MH	25	20	35	10	0	7.8	2	2000	100	20.28	40
MH + O_2	25	20	35	10	3.4	4.4	2	2000	100	20.28	40

Table 2
Catalyst and conditions of the experiments, PM means precious metal catalyst.

Catalyst	Gas	Duration of the experiment, h	GHSV, h^{-1}	Catalyst mass, g	Bed height, cm	T at catalyst outlet, °C	T of furnace, °C
Ni	MH + O_2	450	8800	15.52	2.5	916	950
Ni	MH	500	5400	22.78	4	851	900
Ni	LH	478	5400	22.78	4	850	900
PM1	MH + O_2	570	12,000	5.24	1.6	888	950
PM2	MH + O_2	564	12,000	9.56	1.6	916	950
PM3	MH	503	10,200	13.38	2.1	860	900
PM3	MH	124	12,300	9.58	1.8	920	990–1000
PM3	LH	501	8600	13.38	2.5	862	900
PM3 + Ni	LH	477	5400[a]	7.63 + 14.97	4	868	900

[a] Total GHSV is 5400 h^{-1}, GHSV for PM3 is 15,000 h^{-1} and for Ni 7500 h^{-1}.

Table 3
Geometrical surface area and bulk density of the catalysts.

Catalyst	Bulk density, g/cm^3	Geometrical surface area, mm^2
Ni	1.06	35.3
PM1	0.52	20.3
PM2	0.96	35.3
PM3	1.00	35.3

(O/C_{REF}, Eq. (3)). Reformable carbon refers to the carbon in hydrocarbons in the feed gas.

$$\frac{H_2O}{C_{REF}} = \frac{\dot{n}_{H_2O}}{\dot{n}_{CH_4} + 2\dot{n}_{C_2H_4} + 6\dot{n}_{C_6H_6} + 7\dot{n}_{C_7H_8} + 10\dot{n}_{C_{10}H_8}} \quad (2)$$

$$\frac{O}{C_{REF}} = \frac{\dot{n}_{H_2O} + 2\dot{n}_{O_2} + \dot{n}_{CO} + 2\dot{n}_{CO_2}}{\dot{n}_{CH_4} + 2\dot{n}_{C_2H_4} + 6\dot{n}_{C_6H_6} + 7\dot{n}_{C_7H_8} + 10\dot{n}_{C_{10}H_8}} \quad (3)$$

3. Results of experimental work

3.1. Elemental balances and evolution of the product gases

Hydrogen balance was between 96–103% and nitrogen balance 88–125%. Larger error in nitrogen balance is due that N_2 was not analysed but calculated from the balance. The calculated dry gas flow rates have been given in the Appendix A. The evolution of H_2, CO and CO_2 stayed quite constant over the run in all the experiments. The molar based values of out/in ratios for the product gases are presented in Appendix A. With LH gas, H_2 and CO were formed and CO_2 was consumed with both nickel and precious metal catalyst. With MH and MH + O_2 gas, there was more H_2, CO and CO_2 in the outlet than in the inlet.

3.2. Product conversions and deactivation rates for tar components

Tar conversions are presented in Fig. 3 for the experiments with nickel catalyst and in Fig. 4 for precious metal catalyst. The rates of deactivation after stabilization (about after the first 100 h of the experiments) are presented in Table 4. The conversions and deactivation rates are shown only for the experiments that lasted several hundreds of hours. With nickel catalyst, almost full tar conversion was obtained in autothermal reforming with MH + O_2. In autothermal reforming, however, the temperatures were higher compared to steam reforming experiments. With MH + O_2, the activity of the catalyst declined during the experiment and after 500 h the tar conversion had dropped from 98% to 88%. For steam reforming of MH, the conversion was 88% after 100 h. The decline in tar reforming activity (Table 4) with nickel catalyst was strongest with MH gas and slowest with LH gas, which had lower tar and ethene content and higher H_2O/C ratio than MH gas. Oxygen addition decreased the rate of deactivation with MH gas. However, the lowest rate was obtained with LH.

In autothermal reforming of MH with precious metal catalysts, the total tar conversions of PM1 and PM2 catalysts were in the same range as for nickel catalyst. Full tar conversion was obtained with PM1 and MH + O_2 gas and no deactivation was observed during the experiment (Fig. 4 and Table 4) indicating that the amount

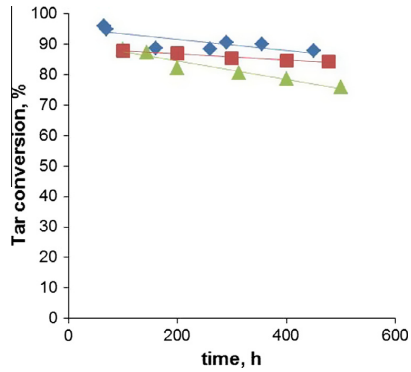

Fig. 3. Conversion of tar compounds with nickel catalyst and different gas compositions: MH + O_2 gas (◇), MH (Δ) and LH (□) gas.

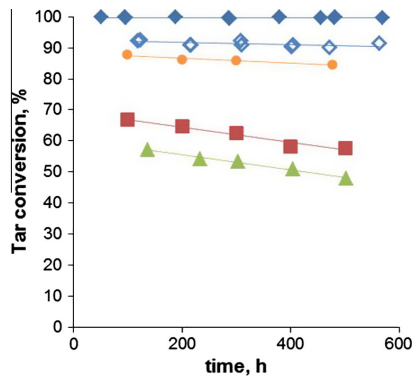

Fig. 4. Tar conversion with precious metal catalyst: MH + O_2 with PM1 (filled ◇), MH + O_2 with PM2 (empty ◇), MH with PM3 (Δ), LH with PM3 (□), LH with PM3 and Ni (○).

Table 4
Change in tar and methane conversion in percentage units per 100 h after the initial activity decrease.

Catalyst	Gas	Total tar %-unit/100 h	Methane %-unit/100 h	Ethene %-unit/100 h
Ni	MH + O_2	−1.4	−1.3	−1.1
Ni	MH	−3.1	−1.5	−1.8
Ni	LH	−1.0	−0.9	−0.1
PM1	MH + O_2	0.0	−3.6	0.0
PM2	MH + O_2	−0.3	0.1	−0.2
PM3	MH	−2.4	0.6	−3.2
PM3	LH	−2.5	−0.2	−0.1
PM3 + Ni	LH	−0.8	−0.7	−0.1

of the catalyst was too large for the possible deactivation to be observable in tar conversion. However, the deactivation could be seen in methane conversion. Also, PM2 with MH + O_2 showed stable activity; however the tar conversion was slightly lower being 92%. These two experiments had the same space velocity of 12,000 h^{-1}. In steam reforming, the conversions remained on lower level, even though the space velocity was lower than in autothermal experiments. The reasons for this were in the lower temperature in steam reforming experiments and possibly also in the different precious metal catalyst, PM3, which might have contained less active metals than the other two used in autothermal reforming experiments.

The deactivation of precious metal catalysts towards tar conversion was less severe than with nickel catalyst in autothermal reforming. In steam reforming, the MH and LH gases had the same deactivation rate in tar conversion although with MH the level of tar conversion was slightly lower than with LH. This may be explained by the slightly higher space velocity with LH gas than with MH gas. If precious metal is compared to nickel, the deactivation rate was lower with LH but higher with MH than with nickel catalyst. In the experiment with combined nickel and PM3 catalyst bed and LH gas, the conversion levels stayed more stable than with PM3 and LH gas. The hydrocarbon conversions showed less deactivation than for precious metal or nickel catalyst alone with LH gas.

3.3. Product conversions and deactivation rates for methane and ethene

The conversions of methane and ethene for the experiments with nickel catalyst are presented in Fig. 5 and for precious metal catalysts in Fig. 6. The highest methane conversions were obtained with MH + O_2 gas with both nickel and precious metal catalysts, most probably due to higher temperature with O_2 as was the case also with tar conversions. With the nickel catalyst the rate of decline of methane conversion was quite similar for all the gas compositions (−0.9,...,−1.5 percentage units/100 h) (Table 4). It was slightly higher for MH gas and slowest for LH gas. Like with tar, PM1 was clearly more active than PM2. Although, the methane and tar reforming activity of PM2 stayed stable, whereas methane reforming activity of PM1 decreased most of all the catalysts 3.6 percentage units per 100 h (Table 4), but on the other hand the activity of PM1 towards tar compounds stayed at 100% for whole 500 h experiment.

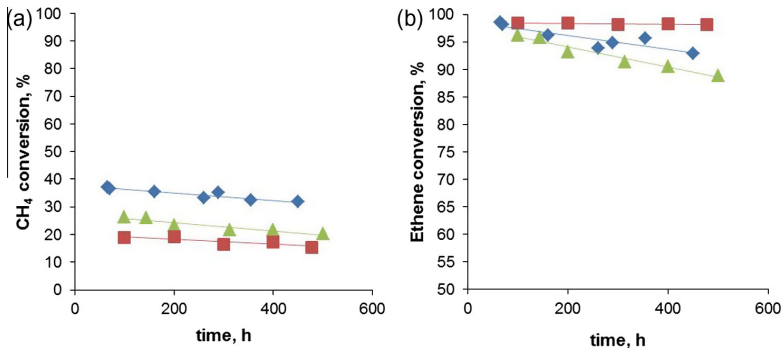

Fig. 5. (a) Methane and (b) ethene conversion with nickel catalyst: MH + O_2 gas (◇), MH (Δ) and LH (□) gas.

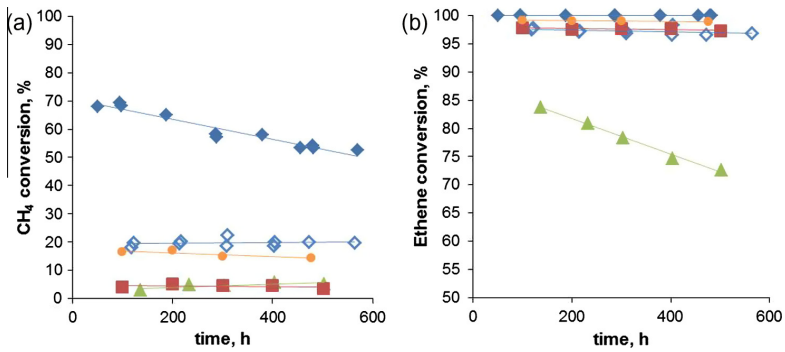

Fig. 6. (a) Methane and (b) ethene conversion with precious metal catalyst: MH + O_2 with PM1 (filled ◇), MH + O_2 with PM2 (empty ◇), MH with PM3 (Δ), LH with PM3 (□), LH with PM3 and Ni (○).

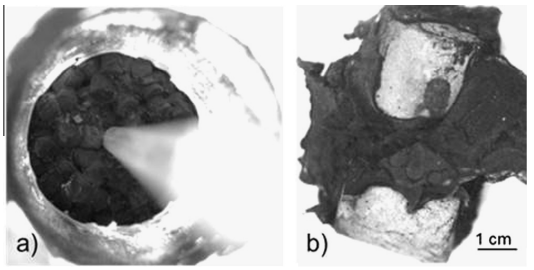

Fig. 7. Pyrolytic coke formation on the catalyst: (a) blocked surface of the catalyst bed, (b) two catalyst particles inside solid carbon encapsulation.

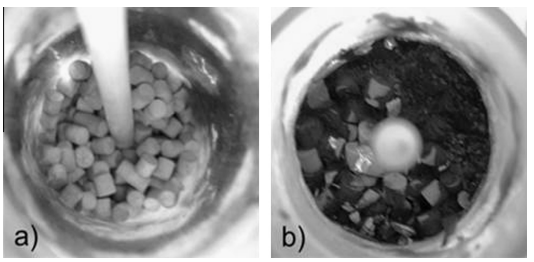

Fig. 8. Top of the catalyst bed after experiment with MH + O_2 gas with (a) PM2 catalyst after 564 h, and (b) nickel catalyst for 450 h.

Ethene conversion with the nickel catalyst stayed stable and almost 100% for LH gas, whereas for MH and MH + O_2 gases the conversion decreased slightly. With the precious metal catalysts, ethene conversion stayed stable and high being >97% for all the other gas compositions except MH gas without oxygen. In that experiment, the conversion level from the beginning was lower than in other experiments with nickel or precious metal and it declined at the rate of 3 percentage units per 100 h, which was the fastest decreasing rate for ethene conversion of all the experiments.

3.4. Carbon formation

Carbon that formed during the experiments was characteristically of pyrolytic type. It was formed from soot, which accumulated on the catalyst bed filling the empty spaces between particles and eventually forming solid graphite, which encapsulated the entire particle as is described also by Rostrup-Nielsen and Christiansen [16]. An example of pyrolytic carbon can be seen in Fig. 7 which presents the top of the carbon-blocked catalyst bed (a) and two catalyst particles (b) from a preliminary test with MH + O_2 gas and nickel catalyst. The entire catalyst bed was filled with pyrolytic carbon but the particles themselves remained intact inside the carbon.

In those experiments where the test could be continued for 500 h, carbon was not formed in such extent that it would have increased the pressure drop over the catalyst bed during the run. With PM2 catalyst, at 916 °C in the catalyst outlet and MH + O_2 gas, the catalyst bed was free of coke (Fig. 8a). With nickel catalyst in exactly same conditions (Fig. 8b) carbon was formed on the catalyst bed even though the accumulation was small compared to cases presented in Fig. 7. The surface structure of different metals has been noticed to affect the carbon formation reactions [16] which was observed as the difference in the carbon formation between the nickel and precious metal catalysts. At higher temperatures, also the gasification of carbon (R4) becomes thermodynamically more favorable and may enhance the carbon removal from the catalysts. The carbon accumulation on nickel catalyst could therefore be due to lower gasification activity of the nickel. Because the carbon formation on the nickel catalyst proved to be more problematic than on precious metal catalyst but the use of precious metal catalyst is hindered by the high price, one interesting option for a reformer design could be a small layer of precious metal catalyst as a pre-reformer followed by a larger nickel catalyst layer.

In steam reforming, the gas compositions with low hydrocarbon content (LH) and medium hydrocarbon content (MH) could be reformed for around 500 h with precious metal and nickel catalyst. Also, the substitution of oxygen by increased temperature was tested in a shorter (124 h), preliminary experiment with precious metal catalyst PM3 and MH gas. The temperature in the outlet of the catalyst bed was about the same as in the experiments with oxygen (920 °C). Instead of improved operation conditions, this led to heavy carbon formation on the reactor walls of above the catalyst bed even though no hard carbon layer was formed on the catalyst bed.

The estimation of the risk for carbon formation for a steady-state, non-equilibrium process with higher hydrocarbons and relatively high temperature is more complicated than for a traditional steam reforming of natural gas. Tar components and especially ethene are known to increase the carbon formation [6,16]. They decompose to carbon through non-reversible reactions (R1), (R2), unlike methane decomposition to carbon which is an equilibrium reaction (R3). Also, the addition of an oxidant (oxygen or H_2O) decreases the risk for carbon formation [6]. Typically H_2O/C_{REF} or O/C_{REF} ratios are used in evaluation of risk of carbon formation in steam reforming and they can also be applied to reforming of biomass gasification gas. The ratios for the gas compositions used in this study are presented in Table 5. The experiments with MH + O_2 gas had higher O/C_{REF} ratio than MH gas, thus explaining the stronger coke formation and deactivation with MH gas than with MH + O_2. Of all the tested gases, the LH gas had the highest H_2O/C_{REF} and O/C_{REF} ratios leading to easy operation for 500 h.

Exact critical ratios for avoiding carbon formation are difficult to specify because the addition of oxygen, the type of the hydrocarbons and the catalyst also affect the ratio. This can be seen especially from the experiments with MH and MH + O_2 gases where H_2O/C_{REF} ratios were the same but the addition of oxygen increased the O/C_{REF} ratio of the MH + O_2 gas significantly allowing easier operation. Generally, based on the results of this study in steam reforming mode, the H_2O/C_{REF} ratio above 4 and O/C_{REF} ratio above 8 can be recommended. When estimating the risk for carbon formation in reforming of biomass gasification gas, both H_2O/C_{REF} and O/C_{REF} ratios should be inspected and the higher risk of carbon formation with nickel catalyst should also be taken into account.

Table 5
Steam-to-reformable carbon, oxygen-to-carbon and oxygen-to-reformable carbon ratios of the gases used in the experiments.

Test gases	H_2O/C_{REF}	O/C_{REF}
MH	3.8	7.6
MH + O_2	3.8	8.0
LH	4.3	10.7

4. Concept assessment

4.1. Examined plant configurations

This section concentrates on the impact of reforming approaches to the overall performance of fuel production from biosyngas. The analysis is based on mass and energy balances calculated with ASPEN Plus process simulation software. The studied reforming alternatives are autothermal and steam reforming, which are examined from the viewpoint of producing two different products: methane or hydrogen. The combination of these alternatives gives four basic configurations, each characterised by distinctive plant designs. The configurations are identified by a sequence of two letters, each having the following meaning:

- first letter identifies the reforming technology: autothermal (A) or steam reforming (S);
- second letter identifies the main product: methane (M) or hydrogen (H).

4.2. Process designs and simulation methodology

The main plant design parameters are summarised in Table 6, while equipment design parameters are given in the Appendix B. All plants are designed to satisfy their own steam usage and excess heat is assumed to be sold to a nearby district heating network. Steam is generated by recovering heat from syngas and fluegas cooling and from methanation exotherm. When electricity produc-

Table 6
Main design parameters for the examined plant configurations.

Configuration		AM	SM	AH	SH
Band conveyor dryer					
Specific heat consumption	kW h/tH_2O_{evap}	1300	1300	1300	1300
Share of LT heat in belt dryer	%	20	20	20	20
Moisture in	wt%	50	50	50	50
Moisture out	wt%	15	15	15	15
Air separation unit (ASU)					
Oxygen purity	mol%	99.5	–	99.5	–
Oxygen delivery pressure	bar	1.05	–	1.05	–
Steam gasifier					
Pressure	bar	Atmospheric	Atmospheric	Atmospheric	Atmospheric
Gasification temperature	°C	820	820	820	820
Combustion temperature	°C	880	880	879	880
Heat loss	%	1.1	1.1	1.1	1.1
Steam/fuel (dry)	kg/kg	0.86	0.89	0.80	0.80
Char to oxidizer/fuel (dry)	kg/kg	0.20	0.20	0.20	0.20
Ceramic filter					
Filtration temperature	°C	820	820	820	820
Catalytic reformer					
Outlet temperature	°C	850	850	850	850
Heat loss (HHV)	%	1.0	1.0	1.0	1.0
Steam/O_2	–	0.7	–	0.7	–
Methane conversion	%	35	10	35	10
Steam/O_2 mixture inlet temp	°C	187		187	
H_2/CO at reformer outlet	–	3.0	3.0	2.9	2.8
Sour shift					
Steam/CO at inlet	–			3.7	3.3
Reactor inlet temp.	°C			310	307
Reactor outlet temp.	°C			404	404
Scrubber					
Temperature at inlet	°C	200	200	200	200
Temp. at stage 1 outlet	°C	60	60	60	60
Temp. at stage 2 outlet	°C	30	30	30	30
Syngas compressor					
Syngas pressure at outlet	bar	16.0	16.0	21.0	21.0
Acid gas removal					
CO_2 removal extent	%	96	96		
Sulphur removal extent	%	99	99		
Syngas methanation					
Inlet pressure to methanation	bar	14.6	14.6		
Outlet pressure from synthesis	bar	11.4	11.4		
Hydrogen recovery					
Inlet pressure to H2PSA	bar			20.0	20.0
Tailgas pressure from H2PSA	bar			1.0	1.0
H_2 recovery	%			86	86
CO_2 recovery					
Inlet pressure to CO2PSA				7	7
Tailgas pressure from CO2PSA				1	1
CO_2 recovery	%			80	80
Gas engine					
Net electric efficiency	%			43.0	43.0
DH efficiency	%			38.3	38.3
Overall efficiency	%			81.3	81.3

Table 7
Properties of forest residue chips used as feedstock.

Proximate analysis, wt% d.b.[a]	
Fixed carbon	25.3
Volatile matter	70.8
Ash	3.9
Ultimate analysis, wt% d.b.	
Ash	3.9
C	53.2
H	5.5
N	0.3
Cl	0
S	0.04
O (difference)	37.06
Other properties	
HHV, MJ/kg	20.67
LHV, MJ/kg	19.34
Bulk density, kg d.b./m^3[b]	293
Sintering temp. of ash, °C	>1000

[a] wt% d.b. = weight percent dry basis.
[b] 1 l batch, not shaken.

tion exceeds the on-site consumption, the excess amount is sold to the power grid.

4.3. Biomass residues to synthesis gas

A schematic diagram of a front-end process with main operating parameters is given in Fig. 1. An atmospheric band conveyor dryer (not shown in figure) is used to dry the biomass residue chips (see Table 7 for properties) from their initial moisture of 50 wt.% down to 15 wt.%. The dried chips are fed to an indirectly heated gasification reactor fluidized with steam and operated at 820 °C. The minimum steam requirement for the gasification reactor is set to 0.8 kg/kg$_{biom,dry}$ based on [29]. The combustion section (oxidizer) of this dual-reactor system is fluidized with air and operated at 880 °C. Bed material, composing of dolomite, is circulated between the reactors. The gasifier converts wood chips into raw product gas containing CO, H_2, CO_2, H_2O, CH_4 and small amount of higher hydrocarbons and tars. Part of the feedstock drifts with circulating bed material to the oxidizer where it is burned with air in order to heat up the bed material. The hot bed material is separated from fluegas and circulated back to the gasification reactor where it provides heat to sustain endothermic gasification reactions. The fluegas is cooled down to 150 °C and the heat is recovered for steam generation. The raw product gas from the gasification reactor is filtrated at 820 °C with ceramic filter elements to separate the entrained dust. After filtration, tars and hydrocarbons are catalytically reformed to light gases at 850 °C. Complete conversion of all components other than methane is assumed. The methane conversion is set to 35% for autothermal and 10% for steam reforming configuration. The heat required to run the endothermic gross reaction is generated either via internal combustion using oxygen (autothermal) or indirectly by gas burners in the furnace radiator box (steam reforming). The steam reforming design produces a separate fluegas stream that is cooled down to 150 °C and the heat is recovered for steam generation. The process configurations downstream from reforming are specific to the targeted end product and are discussed in Sections 4.4 and 4.5.

4.4. Upgrading to methane

The examined plant configurations for the production of biomethane are shown in Fig. 9. Following reforming, the gas is cooled down to 30 °C using syngas coolers and two-stage water scrubber.

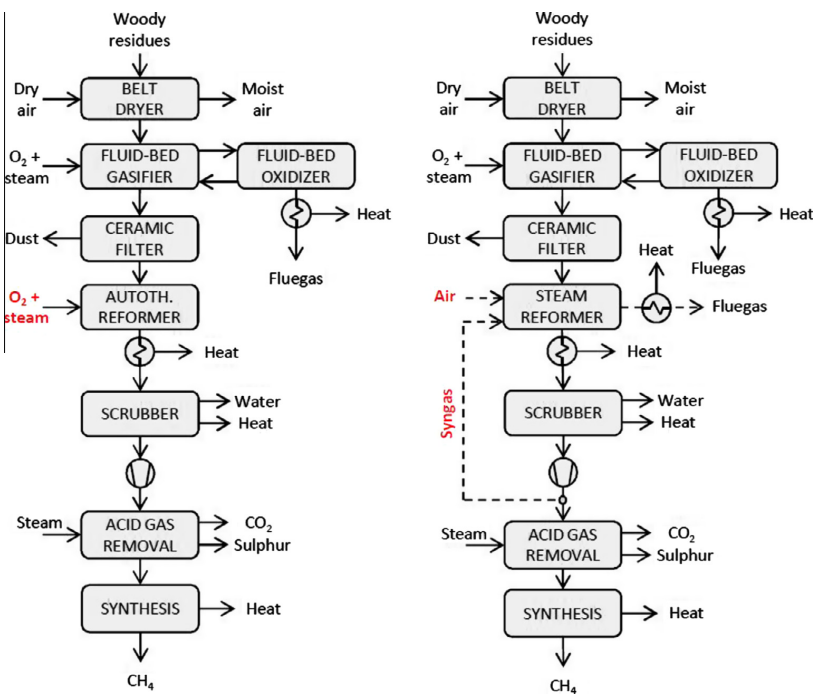

Fig. 9. Examined plant configurations for biomethane (SNG) manufacture.

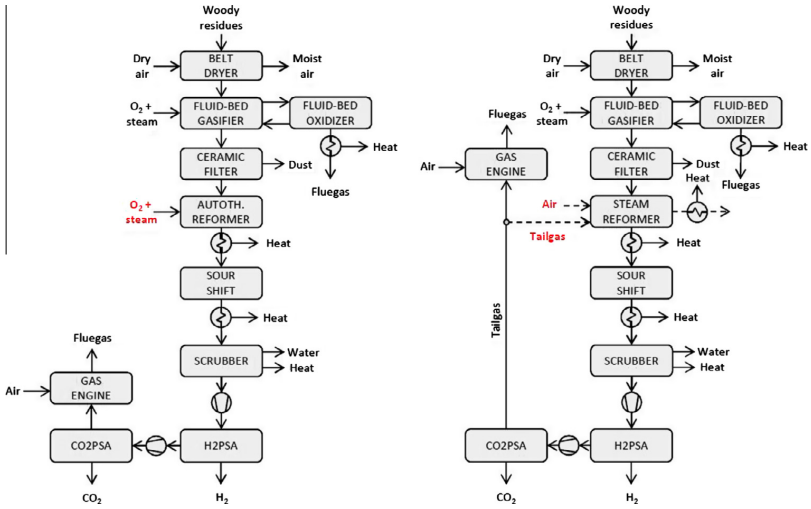

Fig. 10. Examined plant configurations for biohydrogen manufacture.

The waste heat removed is used to raise and superheat steam and to supply heat for the belt dryer. The desired H_2/CO ratio of 3 can be achieved during reforming with catalysts that are also active in water–gas shift reaction R7. The extent of shifting that takes place in the reformer can be controlled by adjusting steam input to the gasifier.[1] For design AM, the correct H_2/CO ratio is achieved with 0.86 and for SM with 0.89 steam/$fuel_{dry}$ ratio (see Table 6).

For a plant configuration that features indirectly heated steam reformer, a slip stream of cooled gas is diverted from the main stream to supply fuelgas for firing in the reformer furnace. Rest of the cooled and condensed gas (all gas in the autothermal reforming configuration) is compressed to 16 bar to facilitate a more efficient separation of acid gases by a physical washing process using chilled methanol as solvent. The treated gas exiting the acid gas removal is fed to a methanation area operated at 15 bar pressure.

The design of the catalytic synthesis section is inspired by a high temperature methanation process called 'TREMP', developed and offered by Haldor Topsøe. The design created for this analysis features 6 adiabatic fixed-bed reactors connected in series and equipped with intercoolers. The inlet pressure to the first reactor is 15 bar. The syngas is first admixed with steam followed by preheating to 300 °C. The amount of steam addition is chosen to limit temperature increase in the first reactor to 700 °C. The hot effluent exiting from the first five reactors is cooled down to 300 °C prior feeding to the next reactor in series. Equilibrium conversions in the reactors are calculated with Aspen using Soave–Redlich–Kwong (SRK) equation of state model. The recovered heat is used to produce high pressure superheated steam for the plant's steam cycle. The effluent from the fifth reactor is cooled enough to condense and separate the associated water before feeding to the last methanation stage. With the above-described configuration, >99.5% conversion of syngas can be achieved. Effluent from the last reactor exits at 11 bar pressure.

[1] While observing the minimum 0.8 kg/kgbiomass,dry limitation.

4.5. Upgrading to hydrogen

The examined plant configurations for the production of biohydrogen are shown in Fig. 10. Following reforming, the gas is cooled down to about 300 °C the waste heat removed being used to raise and superheat steam. The gas is then fed in its entirety to an adiabatic sour shift reactor where carbon monoxide and steam are converted to carbon dioxide and hydrogen. The gas exits the shift reactor at 400 °C having a residual carbon monoxide content of 3.8 or 4.0 vol.% and H_2/CO ratio of 16.1 or 14.9 for AH or SH, respectively. After further cooling with waste heat recovery to 30 °C the gas is compressed to 21 bar followed by recovery of hydrogen from the syngas by pressure swing adsorption process suitable for sulphur containing gases (sour PSA) [30]. The PSA process produces extremely pure hydrogen (from 99 to 99.9999 + vol.%), which is delivered at only about 0.5 bar below the feed gas pressure. However, the tailgas stream, which contains the removed impurities and rest of the hydrogen, needs to be withdrawn at near atmospheric pressure to achieve the high hydrogen yield of 86% [31]. Another PSA unit is then used to separate most of the tailgas CO_2 to improve its heating value. Before separation the tailgas is compressed to 7 bar. The resulting stream of pure CO_2 is vented to atmosphere although a possibility to use it industrially or to sequestate it below ground exists. In configuration SH, a slip stream is diverted from the tailgas for firing purposes in the steam reforming furnace (see Fig. 10). Rest of the tailgas (all in configuration AH) is converted to electricity by internal combustion engine having an electrical efficiency of 43%. Heat from fluegas and engine cooling can be recovered as district heat if heat exchanges are installed at the cost of additional capital investment.

4.6. Mass and energy balances

Mass and energy balances have been simulated for all four plant configurations at the scale of 100 MW (LHV) wet forest residue input. According to the results, presented in detail in Table 8 and summarised in Fig. 11 and 67.5 MW or 66.8 MW of methane can be produced depending on the reforming approach. The by-product district heat output of methane plants is 12.4 MW or

Table 8
Process simulation results for examined plant configurations.

Configuration		AM	SM	AH	SH
Feedstock input					
Biomass to dryer (moist. 50 wt.%)	MW (LHV)	100	100	100	100
Biomass to gasifier (moist. 15 wt.%)	MW (LHV)	112	112	112	112
Biomass dry feed	kg/s	5.9	5.9	5.9	5.9
Oxygen balance					
On-site consumption, t/d		32.7		32.7	
Reformer oxygen input	kg/s	0.4		0.4	
Air separation units output, t/d		32.7		32.7	
Electricity balance					
On-site consumption, MW		−8.4	−6.9	−9.6	−8.0
Oxygen production	MW	−0.4		−0.4	
Oxygen compression	MW	−0.03		−0.03	
Feed screw and lock-hopper pres	MW	−0.1	−0.1	−0.1	−0.1
Feed drying	MW	−0.7	−0.7	−0.7	−0.7
Syngas compression	MW	−4.2	−3.1	−5.7	−4.5
Acid gas removal	MW	−0.2	−0.1		
Synthesis	MW	−0.5	−0.5	−0.4	−0.3
Power Island (all blowers + pumps)	MW	−1.9	−1.9	−1.9	−1.9
Miscellaneous	MW	−0.4	−0.4	−0.5	−0.4
Gross production, MW		8.4	8.8	18.2	18.1
Gas engine	MW			11.3	10.9
Steam turbine (back pressure)	MW	8.4	8.8	6.9	7.3
Steam balance					
On-site consumption (excl. methanation), kg/s		8.0	7.8	7.3	6.9
Gasifier	kg/s	5.4	5.5	5.0	5.0
Reformer	kg/s	0.3		0.3	
AGR solvent regeneration	kg/s	0.6	0.5		
Deaerator	kg/s	0.8	0.8	0.9	0.8
Economiser	kg/s	1.0	1.0	1.1	1.1
Gross production, kg/s		12.6	13.1	10.5	10.3
From syngas cooling (93.5 bar, 500 °C)	kg/s	6.0	5.9	6.7	6.4
From fluegas cooling (93.5 bar, 500 °C)	kg/s	3.8	3.8	3.8	3.8
From synthesis exotherm (93.5 bar, 500 °C)	kg/s	2.7	3.3		
Turbine extractions, kg/s		7.7	7.5	7.0	6.6
HP steam (25 bar, 330 °C)	kg/s	1.0	1.0	1.1	1.1
IP steam (2.2 bar, 123 °C)	kg/s	6.7	6.5	5.9	5.6
Turbine back pressure	bar	0.8	0.8	0.8	0.8
Energy outputs					
Methane	MW (LHV)	67.5	66.8	–	–
Hydrogen	MW (LHV)	–	–	53.8	53.4
Net electricity output	MWe	0.0	2.0	8.5	10.1
District heat (steam cycle)	MWth	4.2	6.8	6.0	9.3
District heat potential (engine)	MWth	0.0	0.0	10.1	9.7
District heat (methanation)	MWth	8.2	7.1	–	–
Gas to combustion	MW (LHV)	–	–	26.3	25.2

13.9 MW again depending on the reforming approach. The overall efficiencies are thus 79.9 MW or 80.7 MW for the two methane producing plant configurations. The gross electricity production by the steam turbine exceeds the on-site consumption of the methane plant by 2.0 MW for the steam reforming configuration, while additional electricity consumption in the autothermal reforming configuration lowers this balance to zero.

Corresponding results for hydrogen plants show that 53.8 or 53.4 MW of high-purity hydrogen can be produced from 100 MW (LHV) of wet biomass depending on the reforming approach. The by-product district heat output is in total either 16.1 MW or 19.0 MW again depending on the reforming approach. In comparison to methane plants, much more by-product electricity is generated as a result of PSA tailgas combustion in an internal combustion engine. The electricity surplus is 10.1 MW for the steam reforming configuration and 8.5 MW for the autothermal configuration.

Judging from these results, the reforming approach seems to have surprisingly limited impact to the amount of methane or hydrogen produced. However, it is expected that some of the impacts will materialise only as changes in plant capital cost and

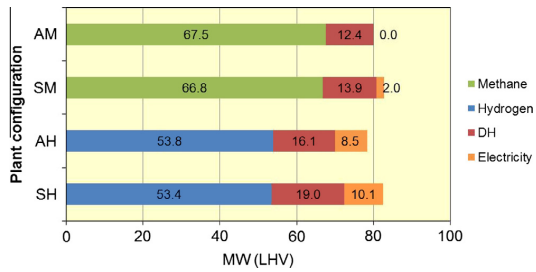

Fig. 11. Summary of the overall performance results for the examined plant configurations each processing 100 MW (LHV) of wet biomass.

are therefore not captured by our present analysis. For example, the fully indirectly heated configurations SM and SH do not require investment in oxygen production, which should lead to potentially large savings in capital. In addition, the CO_2 formed by internal

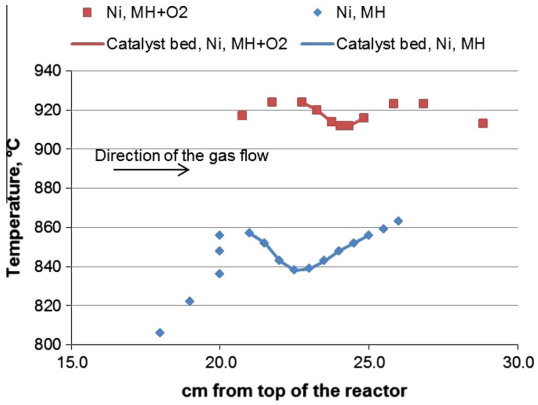

Fig. A1. The measured temperature profiles.

combustion with oxygen (cases AM and AH) mixes with the synthesis gas instead of exiting as a separate stream as is the case with steam reforming. This additional CO_2 increases synthesis gas volume downstream from reforming, making subsequent equipment larger and thus more expensive in comparison to plants based on steam reforming.

5. Conclusions

In this work, the feasibility of the two reforming concepts, autothermal and steam reforming was studied. The both modes were investigated experimentally in a laboratory scale reformer and on a conceptual level with the help of process simulation. Gas compositions representing the gases from different biomass gasification sources were tested with nickel and precious metal reforming catalysts. Both autothermal and steam reforming concepts were tested with the gas that contained medium amount of hydrocarbons (MH) and the operation was found to be easier with oxygen addition. The rate of deactivation in autothermal reforming mode was also lower than in steam reforming mode. The gas with low hydrocarbon content (LH) could be steam reformed without carbon blockages on both nickel and precious metal catalyst.

The risk for carbon formation was assessed by calculating H_2O/C_{REF} and O/C_{REF} molar ratios for each gas composition. The recommended critical ratios for both nickel and precious metal catalysts were estimated to be above 4 for H_2O/C_{REF} and above 8 for O/C_{REF} ratio in the tested temperature range. Both of these ratios should be inspected when analyzing the risk for carbon formation and also the effect of the catalyst should be taken into consideration. The nickel catalyst was found to be more prone for pyrolytic carbon accumulation than precious metal catalyst which was considered to be result of higher activity of precious metal catalyst towards gasification of carbon.

The experiments of this study were made with model gasification gas in laboratory. The gas contained the impurities that are the main factors to catalyst deactivation in biomass gasification: hydrocarbons (tar compounds and ethene) that may lead to coke formation and H_2S, a catalyst poison. However, real biomass gasification gas contains more complex tar composition and trace impurities and thus the catalysts should be tested in real conditions for final evaluation of feasibility.

Based on the concept assessment, the choice of reformer technology was found to have only limited impact on the amount of methane or hydrogen that can be produced from biomass. However, some of the impacts are expected to materialise in the plant capital costs instead. Therefore it can be concluded that the option with lower capital investment is also likely to have lower cost of fuel production, due to the small differences in performance.

Table A1
Calculated gas flows and molar based out/in ratios for H_2, CO and CO_2.

	Min	Max
Ni, MH + O_2		
Gas flow, dm^3_N/min	1.35	1.53
H_2 out/in	1.51	1.74
CO out/in	1.15	1.27
CO_2 out/in	1.16	1.34
Ni, MH		
Gas flow, dm^3_N/min	1.41	1.48
H_2 out/in	1.60	1.71
CO out/in	1.26	1.30
CO_2 out/in	1.05	1.11
Ni, LH		
Gas flow, dm^3_N/min	1.69	1.69
H_2 out/in	1.14	1.16
CO out/in	1.36	1.40
CO_2 out/in	0.87	0.89
PM1, MH + O_2		
Gas flow, dm^3_N/min	1.46	1.55
H_2 out/in	1.76	2.02
CO out/in	1.34	1.41
CO_2 out/in	1.12	1.24
PM2, MH + O_2		
Gas flow, dm^3_N/min	1.40	1.44
H_2 out/in	1.40	1.50
CO out/in	1.16	1.23
CO_2 out/in	1.13	1.22
PM3, MH		
Gas flow, dm^3_N/min	1.42	1.45
H_2 out/in	1.33	1.38
CO out/in	1.09	1.12
CO_2 out/in	1.10	1.17
PM3, LH		
Gas flow, dm^3_N/min	1.58	1.61
H_2 out/in	1.03	1.10
CO out/in	1.18	1.26
CO_2 out/in	0.91	0.97
PM3 + Ni, LH		
Gas flow, dm^3_N/min	1.70	1.71
H_2 out/in	1.13	1.15
CO out/in	1.38	1.40
CO_2 out/in	0.86	0.87

Acknowledgments

The authors would like to thank Katja Heiskanen, Päivi Jokimies and Mari-Leena Koskinen-Soivi for the experimental and analytical work. Finnish Funding Agency for Technology and Innovation (Tekes), Outotec Oyj, Helsingin Energia, Metso Power Oy, Huoltovarmuuskeskus, Gasum Oy, Neste Oil Oyj and Svenskt Gastekniskt Center AB for the financial support through VETAANI project (contract number 238/31/11) are acknowledged for financial support. VTT's co-operation partners Neste Oil and Stora Enso and their joint venture company NSE Biofuels are also acknowledged for their support and efforts for the BTL process development in 2007–2011.

Appendix A

Two typical examples of the measured temperature profiles of the catalyst bed are presented in Fig. A1. The calculated gas flow rates and molar based in/out ratios for the product gases (H_2, CO and CO_2) are given in Table A1.

Table B1
Equipment design parameters for the examined plant configurations.

Item	Design parameters	Notes
Air separation unit	Oxygen delivered from ASU at 1.05 bar pressure. Oxygen product (mol.%): O_2 = 99.5%, N_2 = 0.5%, Ar = 0%. Power consumption 263 kW h/ton O_2	a
Feedstock preparation and handling	Feeding screw power consumption 7 kJ/kg biomass. Lock-hopper inert gas consumption: 0.07642 $Nm^3/kg_{Biomass}$ for a double lock-hopper system that uses purge gas from LH to partly pressurise another LH. For a single lock-hopper system inert gas consumption 50% higher	b
Atmospheric band conveyor dryer	Biomass moisture: inlet 50 wt.%, outlet 15 wt.%, hot water: T_{IN} = 90 °C, T_{OUT} = 60 °C, steam: 1 bar, 100 °C heat consumption 1300 kW h/ton$H_2O_{EVAP.}$, power consumption 32 kW h/ton$_{DryBiomass}$	c
Fluidised-bed steam gasifier	Heat loss = 1% of biomass LHV. Δp = −0.2 bar. Gasifier modelled in two steps with RStoic and RGibbs using Redlich–Kwong–Soave equation of state with Boston–Mathias modification (RKS–BM). Hydrocarbon formation (kmol/kg of fuel volatiles): CH_4 = 5.864, C_2H_4 = 0.727, C_2H_6 = 0.2378, C_6H_6 = 0.1787. Tars modelled as naphthalene: $C_{10}H_8$ = 0.0261, All fuel nitrogen converted to NH_3. All other components assumed to be in simultaneous phase and chemical equilibrium. Oxidizer modelled as RStoic, Δp = −0.1 bar, lambda = 1.20	d, e
Ceramic hot-gas filter	Δp = −0.2 bar. Inlet temperature 820 °C	e
Catalytic reformer	Modelled as RGibbs using Redlich–Kwong–Soave equation of state with Boston–Mathias modification (RKS–BM). Phase and chemical equilibrium conversion for C_2+ and tar. For methane conversion see case designs. Δp = −0.2 bar. Steam reformer furnace lambda = 1.20	d, e
Sour shift	T_{out} = 404 °C, steam/CO = 1.8 mol/mol, Δp = −0.2 bar. Modelled as REquil using Redlich–Kwong–Soave equation of state with Boston–Mathias modification (RKS–BM). Equilibrium reactions: $CO + H_2O = CO_2 + H_2$, $T_{APPR.}$ = 10 K. $COS + H_2O = CO_2 + H_2S$, $T_{APPR.}$ = 0 K. $HCN + H_2O = CO + NH_3$, $T_{APPR.}$ = 10 K	f, e
Scrubber	Scrubbing liquid: water. T_{INLET} 200 °C. Two-step cooling: T^1_{OUT} = 60 °C, T^2_{OUT} = 30 °C. Complete ammonia removal. Modelled as flash using Soave–Redlich–Kwong (SRK) equation of state model	e
Rectisol acid gas removal	99% H_2S capture, for CO_2 capture level see case designs. Utilities: electricity (other than for refrigeration) = 1900 kJ/kmol (CO_2 + H_2S); refrigeration 3 × duty needed to cause −12 K temperature change in the syngas; 5 bar steam = 6.97 kg/kmol (H_2S + CO_2)	g
High temperature methanation	Six adiabatic fixed-bed reactors connected in series and equipped with intercoolers. Pressure at system inlet = 15 bar, pressure at system outlet 11 bar. T_{INPUT} to reactors 300 °C. T_{OUTPUT} from the first reactor restricted to 700 °C with steam dilution. Gas dried before feeding to last reactor. Syngas conversion to methane ⩾99.5%. Equilibrium reactions: $CO + 3H_2 = CH_4 + H_2O$, $T_{APPR.}$ = 20 K; $CO_2 + 4H_2 = CH_4 + 2H_2O$, $T_{APPR.}$ = 20 K. Reactors modelled as REquils using Soave–Redlich–Kwong (SRK) equation of state model	e
Heat exchangers	$\Delta p/p$ = 2%; ΔT_{MIN} = 15 °C (gas–liq), 30 °C (gas–gas). Heat loss = 1% of heat transferred	g
Heat recovery and steam system	Flue gas T_{OUT} = 150 °C, feed water pressure 110 bar, steam drum blowdowns: 2% of inlet flow, deaerator T_{OUT} = 120 °C	e
Steam turbine	Inlet steam parameters: 93.5 bar, 500 °C; for extraction steam parameters see case designs; $\eta_{ISENTROPIC}$ = 0.78, $\eta_{GENERATOR}$ = 0.97, $\eta_{MECHANICAL}$ = 0.98.	c, e, h
Compressors	Stage pressure ratio < 2, $\eta_{POLYTROPIC}$ = 0.85, η_{DRIVER} = 0.92, $\eta_{MECHANICAL}$ = 0.98.	i
Multistage compressors (>4.5 kg/s)	Stage pressure ratio <2, $\eta_{POLYTROPIC}$ = 0.87, η_{DRIVER} = 0.92, $\eta_{MECHANICAL}$ = 0.98, $T_{INTERCOOLER}$ = 35 °C, $\Delta p/p_{INTERCOOLER}$ = 1%.	j
Multistage compressors (<4.5 kg/s)[6]	Stage pressure ratio < 2, $\eta_{POLYTROPIC}$ = 0.85, η_{DRIVER} = 0.90, $\eta_{MECHANICAL}$ = 0.98, $T_{INTERCOOLER}$ = 35 °C, $\Delta p/p_{INTERCOOLER}$ = 1%	j
Pumps	$H_{HYDRAULIC}$ = 0.75, η_{DRIVER} = 0.90	i

a – Taken from Smith et al. [32].
b – Taken from Swanson et al. [33]. The original value in the reference was given for bagasse (160 kg/m), which is here fitted for forest residues (293 kg/m) assuming that LH is filled with feedstock up to 90%.
c – Based on personal communication with Andras Horvath, Carbona-Andritz, May 15th 2012.
d – Modelling principles taken from Refs. [34,35].
e – Operating parameters chosen by author.
f – Outlet temperature and steam/CO ratio based on personal communication with Wolfgang Kaltner, Süd-Chemie AG, July 9th, 2012.
g – Taken from Liu et al. [36].
h – Based on personal communication with Reijo Kallio, Å F-Consult, October 2012.
i – Taken from Chiesa et al. [37].
j – Taken from Glassman [38].

Appendix B

In order to enable the reader to reproduce the concept assessment presented in this paper, detailed process design parameters are given in Table B1.

References

[1] Sutton D, Kelleher B, Ross JRH. Review of literature on catalysts for biomass gasification. Fuel Process Technol 2001;73:155–73.
[2] Woolcock PJ, Brown RC. A review of cleaning technologies for biomass-derived syngas. Biomass Bioenergy 2013;52:54–84.
[3] Dayton D. A review of the literature on catalytic biomass tar destruction milestone completion report. NREL/TP-510-32815; 2002..
[4] Shen Y, Yoshikawa K. Recent progresses in catalytic tar elimination during biomass gasification or pyrolysis—a review. Renew Sustain Energy Rev 2013;21:371–92.
[5] Xu Charles C, Donald J, Byambajav E, Ohtsuka Y. Recent advances in catalysts for hot-gas removal of tar and NH3 from biomass gasification. Fuel 2010;89:1784–95.
[6] Yung MM, Jablonski WS, Magrini-Bair Ka. Review of catalytic conditioning of biomass-derived syngas. Energy Fuels 2009;23:1874–87.
[7] Anis S, Zainal Za. Tar reduction in biomass producer gas via mechanical, catalytic and thermal methods: a review. Renew Sustain Energy Rev 2011;15:2355–77.
[8] Abu El-Rub Z, Bramer Ea, Brem G. Review of catalysts for tar elimination in biomass gasification processes. Ind Eng Chem Res 2004;43:6911–9.
[9] Chan FL, Tanksale A. Review of recent developments in Ni-based catalysts for biomass gasification. Renew Sustain Energy Rev 2014;38:428–38.
[10] Leppälahti J, Simell P, Kurkela E. Catalytic conversion of nitrogen compounds in gasification gas. Fuel Process Technol 1991;29:43–56.
[11] Rönkkönen H, Simell P, Reinikainen M, Krause O, Niemelä MV. Catalytic clean-up of gasification gas with precious metal catalysts – a novel catalytic reformer development. Fuel 2010;89:3272–7.
[12] Caballero MA, Corella J, Aznar M-P, Gil J. Biomass gasification with air in fluidized bed. Hot gas cleanup with selected commercial and full-size nickel-based catalysts. Ind Eng Chem Res 2000;39:1143–54.
[13] Wang T, Chang J, Cui X, Zhang Q, Fu Y. Reforming of raw fuel gas from biomass gasification to syngas over highly stable nickel–magnesium solid solution catalysts. Fuel Process Technol 2006;87:421–8.
[14] Wang T, Li Y, Wang C, Zhang X, Ma L, Wu C. Synthesis gas production with NiO–MgO/γ-Al_2O_3/cordierite monolithic catalysts in a pilot-scale biomass-gasification-reforming system. Energy Fuels 2011;25:1221–8.
[15] Simell P, Hannula I, Tuomi S, Nieminen M, Kurkela E, Hiltunen I, et al. Clean syngas from biomass—process development and concept assessment. Biomass Convers Biorefin 2014.
[16] Rostrup-Nielsen JR, Christiansen LJ. Concepts in syngas manufacture. London: Imperial College Press; 2011.

[17] Jackson SD, Thomson SJ, Webb G. Carbonaceous deposition associated with the catalystic steam-reforming of hydrocarbons over nickel alumina catalysts. J Catal 1981;70:249–63.
[18] Kihlman J, Sucipto J, Kaisalo N, Simell P, Lehtonen J. Carbon formation in catalytic steam reforming of natural gas with SOFC anode off-gas. Int J Hydrogen Energy 2014;40:1548–58.
[19] Hepola J. Sulfur transformations in catalytic hot-gas cleaning of gasification gas. VTT Publications 425. Espoo; 2000..
[20] Kurkela E, Kurkela M. Advanced biomass gasification for high-efficiency power. Espoo: Publishable Final activity Report of PiGPower Project; 2009.
[21] Hannula I, Lappi K, Simell P, Kurkela E, Luoma P, Haavisto I. High efficiency biomass to power operation experiences and economical aspects of the novel gasification process. In: 15th Eur Biomass Conf Exhib from Res to Mark. Deploy., Berlin; 2007..
[22] Anonym. Gasification of biomass is a success. <http://www.aaenas.dk/PDF/EU_902321_Biomass%20Gasification.pdf> [accessed 27.10.14]..
[23] Hiltunen I, Kurkela E, Simell P. Method of reforming gasification gas. WO11107661A; 2011..
[24] Kurkela E, Simell P. Multiple stage method of reforming a gas containing tarry impurities employing a zirconium-based catalyst. WO2007FI00090; 2007..
[25] Kurkela E, Ståhlberg P, Simell P. Method and process for cleaning a product gas of a gasification reactor. EP 1165727 B1; 2005..
[26] Simell P, Kurkela E. Method for the purification of gasification gas. EP1404785 B1; 2007..
[27] Sabatier P, Senderens J-B. Nouvelles syntheses du methane. Comptes Rendus Des Seances L'academie Des Sci 1902;314:514–6.
[28] Kopyscinski J, Schildhauer TJ, Biollaz SMA. Production of synthetic natural gas (SNG) from coal and dry biomass – a technology review from 1950 to 2009. Fuel 2010;89:1763–83.
[29] Tuomi S, Kurkela E, Simell P, Reinikainen M. Behaviour of tars on the filter in high temperature filtration of biomass-based gasification gas. Fuel 2015;139:220–31.
[30] Hufton J, Golden T, Quinn R, Kloosterman J, Wright A, Schaffer C, et al. Advanced hydrogen and CO_2 capture technology for sour syngas. Energy Proc 2011;4:1082–9.
[31] Appl M. Ammonia, methanol, hydrogen, carbon monoxide. Modern Production Technologies; 1997..
[32] Smith A, Klosek J. A review of air separation technologies and their integration with energy conversion processes. Fuel Process Technol 2001;70:115–34.
[33] Swanson M, Musich M, Schmidt D, Schultz J. Feed system innovation for gasification of locally economical alternative fuels (figleaf) final report; 2002..
[34] Hannula I, Kurkela E. A semi-empirical model for pressurised air-blown fluidized-bed gasification of biomass. Bioresour Technol 2010;101:4608–15.
[35] Hannula I, Kurkela E. A parametric modelling study for pressurised steam/O_2-blown fluidised-bed gasification of wood with catalytic reforming. Biomass Bioenergy 2012;38:58–67.
[36] Liu G, Larson ED, Williams RH, Kreutz TG, Guo X. Making Fischer-Tropsch fuels and electricity from coal and biomass: performance and cost analysis. Energy Fuels 2011;25:415–37.
[37] Chiesa P, Consonni S, Kreutz T. Co-production of hydrogen, electricity and CO from coal with commercially ready technology. Part A: performance and emissions. Int J Hydrogen Energy 2005;30:747–67.
[38] Glassman A. Users manual for updated computer code for axial-flow compressor conceptual design. Ohio: Toledo; 1992.

IV

Kaisalo, N., Simell, P., Lehtonen, J. (2016) Benzene steam reforming kinetics in biomass gasification gas cleaning. *Fuel* **182**, 696-703.

Fuel 182 (2016) 696–703

Contents lists available at ScienceDirect

Fuel

journal homepage: www.elsevier.com/locate/fuel

Full Length Article

Benzene steam reforming kinetics in biomass gasification gas cleaning

Noora Kaisalo [a,*], Pekka Simell [a], Juha Lehtonen [b]

[a] VTT Technical Research Centre of Finland, P.O. Box 1000, FI-02044 VTT, Finland
[b] Department of Biotechnology and Chemical Technology, Aalto University, P.O. Box 16100, FI-00076 Aalto, Finland

HIGHLIGHTS

- Effect of gasification product compounds on steam reforming of benzene was studied.
- H_2 decelerate and CO_2 accelerate the reforming kinetics.
- The acceleration by CO_2 could not be explained only by simultaneous dry reforming.
- Langmuir-Hinshelwood model described air gasification gas reasonably well.

ARTICLE INFO

Article history:
Received 27 March 2016
Received in revised form 4 June 2016
Accepted 7 June 2016

Keywords:
Biomass gasification
Steam reforming
Nickel catalyst
Kinetics

ABSTRACT

Benzene steam reforming kinetics was studied in conditions relevant to biomass gasification gas cleaning on Ni/Al_2O_3 catalyst i.e. temperature range 750–900 °C and in presence of H_2S. The benzene concentration was 600–3500 ppm. The qualitative effect of the main gasification product gas compounds on the benzene steam reforming kinetics was studied. The first order kinetic model in respect to benzene was used to compare the effect of H_2, CO and CO_2. It was observed that especially H_2 decelerated and CO_2 accelerated the benzene steam reforming kinetics. With a gas mixture representing air gasification gas, the Langmuir-Hinshelwood type model taking account effect of H_2 in denominator described the benzene decomposition well. However, the model did not describe the kinetics of benzene steam reforming for the gas representing O_2/H_2O gasification gas.

1. Introduction

Thermochemical conversion of biomass by gasification is one route to produce renewable fuels and chemicals. The gas produced by biomass gasification contains impurities that need to be cleaned before the gas can be utilized for fuel production. The hydrocarbon impurities (light hydrocarbons and tar) in the gasification gas can be converted into syngas by steam reforming. In addition to hydrocarbon impurities, the gas contains, among others, H_2S which is a known catalyst poison. The H_2S content in the gasification gas produced from forest residues is typically around 40–120 ppm [1].

Kinetics of tar decomposition in biomass gasification conditions have been studied with many catalysts such as dolomite, olivine, steam reforming type nickel catalysts and precious metal catalysts [2]. The dolomite and olivine catalysts are not as active as nickel or precious metal catalysts. They are more typically used in-situ as gasifier bed materials to reduce the tar concentration in the outlet gas than as a secondary bed to completely purify gasification gas from tar compounds, whereas nickel and precious metal catalysts are used in the secondary reformer.

In kinetic studies, tar is typically studied by combining tar compounds to one or several lumps or by using tar model compounds. Furthermore, the first order kinetics is typically assumed towards tar or tar model compounds. Palma [2] has collected in a review article kinetic parameters from different studies using model compounds or real gasification gas. In the studies with real gasification gas, the gas composition and conditions cannot be varied as freely as in the laboratory scale experiments and the effect of different compounds on kinetics cannot be studied so easily. On the other hand, most of the laboratory studies with model compounds have been conducted without H_2S. The conditions for the kinetic studies has to be carefully chosen since steam reforming is a fast, strongly endothermic reaction leading easily to mass transfer limitations and temperature gradients in the catalyst bed. The effectiveness factor is low in industrial scale reactors [3].

Considering studies of individual tar components, Jess [4] has studied steam reforming kinetics of various aromatic compounds, including benzene, with simulated coke oven gas with Ni/MgO catalyst. The gas mixture studied with contained 0.2 vol% of benzene,

* Corresponding author.
E-mail address: noora.kaisalo@vtt.fi (N. Kaisalo).

http://dx.doi.org/10.1016/j.fuel.2016.06.042
0016-2361/

Nomenclature

a	superficial surface area of the catalyst per volume of the particle (cm^2/cm^3)
c_i	concentration of a compound i (mol/m^3)
d_p	diameter of the particle (mm)
E_a	activation energy (kJ/mol)
ΔH_i	adsorption enthalpy of a compound i (kJ/mol)
K_i	equilibrium constant for adsorption of a compound i (–)
k′	apparent reaction rate constant ($m^3/(kg_{cat} * h)$)
k_c	mass transfer coefficient between gas and particle (cm/s)
L	length of the catalyst bed (mm)
m_{cat}	mass of the catalyst (kg)
n_i	molar flow of a compound i (mol/h)
p_i	partial pressure of a compound i (Pa)
Pe_p	particle Peclet number (–)
R	gas constant (J/(K * mol))
r_i	rate of reaction ($mol/(kg_{cat} * h)$)
RSS	residual sum of squares (mol^2/h^2)
T	temperature (°C)
X	conversion of benzene (–)
z	dimensionless weight of the catalyst bed (–)

Greek letters

α, β	reaction orders (–)
η	internal effectiveness factor (–)
θ_S	surface coverage by sulphur (–)

Subscripts

ref	reference temperature, 850 °C
exp	experimental result
calc	calculated value

H_2 30 vol% and H_2O 13 vol% in nitrogen at 410–800 °C. No H_2S was used in the experiments. For benzene reforming, first order kinetics was assumed. The pre-exponential factor was $2 * 10^{11}\ m^3\ s^{-1}\ kg^{-1}$ and the activation energy 196 kJ/mol.

Swierczynski et al. [5], in turn, have studied toluene steam reforming with Ni/olivine catalyst. The gas mixture used in the experiments contained toluene 4709 ppm, 7.5% H_2O and Argon to balance. H_2S was not included in this study either. They assumed as well the first order kinetics for toluene steam reforming and the pre-exponential factor was $3.14 * 10^{13}\ m^3\ kg_{cat}^{-1}\ h^{-1}$ and the activation energy was exactly the same as in the study of Jess [4] for benzene, 196 kJ/mol. Carbon monoxide was the primary reaction product but with higher space times, also CO_2 was formed via water gas shift reaction.

Devi et al. [6] have studied steam and dry reforming of naphthalene on olivine without H_2S in the gas. They studied the effect of gas compounds on naphthalene conversion at 900 °C. Similar naphthalene conversion was obtained at steam and dry reforming modes. However, with gasification gas (air gasification type composition), the conversion was lower because the conversion was decreased by the presence of hydrogen. They used power law model for naphthalene steam reforming. The reaction order for naphthalene was 2.04, for H_2 −0.74, CO 0.2, CO_2 0.94 and H_2O 1.79.

Simell et al. have studied both steam [7] and dry reforming [8] kinetics of benzene on dolomite catalyst. The steam reforming kinetics of benzene could be described by Langmuir-Hinshelwood mechanism. In the conditions of the study, steam did not have an effect on reaction rate but H_2 decreased the reaction rate. The rate determining step in the model was single site adsorption of benzene on the catalyst.

Corella et al. [9] have studied steam reforming kinetics of tar in real gasification gas from an air gasifier. They divided the tar compounds in different lumps and modelled the rate of reforming for the tar lumps. As a catalyst they used nickel catalyst with particle size of 7–14 mm. The kinetics were likely limited by mass transfer since in their earlier, study they used smaller particle size of the same catalyst and reported with that particle size that the kinetics were controlled by internal diffusion [10].

In this study, the qualitative effect of main gasification gas compounds on steam reforming kinetics of benzene was studied in presence of H_2S on nickel catalyst. The temperature range 750–900 °C was chosen to cover the practical reformer temperatures, which are required to avoid the complete deactivation of the catalyst by H_2S [11]. Benzene was chosen as a model compound because it is thermally very stable aromatic compound [12]. Consequently, the reformer design could be based on steam reforming rate data of benzene in cases where only tar reforming is necessary. An example is a biomass gasification plant producing only SNG, where low methane conversion in the reforming is an advantage.

2. Experimental

2.1. Laboratory experiments

The experiments were carried out in an atmospheric plug flow reactor system described in [13]. The reactor was a quartz tube of 10 mm inner diameter with 4 mm thermocouple pocket in the centre of the reactor. The reactor was placed in a three zone furnace. The catalyst was placed on a quartz sinter. The gases were fed by mass flow controllers from the gas cylinders. The gas compositions used in the experiments are presented in Table 1. The gasification gas 1 represented the product gas of air gasifier. The gasification gas 2 represented the gas from steam-oxygen blown gasifier; however the H_2O concentration was kept the same as in gasification gas 1. The gases were supplied by Aga and their purities were as follows: CO 99.97%, CO_2 99.99%, H_2 99.999%, CH_4 99.995%, N_2 99.999, H_2S 0.500 mol% in N_2. Benzene (Merck, >99.7%) and water (ion exchanged) were fed by HPLC pumps. Benzene was fed to the heated line with other gas components, whereas water was fed through a vaporizer before mixing it to the gases. The H_2S concentration of 100 ppm in dry gas was chosen based on typical concentration in the biomass gasification gas and it was kept constant in all the experiments.

Benzene and other hydrocarbons were analysed by GC/FID (Agilent 7890A). In some of the experiments with gas mixtures of Bz + H_2O and Bz + H_2O + H_2, the permanent gases (H_2, CO, CO_2, N_2) and H_2O were analysed by GC/TCD (Agilent 6850) to examine the

Table 1
Gas compositions in the experiments, the gas mixtures contained N_2 for balance.

	Dry gas				Wet gas	
	CO (vol%)	CO_2 (vol%)	H_2 (vol%)	H_2S (ppm)	H_2O (vol%)	C_6H_6 (ppm)
Bz + H_2O	0	0	0	100	10	600–3500
	0	0	0	100	4.25–12.76	3500
Bz + CO_2	0	14.9	0	100	0	3500
Bz + H_2O + CO	12.5	0	0	100	10	3500
Bz + H_2O + CO_2	0	15	0	100	10	3500
Bz + H_2O + H_2	0	0	11	100	10	3500
Gasification gas 1	12.5	15	11	100	10	3500
Gasification gas 2	25	20	35	100	10	3500

reaction products and stoichiometry. More detailed description of these gas chromatographs can be found in [13].

The experiments with the gas mixtures of Bz + H_2O were conducted in the temperature range 750–900 °C and the other gas compositions in the range of 800–900 °C. The total gas flow rate in the experiments was 1 l/min. The catalyst was reduced in-situ for 1 h at 900 °C with the mixture of H_2:N_2 50:50, 1 l/min. The first experimental condition was always run for at least 4 h to stabilize the catalyst activity. In each set point, the reaction conditions were kept constant for around 1.5–2.5 h. Every fifth set point was a reference set point where the catalyst activity was checked. The results were calculated typically from the average of three GC samples.

The catalyst used in the experiments was a commercial Ni/α-Al_2O_3 catalyst, containing 14.7 wt% of NiO, with a particle size of 200–300 μm. The amount of the nickel catalyst used in the experiments was 0.6 g. To ensure isothermal behaviour, the catalyst was diluted with SiC to 1:1 volume ratio. The particle size of SiC was 300–355 μm. The height of the diluted bed was 1.1 cm. The thermal conversion of benzene was tested with SiC (Pan Abrasives) at 900 °C. The SiC bed was of the same volume as the nickel catalyst bed. The gas composition in the experiment contained benzene 3500 ppm, 10% H_2O, 100 ppm H_2S and N_2 for balance.

The temperature of the catalyst bed was measured by a K-type thermocouple that was placed in the middle of the catalyst bed. For some of the experimental points, the axial temperature profile was measured and the maximum temperature gradient measured in the catalyst bed was ±4 °C from the temperature in the middle of the bed. The temperatures measured in the middle of the bed are used in the results.

2.2. Reactor model

A plug flow pseudo-homogenous model was used for the reactor system. Furthermore, the reactor was assumed as isothermal based on the small axial temperature gradient measured over the bed. In the evaluation of flow properties and mass transfer limitations, benzene steam reforming reaction was assumed to be a first order reaction (1).

$$-r_{bz} = k' * c_{bz} \tag{1}$$

The plug flow assumption was checked by known criteria and it was concluded that the axial and radial dispersion can be neglected. The ratio of the length of the bed to the particle size was larger than the criterion for axial dispersion (2) [14] even with high conversion of benzene (90%). The channelling criterion [14] was fulfilled as well; the ratio of the tube diameter to catalyst particle diameter was 24, which is above the limit 10, when the thermocouple pocket was reduced from the diameter of the reactor.

$$\frac{L}{d_p} = \frac{8\alpha}{Pe_p} \ln\left(\frac{1}{1-X}\right) \tag{2}$$

2.2.1. Mass transfer limitations

The internal and external mass transfer limitations were investigated by calculations. The reaction conditions used for calculations were the gas mixture of Bz + H_2O at 900 °C. For diffusion limitations in the particle, Thiele modulus and Weisz-Prater criterion [15] were calculated. The value for Thiele modulus was 0.21 and the internal effectiveness factor was 0.997, which lead to Weisz-Prater criterion value of $0.04 \ll 1$. For intraparticle resistances, Mears' criterion [16] was calculated (3). Thus, it could be concluded that internal or external mass transfer limitations did not limit the reaction rate.

$$\frac{\eta * k' * m_{cat}}{k_c a} = 0.002 < 0.1 \tag{3}$$

2.2.2. Parameter estimation

The parameter estimation was performed with MATLAB®. The objective function was residual sum of squares (4). It was minimized by Nelder-Mead simplex and Levenberg-Marquart algorithms. For the first order kinetics, the initial guesses for parameters were calculated by the linearization of Arrhenius equation. The model parameters were first estimated by Nelder-Mead simplex and then refined with Levenberg-Marquart algorithm. The molar flow of benzene was used as an objective variable. The model equation was described as an ordinary differential Eq. (5) and solved by ODE15s solver.

$$\mathrm{RSS} = \Sigma(\dot{n}_{i,exp} - \dot{n}_{i,calc})^2 \tag{4}$$

$$\frac{dn_i}{dz} = -r_i * m_{cat} \tag{5}$$

Arrhenius (6) and Van't Hoff (7) equations were used in the temperature centralized forms to minimize the correlation between the parameters and to enhance the convergence of the model.

$$k' = k_{ref} * \exp\left(-\frac{E_a}{R} * \left(\frac{1}{T} - \frac{1}{T_{ref}}\right)\right) \tag{6}$$

$$K = K_{ref} * \exp\left(-\frac{\Delta H_i}{R} * \left(\frac{1}{T} - \frac{1}{T_{ref}}\right)\right) \tag{7}$$

3. Results and discussion

3.1. Thermal reactions

The conversion of benzene by thermal reactions was studied at 900 °C, with gas flow of 1 l/min (H_2O 10% + C_6H_6 3500 ppm) with SiC. The conversion of benzene was only 3.7%. In these conditions, small amount of unidentified tar compounds (15 ppm calculated with the response factor for benzene) were formed. The thermal reactions of benzene in the conditions of this study were considered negligible for further result calculation and discussion.

3.2. Reactions and stoichiometry

Benzene steam reforming may take place via two steam reforming reactions (8) and (9). In addition to steam reforming reactions, water gas shift reaction (WGS) (10) may take place and affect the product distributions. According to Xu and Froment [17], all the three reactions (8)–(10) take place in parallel and the production of CO_2 cannot be explained only by WGS or only by the reaction (9). High temperatures may lead to thermal cracking of benzene (11). Biomass gasification gas contains CO_2 making also dry reforming reaction (12) possible route for benzene decomposition.

$$C_6H_6 + 6H_2O \rightarrow 6CO + 9H_2 \tag{8}$$

$$C_6H_6 + 12H_2O \rightarrow 6CO_2 + 15H_2 \tag{9}$$

$$CO + H_2O = CO_2 + H_2 \tag{10}$$

$$C_6H_6 \rightarrow wC_xH_y + zH_2 \tag{11}$$

$$C_6H_6 + 6CO_2 \rightarrow 12CO + 3H_2 \tag{12}$$

The stoichiometry of the reactions was inspected at 900 °C for the benzene steam reforming experiments and steam reforming in presence of H_2 (Table 2). For these experimental points, the product gases were measured and the elemental balances were calculated. In balance calculation, the water concentration was calculated by setting the oxygen balance to 1. Other values used in calculation were measured values. The elemental balances (out/in) were in steam reforming experiment and in presence of hydrogen respectively for carbon 1.06 and 1.03, hydrogen 0.98

Table 2
Measured stoichiometry in steam reforming without and with hydrogen at 900 °C (mol formed/mol of benzene reacted) compared to the stoichiometry of steam reforming reaction (8).

	Bz + H_2O	Bz + H_2O + H_2	Steam reforming reaction
Benzene conversion (%)	65	62	
CO/Bz	4.8	5.7	6
CO_2/Bz	0.7	0.0	0
H_2/Bz	9.7	10.8	9
H_2O/Bz	6.1	5.7	6
H_2/CO	2.0	1.9	1.5

and 0.99, and nitrogen 0.97 in both cases. No significant carbon formation was inspected when the catalyst was replaced after several experimental conditions.

The ratios of formed products to reacted benzene indicate that the main reaction was steam reforming reaction (8). With the nickel catalyst, no other hydrocarbons were detected in the outlet gas. In benzene steam reforming, small amount of CO_2 (1400 ppmv) was also formed which may be either formed by steam reforming (9) or water gas shift (10) reaction. When the inlet gas mixture contained hydrogen, no CO_2 was detected as a product, likely due to WGS equilibrium change. Carbon monoxide has been reported to be the primary product as well by Swierczynski et al. [5] who studied toluene steam reforming on Ni/olivine catalyst and by Jess [4] who studied tar reforming on Ni/MgO. Jess [4] attributed the CO_2 formation to the WGS reaction. According to methane steam reforming literature [17], both of the reactions (9) and (10) are responsible for the CO_2 formation. With dolomite catalyst, Simell et al. [7] have obtained quite different product distribution. In their study, the ratio of reacted benzene to CO_2 formed was 3–3.8. However, they as well considered CO as the primary product and the CO_2 formation was explained by the WGS reaction. Swierczynski et al. [5] observed that CO_2 content decreased with the increase of temperature due to the reverse WGS reaction.

3.3. Kinetics of benzene steam reforming

3.3.1. Reaction order for benzene and steam

At first, benzene steam reforming was studied by using a mixture of benzene and steam (Bz + H_2O, Table 1) with 100 ppm of H_2S and N_2 for balance. The reaction order for benzene and steam were defined by changing the H_2O and benzene concentrations in the gas and by fitting the parameters to a power law model (13). The parameter estimates with 95% confidence limits and correlation between parameters are presented in Table 3. The reaction order for benzene was close to one, which is typically used in literature [4,5,9]. For H_2O, the reaction order was close to zero, which is as well in line with literature. Accordingly, Rostrup-Nielsen and Christiansen [3] have reported that steam does not have an effect on steam reforming rate of methane on nickel catalyst above 600 °C. Similar observations are also reported by Simell et al. [7] for steam reforming of benzene on dolomite catalyst and by Swierczynski et al. [18] for toluene steam reforming on Ni/olivine

Table 3
Parameter estimates for power law model for Bz + H_2O mixture.

Parameter	Estimate	95% confidence limit	Correlations			
k_{ref} ($m^3/(kg_{cat} * h)$)	98.3	46.3	1			
E_a (kJ/mol)	220.1	13.7	0.544	1		
α	0.91	0.14	0.996	0.595	1	
β	0.15	0.09	0.279	0.051	0.281	1

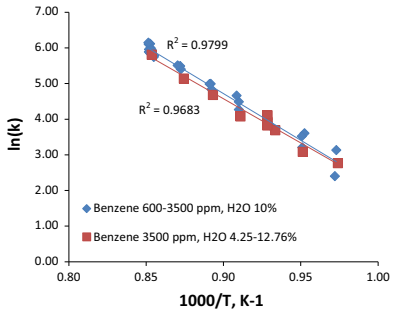

Fig. 1. The Arrhenius plot for benzene and steam concentration change.

catalyst. To illustrate the fit of first order kinetics for benzene and zero order for H_2O, the Arrhenius plots for the different benzene and H_2O inlet concentrations are presented in Fig. 1. The Arrhenius plots were calculated analytically by linearization method from two different datasets: one in which the benzene inlet concentration was varied from 600 ppm to 3500 ppm and the other in which H_2O concentration was varied between 4.25 and 12.76% at the benzene level of 3500 ppm.

$$-r_{Bz} = k' c_{Bz}^{\alpha} c_{H_2O}^{\beta} \quad (13)$$

3.3.2. Effect of main gasification gas compounds on benzene reforming rate

The effects of main gasification gas compounds (H_2, CO, CO_2) on the steam reforming rate of benzene were investigated by adding them individually to the mixture of benzene and H_2O. The first order kinetics was fitted separately to different data sets and the parameter estimates are presented in Table 4. The parameter estimation was done separately for the different gas mixtures to see the qualitative effect of main gas compounds on benzene steam reforming. For the mixture Bz + H_2O, all the data with different benzene and water concentrations were used in the estimation of parameters. The clearest effect on steam reforming rate was caused by H_2 and CO_2; H_2 decreasing and CO_2 enhancing the rate, whereas CO only slightly increased the rate. In addition to the parameter estimation by non-linear least squares, the linearization method for the Arrhenius plot (Fig. 2) was used to better illustrate the behaviour of different gas compositions. As can be from Fig. 2, the repeated data points have some variation. The data points are from the experiments with different catalyst packings, different time on stream and gas compositions that the catalyst has experienced may vary. However, if the catalyst was noticed to have been deactivated in the reference set point, the deactivated data points have been rejected and not used in the modelling.

The first order kinetic parameters obtained by Jess [4] for benzene steam reforming on nickel catalyst with gas containing H_2 had lower activation energy of 196 kJ/mol than in this study. If the pre-exponential factor reported by Jess [4] was converted to k_{ref} at 850 °C, it could be noticed that it was higher than in this study. Higher k_{ref} and lower activation energy is likely due to absence of H_2S in the experiments conducted by Jess. In steam reforming of toluene without product gases in the feed, Swierczynski et al. [5] obtained as well higher reaction rate than in this study on Ni/olivine catalyst in the absence of H_2S.

Benzene dry reforming (12) was studied without H_2O in the feed. The rate of dry reforming was clearly lower than the steam reforming rate. The observation of this study is in line with the literature data indicating that with nickel catalysts the dry reforming

Table 4
The parameter estimates for first order kinetics calculated by linearization for different gas compositions.

	k_{ref} ($m^3/(kg_{cat} * h)$)	95% confidence limit	E_a (kJ/mol)	95% confidence limit	Correlation	RSS
$Bz + H_2O$	133	±7	230	±13	−0.650	$2.28 * 10^{-6}$
$Bz + CO_2$	34	±19	295	±36	−0.890	$1.79 * 10^{-7}$
$Bz + H_2O + H_2$	59	±24	378	±100	−0.939	$3.18 * 10^{-6}$
$Bz + H_2O + CO$	173	±58	206	±98	−0.580	$1.94 * 10^{-6}$
$Bz + H_2O + CO_2$	247	±12	169	±15	−0.204	$2.96 * 10^{-8}$
Gasification gas 1	103	±32	307	±73	−0.907	$4.83 * 10^{-6}$
Gasification gas 2	212	±46	272	±79	−0.348	$4.07 * 10^{-7}$

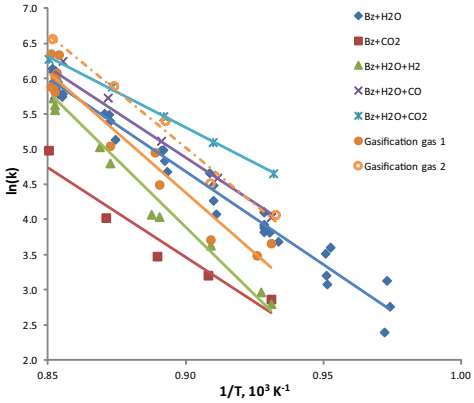

Fig. 2. The Arrhenius plot for the different gas compositions calculated by the linearization method.

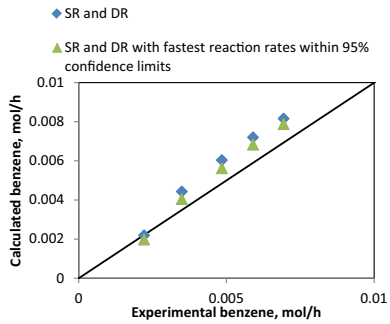

Fig. 3. The simulated parity plot of the benzene molar flow in $Bz + H_2O + CO_2$ mixture with the first order model for steam and dry reforming reactions.

is slower than steam methane reforming [19]. Wei and Iglesia [20], in turn, reported the same reaction rate for steam and dry reforming of methane. However, also the opposite behaviour was observed by Simell et al. [8] for a dolomite catalyst. The slower kinetics of dry reforming was explained by Mortensen and Dybkjær [19] by high CO coverage, which has also been reported in lower temperature steam reforming to limit the reaction rate [21]. However, at high temperatures, methane dissociation has been identified as the rate determining step [21]. From Arrhenius plot (Fig. 2), it seems that the first order kinetics does not well describe the dry reforming even though the RSS of non-linear least squares method is small (Table 4). However, the benzene conversion range (5–33%) in dry reforming experiments was more limited than in steam reforming case. For reliable kinetics for benzene dry reforming, more data would be required.

The higher benzene reforming rate with the mixture containing both H_2O and CO_2 might have been due to a dual effect of H_2O and CO_2. The rate of benzene conversion was simulated by two parallel reforming reactions (8) and (12) with the estimated first order kinetic parameters (Table 4). However, the simulated benzene outlet concentration was higher than the measured value, Fig. 3. To check that the lower benzene reforming rate was not only due to confidence limits in parameter estimation, the lowest activation energies and the highest k_{ref} within the confidence limits were chosen as the parameter values for simulation of the two reactions. Thus, there might be some beneficial effect of co-adsorption of CO_2 and H_2O to reforming rate, which increases the reaction rate. Because in dry and steam reforming mechanisms, the surface species O^* and HO^* are reacting with adsorbed hydrocarbons [19,20], and consequently both CO_2 and H_2O bring more oxygen to the surface for adsorbed carbon from hydrocarbons to react to carbon oxides, although CO_2 has low adsorption energy and thus, low coverage on the nickel surface [21].

In benzene steam reforming study by Simell et al. [7], CO or CO_2 was not assumed to affect the benzene reforming rate and dry reforming reaction was not included. The results in this study, however, indicate that especially CO_2 had a rate enhancing effect for benzene steam reforming. However, the CO_2 is likely to have a different effect on dolomite than on nickel catalyst.

With the air gasification type of gas (Table 1, gasification gas 1), the rate was lower than with only $Bz + H_2O$ but higher than when only H_2 was added to the $Bz + H_2O$ mixture. This was likely due to enhancing effect of CO_2 on the decomposition rate of benzene. With the gasification gas 2, the rate of benzene steam reforming was higher than with gasification gas 1 or with the $Bz + H_2O$ mixture.

To illustrate the effect of temperature on the rate constant, the Arrhenius plot for different gas mixtures is presented in Fig. 2. Interestingly at 900 °C, the reaction rate was quite the same for all the gas mixtures when steam is present. The effect of main gasification gas compounds on the reforming rate became more evident when the temperature was decreased. The rates of chemical reactions decrease with temperature, but in this case the reduction of the rate is also likely due to more severe poisoning of the catalyst by H_2S when temperature decreases. The adsorption of H_2S on the catalyst surface depends on the temperature; the surface coverage decreases with the increase of temperature [3].

H_2S is likely to influence the kinetics of reforming since it adsorbs preferentially on the edges and corners of nickel crystals which are, as well, the most active sites for reforming leaving less active facet sites free for reforming reactions [21]. The higher activation energies obtained in this study than for example by Jess [4] could be explained by H_2S poisoning leaving only less active facets for reforming. However, if the surface coverage for sulphur on nickel is calculated according to Rostrup-Nielsen and Christiansen [3] (Eq. (14)), for the gas composition containing 10% of H_2, the sulphur coverage is 1 at 900 °C. At lower temperatures, the surface coverage would be above 1 according to Eq. (14). However, the catalyst is still active and thus, there has to be some free sites for

Table 5
The parameter estimates with 95% confidence intervals, the RSS for models fitted with data sets Bz + H_2O and Bz + H_2O + H_2 and the RSS for simulation with gasification gases.

	A	B	C
Model equation	$-r_{bz} = \frac{k_1 * c_{bz}}{1+K_{H_2} * c_{H_2}}$	$-r_{bz} = \frac{k_1 * c_{bz}}{1+\sqrt{K_{H_2}} * c_{H_2}}$	$-r_{bz} = \frac{k_1 * c_{bz}}{(1+\sqrt{K_{H_2}} * c_{H_2})^2}$
k_{ref}	142.5 ± 15.95	172.5 ± 43.18	165.9 ± 31.06
E_a	226 ± 29.72	212.2 ± 63.49	217 ± 49.01
$K_{ref}(H_2)$	0.896 ± 0.5023	1.343 ± 1.832	0.2023 ± 0.1996
ΔH_{H2}	−336.6 ± 178.5	−455.2 ± 370.8	−415.5 ± 287.8
RSS	$6.1437 * 10^{-6}$	$6.6255 * 10^{-6}$	$6.5151 * 10^{-6}$
RSS for gasification gas 1	$1.6000 * 10^{-5}$	$1.6187 * 10^{-5}$	$1.6366 * 10^{-5}$
RSS for gasification gas 2	$4.8322 * 10^{-5}$	$3.7844 * 10^{-5}$	$4.0395 * 10^{-5}$

Table 6
The correlation coefficients for parameter estimates of the models A, B and C.

Model A				
k_{ref}	1			
E_a	−0.627	1		
$K_{ref}(H_2)$	0.540	−0.341	1	
ΔH_{H2}	−0.338	0.555	−0.799	1
Model B				
k_{ref}	1			
E_a	−0.868	1		
$K_{ref}(H_2)$	0.938	−0.783	1	
ΔH_{H2}	−0.748	0.932	−0.738	1
Model C				
k_{ref}	1			
E_a	−0.822	1		
$K_{ref}(H_2)$	0.892	−0.700	1	
ΔH_{H2}	−0.654	0.894	−0.664	1

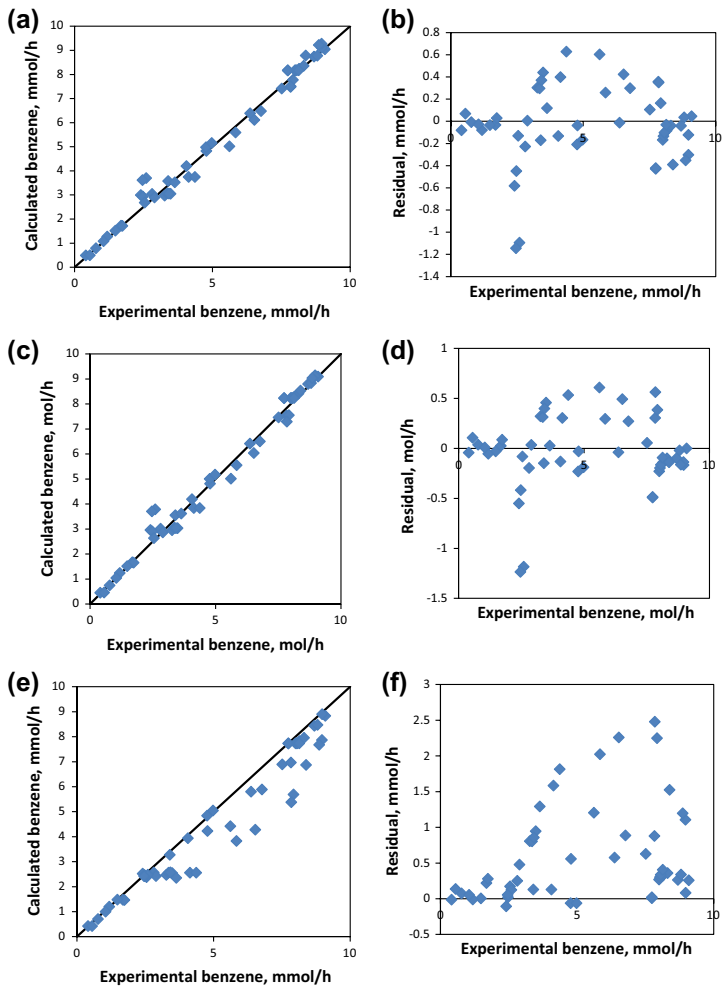

Fig. 4. (a) The parity and (b) residual plot for the model A of the parameter estimation for gas mixtures Bz + H_2O and Bz + H_2O + H_2, (c) and (d) for the model B and (e) and (f) for the model C, respectively.

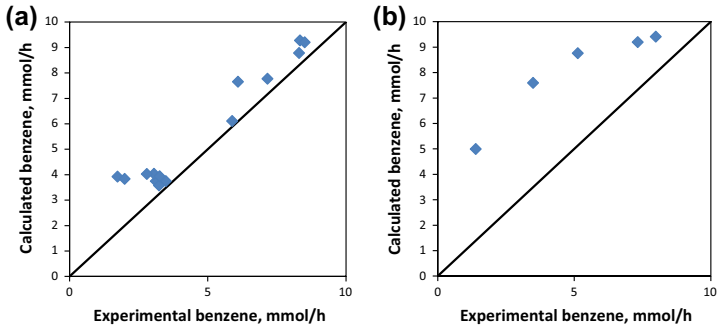

Fig. 5. The parity plot for the model A simulated with (a) gasification gas 1 and (b) gasification 2.

reforming. Also, it is noted by Rostrup-Nielsen and Christiansen [3] that Eq. (14) is not valid for sulphur coverages close to one. According to Rostrup-Nielsen [22], the methane steam reforming rate depends on the sulphur coverage of nickel by a factor $(1-\theta_S)^3$ meaning that if the surface is completely covered by sulphur, the catalyst is completely inactive. However, the catalyst in this study maintained its activity towards benzene steam reforming despite of sulphur poisoning. This might be due to that the surface coverage equation does not hold for as high coverages [3] or the sulphur is preferentially adsorbed on corners and edges in multiple layers leaving some facet sites free for benzene adsorption on the surface enabling steam reforming reaction. Hepola et al. [23] have studied sulphur adsorption on nickel catalysts in conditions relevant to cleaning of biomass gasification gas. They reported that the nickel surface was reconstructed with high sulphur coverages and sulphur was adsorbed in multi-layer or sub-surface form. Thus, sulphur might, as well, create new active sites for benzene steam reforming instead of completely deactivating the catalyst.

$$\theta_S = 1.45 - 9.53 * 10^{-5} * T * \ln\left(\frac{p_{H_2S}}{p_{H_2}}\right) \quad (14)$$

3.3.3. Langmuir-Hinshelwood type models

Several Langmuir-Hinshelwood type models were tested assuming that the rate determining step was benzene adsorption [7]. The tested models and their parameter estimates are presented in Table 5 and the correlations of model parameters are presented in Table 6. The model A was taken from the study of Simell et al. [7]. In the model B, the benzene adsorption was assumed as single site and hydrogen adsorption as dissociative. In the model C, the benzene adsorption was assumed as dual site and the hydrogen adsorption as dissociative. The dual site benzene adsorption was assumed based on the literature of higher hydrocarbon reforming kinetics [24]. The gas mixtures used in the parameter estimation were Bz + H_2O and Bz + H_2O + H_2. The RSS values were closely the same for all the models. Parity plots and residuals for the models are presented in Fig. 4. The model A was the simplest model and the RSS is slightly smaller for that than for the models B or C, thus it was selected as the best model.

The adsorption enthalpy reported in the literature for hydrogen adsorption on nickel catalyst has been clearly lower −93.4 kJ/mol for Ni/α-Al_2O_3 [25] and −82.90 kJ/mol for Ni/magnesium spinel catalyst [17] than estimated in this study. The difference might be due to the correlations of the parameters or H_2S poisoning of the catalyst. The estimated adsorption enthalpy also had a large confidence interval.

The two gasification gas compositions were simulated with all the models and the RSS values for these are included in Table 5 and parity plots in Fig. 5. The models fit reasonably with gasification gas 1 (Fig. 5a) because the concentrations of CO_2 and CO were smaller than in gas 2 and thus their rate increasing effect was not so strong. However, with the gas 2, the models seemed not to fit the data well. Fig. 5b presents the parity plot when model A was tested for gasification gas 2 with the parameter estimates in Table 5. Consequently, CO_2 and CO should be included in the model; H_2 alone was not enough to describe the benzene reforming. However, more data would be required to obtain more reliable parameter estimates.

4. Conclusions

The effect of the main gasification gas components on benzene steam reforming rate was studied under atmospheric pressure in the temperature range 750–900 °C. Based on the measured products, the main reaction was identified to be the steam reforming reaction of benzene producing CO and H_2. Isothermal pseudo-homogenous plug flow model was concluded to be suitable for kinetic modelling and simulations. From the first order kinetic models with different gas compositions, it could be concluded that CO_2 and CO enhance the reforming rate of benzene and H_2 decelerate the rate. The enhancing effect of CO_2 could not be explained by parallel steam and dry reforming reactions taking place.

The Langmuir-Hinshelwood type model A with H_2 in denominator described the system with air gasification gas reasonably well but not the O_2/H_2O gasification gas. This is probably due to higher concentrations of products in the gas. The effect of main gasification gas compounds could be described in this study qualitatively, however, more data would be required for more sophisticated model that could explain the effect of CO_2 on the steam reforming rate and that would take account temperature dependence of H_2S poisoning.

Acknowledgment

The authors would like to thank Hakan Oyaci, Katja Heiskanen and Päivi Jokimies for the experimental work. Finnish Funding Agency for Technology and Innovation (Tekes), Outotec Oyj, Helsingin Energia, Metso Power Oy, Huoltovarmuuskeskus, Gasum Oy, Neste Oil Oyj and Svenskt Gasteknisk Center AB for the financial support through VETAANI project (contract number 238/31/11) are acknowledged for financial support.

References

[1] Simell P, Hannula I, Tuomi S, Nieminen M, Kurkela E, Hiltunen I, et al. Clean syngas from biomass—process development and concept assessment. Biomass Convers Biorefinery 2014;4:357–70.

[2] Palma C Font. Modelling of tar formation and evolution for biomass gasification: a review. Appl Energy 2013;111:129–41.
[3] Rostrup-Nielsen JR, Christiansen LJ. Concepts in syngas manufacture. London: Imperial College Press; 2011.
[4] Jess A. Catalytic upgrading of tarry fuel gases: a kinetic study with model components. Chem Eng Process Process Intensif 1996;35:487–94.
[5] Swierczynski D, Courson C, Kiennemann A. Study of steam reforming of toluene used as model compound of tar produced by biomass gasification. Chem Eng Process Process Intensif 2008;47:508–13.
[6] Devi L, Ptasinski KJ, Janssen FJJG. Decomposition of naphthalene as a biomass tar over pretreated olivine: effect of gas composition, kinetic approach, and reaction scheme. Ind Eng Chem Res 2005;44:9096–104.
[7] Simell PA, Hirvensalo EK, Smolander VT. Steam reforming of gasification gas tar over dolomite with benzene as a model compound. Ind Eng Chem Res 1999;38:1250–7.
[8] Simell PA, Hakala NAK, Haario HE, Krause AOI. Catalytic decomposition of gasification gas tar with benzene as the model compound. Ind Eng Chem Res 1997;36:42–51.
[9] Corella J, Caballero MA, Aznar M-P, Brage C. Two advanced models for the kinetics of the variation of the tar composition in its catalytic elimination in biomass gasification. Ind Eng Chem Res 2003;42:3001–11.
[10] Corella J, Orío A, Toledo J-M. Biomass gasification with air in a fluidized bed: exhaustive tar elimination with commercial steam reforming catalysts. Energy Fuels 1999;13:702–9.
[11] Hepola J. Sulfur transformations in catalytic hot-gas cleaning of gasification gas. VTT Publications 425. Espoo; 2000. http://www.vtt.fi/inf/pdf/publications/2000/P425.pdf.
[12] Bruinsma OSL, Tromp PJJ, de Sauvage Nolting HJJ, Moulijn JA. Gas phase pyrolysis of coal-related aromatic compounds in a coiled tube flow reactor, 2. Heterocyclic compounds, their benzo and dibenzo derivatives. Fuel 1988;67:334–40.
[13] Kihlman J, Sucipto J, Kaisalo N, Simell P, Lehtonen J. Carbon formation in catalytic steam reforming of natural gas with SOFC anode off-gas. Int J Hydrogen Energy 2015;40:1548–58.
[14] Kapteijn F, Moulijn JA. Laboratory reactors. In: Ertl G, Knözinger H, Weitkamp J, editors. Handb. Heterog. Catal.. Weinheim: VCH Verlagsgesellschaft mbH; 1997. p. 1363–4.
[15] Fogler SF. Elements of chemical reaction engineering. 4th ed. Upper Saddle River: Prentice Hall; 2006. p. 839.
[16] Mears DE. Tests for transport limitations in experimental catalytic reactors. Ind Eng Chem Process Des Dev 1971;10:541–7.
[17] Xu J, Froment GF. Methane steam reforming, methanation and water-gas shift: I. Intrinsic kinetics. AIChE J 1989;35:88–96.
[18] Świerczyński D, Libs S, Courson C, Kiennemann A. Steam reforming of tar from a biomass gasification process over Ni/olivine catalyst using toluene as a model compound. Appl Catal B Environ 2007;74:211–22.
[19] Mortensen PM, Dybkjær I. Industrial scale experience on steam reforming of CO_2-rich gas. Appl Catal A Gen 2015;495:141–51.
[20] Wei J, Iglesia E. Isotopic and kinetic assessment of the mechanism of reactions of CH_4 with CO_2 or H_2O to form synthesis gas and carbon on nickel catalysts. J Catal 2004;224:370–83.
[21] Rostrup-nielsen JR, Sehested J, Norskov J. Hydrogen and synthesis gas by steam- and CO_2 reforming. Adv Catal 2002;47:65–139.
[22] Rostrup-Nielsen JR. Sulfur passivated nickel catalysts for carbon-free steam reforming of methane. J Catal 1984;85:31–43.
[23] Hepola J, McCarty J, Krishnan G, Wong V. Elucidation of behavior of sulfur on nickel-based hot gas cleaning catalysts. Appl Catal B Environ 1999;20:191–203.
[24] Rostrup-Nielsen JR. Catalytic steam reforming. Berlin: Springer-Verlag; 1984. p. 54.
[25] Hou K, Hughes R. The kinetics of methane steam reforming over a Ni /α-Al_2O catalyst. Chem Eng J 2001;82:311–28.

V

Simell, P., Hannula, I., Tuomi, S., Nieminen, M., Kurkela, E., Hiltunen, I., Kaisalo, N., Kihlman, J. (2014) Clean syngas from biomass—process development and concept assessment. *Biomass Conversion and Biorefinery* **4**, 357-370.

Aalto-DD 132/2017
VTT SCIENCE 160

ISBN 978-952-60-7525-9 (printed)
ISBN 978-952-60-7524-2 (pdf)
ISSN-L 1799-4934
ISSN 1799-4934 (printed)
ISSN 1799-4942 (pdf)

978-951-38-8561-8 (printed)
978-951-38-8560-1 (pdf)
2242-119X
2242-119X (printed)
2242-1203 (pdf)

Aalto University
School of Chemical Engineering
Department of Chemical and Metallurgical Engineering
www.aalto.fi

BUSINESS + ECONOMY

ART + DESIGN + ARCHITECTURE

SCIENCE + TECHNOLOGY

CROSSOVER

DOCTORAL DISSERTATIONS